

## **A COMPLEX ANALYTICAL METHOD FOR PARCHMENT CHARACTERIZATION**

B. Dolgin <sup>(1)</sup>, V. Bulatov <sup>(2)</sup>, I. Schechter <sup>(2)</sup>

<sup>(1)</sup> *Nuclear Research Center Negev, PO Box 9001,  
Beer-Sheva 84190, Israel*

<sup>(2)</sup> *Schulich Faculty of Chemistry, Technion-Israel Institute of  
Technology, Haifa 32000, Israel*

### **ABSTRACT**

Parchments are interesting archeological objects. A wide variety of modern analytical techniques have been applied in order to get better insight on parchment preservation stage as well as to contribute to their conservation and restoration. However, no practical method to help the museum workers and laboratory experts in these routine jobs exists. Several requirements have to be satisfied to obtain an appropriate procedure capable of parchment characterization as an entire analytical object. Due to the unique character of common archeological objects, non-destructive techniques or those requiring no (or only minimal) sampling, are preferred. The second problem in this method development deals with the nature of objects under the study. Archeological objects (and parchment particularly) regularly have complex shapes and structures and their origin is rarely known, and they can be found in various states of conservation. Their degree of deterioration can modify the chemical and the physical composition mainly of the surface layers, which are directly accessible to analysis. However, the information obtainable from deeper layers can sometimes be more helpful. Therefore, an application of a single analytical technique to describe parchment conditions often is not advantageous and a special experimental approach, which combines several examination techniques and chemical analysis should be favored. In this context, an assortment of five analytical techniques (synchronous fluorescence, laser induced breakdown spectroscopy, visual color imaging, characterization using high voltage application and near infrared analysis) as well as every technique alone represents one of the best choices, since it

combines simplicity, good analytical performance and robustness, non-destructiveness and non-invasiveness. The aim of this work was to develop a guide procedure for characterizing archeological objects using complex non-destructive analytical methodology. Using this guide, the entire parchment analysis can be performed very fast *in situ* and archeological items can be identified in real time during an on-line data collection. Furthermore, it allows several constituents of interest to be measured simultaneously leading to accurate and objective identification of authentic items.

### **List of abbreviations**

**ANOVA** Analysis of variance

**CV** Cross-validation

**DA** Discriminant analysis

**ESR** Electron spin resonance

**FT** Fourier transform

**ICP** Inductively coupled plasma

**IDAP** Improved Damage Assessment of Parchment

**IR** Infrared

**LIBS** Laser induced breakdown spectroscopy

**MAP** Methods in the Micro-Analysis of Parchment

**MD** Mahalanobis distance

**MLR** Multiple Linear Regression

**MSC** Multiplicative scatter correction

**MPLS** Modified partial least squares

**NIR** Near-infrared

**OES** Optical emission spectroscopy

**PC** Principal component

**PCA** Principal component analysis

**PCR** Principal component regression

**RGB** Red Green Blue

**PLS** Partial least squares

**PMMA** Polymethylmetacrylate

**PRESS** Prediction error sum of squares

**SEC** Standard error of calibration

**SECV** Standard error of cross-validation

**SEM** Scanning electron microscopy

**SEP** Standard error of the NIR analysis prediction

**SEP(C)** Standard error of prediction corrected for bias

**SF** Synchronous fluorescence

**SNV** Standard normal variate

**UV** Ultraviolet

## **1. INTRODUCTION**

### **1.0. General aspects**

Parchment is composed of organic matter; therefore, it undergoes considerable aging and deterioration during the years after production. This fact poses a severe problem to archeologists and restorers when attempting to characterize a given ancient sample in terms of its present condition and evident origin. In fact, it has been observed that the degradation processes continue even under the stable conditions prevalent in museums. Therefore, a proper method for monitoring the parchment conditions is needed for ensuring optimal conservation and restoration.

Parchments are multifarious objects and their matrix is complicated; therefore, both chemical and physical properties of parchment samples have to be taken into account in the study of its deterioration. This study is focused on the development of new analytical procedures for analysis of ancient parchments.

In the following study, we attempt the development of a new analytical tool and apply it to the characterization of the authentic archeological objects. The objects included real samples of the Jewish national heritage such as the Dead Sea Scrolls. Most of these objects are unique and valuable, thus it is important to derive a non-destructive technique of characterization in order to preserve the objects for future generations. We used multivariate analysis techniques based on non-destructive methods for the entire parchment characterization.

This work describes in detail the process of the new complex analytical tool development including the possibilities and limitations of each method described. The first chapter serves as background for all following topics. Firstly, we attempt to describe the parchment manufacturing and deterioration steps. The discussion will then shift to methods used recently for the characterization of ancient parchment. Methods proposed in this study

will be described. Chapter 2 provides detailed descriptions of each applied method as well as results and discussion. Interesting examples of some diagnostic tools used for modern/ancient parchment characterization are also included in this chapter. Finally, the proposed analytical procedure for the entire parchment characterization will conclude the review (Chapter 3).

### 1.1. Parchment definition

Ancient parchment is a product of animal skin. It is used for writing, sometimes on both sides; first on a scroll, and from the second century BC in book form. Currently, in Israel it is used mainly for religious purposes.

Parchment supplanted papyrus as the most popular writing support material in the fourth century, although it was known earlier. Parchment is made of the untanned skins of animals, usually sheep, goats and calves. The term parchment comes from the city of Pergamum (Asia Minor) where an improved method of scraping and preparing leather was developed in the 2nd century BC. Parchment was largely replaced by paper in the sixteenth century (with the rise of printing), but remained in use for certain high-grade bookbinding.



Fig. 1: Deteriorated parchment appearance (page of ancient book, found in Hebrew University Library, Jerusalem).

Conservators/restorers often characterize a parchment based on a visual assessment. Changes in texture, color, and the form of the parchment sample have to be analyzed. At a high degree of deterioration, even a non-expert eye can distinguish transformations in parchment appearance. An example of deteriorated parchment is provided in **Figure 1**. At the same time, more advanced and objective methods of analysis evidently can be of help to obtain a better description of the deterioration stage and to aid in the treatment decision/making process [Larsen]. Therefore, this study is particularly important for the following reasons:

- Restorers need a tool for identification of historical objects;
- It may help in the authentication of original artifacts;
- Environmental risk valuation;
- Patrimonial objects restoration;
- Achievement of suitable preservation.

## 1.2. Parchment manufacturing

Skin is composed of three layers: the outer layer being the epidermis (rich in keratin), the collagen-rich dermis layer and an underlying layer of fat-producing cells (**Figure 2**). The *epidermis* is the thin layer of skin containing melanocytes, which are cells that produce melanin (skin pigment). The *dermis* is the middle layer of the skin. The dermis is held together by a protein called *collagen*, made by fibroblasts. The *subcutis* is the deepest layer of skin. The subcutis, consisting of a net of collagen and fat cells, helps conserve the body's heat and protects the body from injury by acting as a shock absorber.

Parchment is prepared from animal skin by a procedure involving a number of steps [Kennedy et al., Guidelines for the Conservation of Leather and Parchment Bookbinding]. The first step in the process is flaying the skin from the animal mechanically. The second step is drying the skin to avoid degeneration. There are several methods of drying the skin: in air, dry-salting with sodium chloride, wet salting (brining) and liophylization (freeze drying). Ideally the moisture content of the skin would be reduced to approximately 40% at this stage. The next step in parchment preparation is washing in cold running water to remove all blood, dung, dirt and salt. The next stage is liming - soaking in a solution containing lime [ $\text{Ca(OH)}_2$ ]. The major chemical modification the collagen undergoes during liming is the hydrolysis

of some amino groups attached to aspartic and glutamic acid residues (a small portion of arginine residues is converted to ornithine and urea releases). The liming process may be carried out with caustic soda in the case of greasy skins. On drying, calcium carbonate  $[CaCO_3]$  is formed on the parchment surface when the lime residue reacts with the carbon dioxide from the air. The skin is then scraped with knives to remove the hair, fat materials, muscle tissue and the last traces of dirt, grease, pigmentation and lime. The wet skin is dried under tension. As a result, the fibrous collagen network in final parchment is aligned parallel to the surface layer.

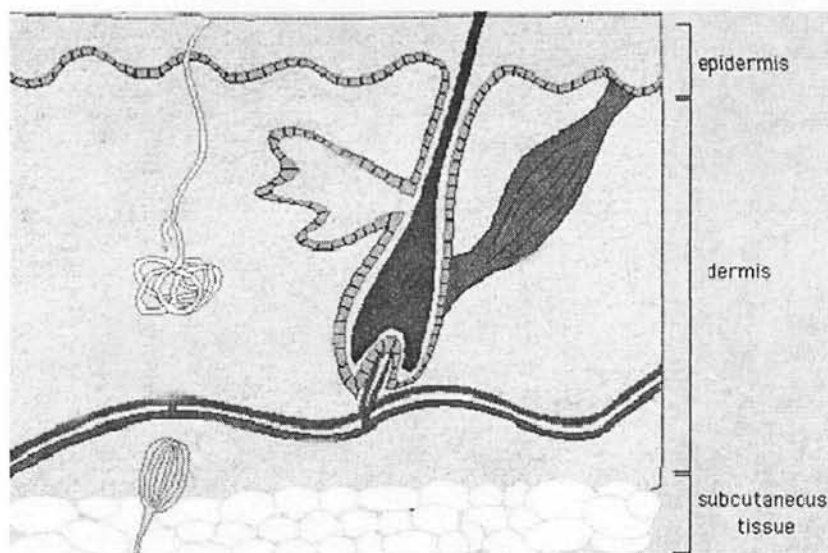


**Fig. 2:** The schematic structure of skin. (adapted from: [www.enchantedlearning.com/subjects/anatomy/skin](http://www.enchantedlearning.com/subjects/anatomy/skin)).

The last stage is finishing – mechanical thinning of parchment, bleaching, dying, scrapping, cleaning the surface and polishing. The term *flesh* side of the parchment refers to the side connected to animal, and the term *grain* side refers to the outer surface of skin. The flesh side is generally whiter and softer than the grain side. The grain side sometimes may carry speckled traces of hair follicles. Finished parchment consists almost exclusively of dermis layer, which is composed of ~95% collagen.

### 1.3. Collagen structure within parchment

The collagens are arguably the dominant proteins of the body [Fessas et al.; Kennedy et al.; Wess et al.]. At least 20 collagen types have been characterized, numbered in a series from collagen I to collagen XIX, the most abundant ones belonging to the fibrillar subfamily. The structure of collagen at different levels of representations can be observed in **Figure 3**.

Collagen fibers are composed of fibrils, which are made up of collagen molecules. Fibers are approximately 50-300  $\mu\text{m}$  in diameter, and are composed of tightly packed collagen fibrils. The collagen fibrils are approximately cylindrical with diameters ranging between 10-500 nm, and in skin mainly from 40-100 nm. This diameter varies with age, collagen type, composition and tissue source. Collagen molecules are approximately 300 nm in length [Kennedy et al.]. The molecular weight is approximately  $3 \times 10^5$  grams per mole, and a mean residue weight (the molecular weight of the polymer divided by the number of monomers, i.e. weight per unit length) of approximately 100 grams per mole [Majewsky, 2001].

Type I collagen is the predominant type being found in skin (relative proportion of about 80-90%), type III collagen at about 8-12% (the percentage is age-dependent) and type V collagen at 5%. The structure unit of all collagen types is formed by three polypeptide chains, called alpha helices, with a repetitive sequence pattern, Gly-X-Y, where X is frequently proline and Y is hydroxyproline. Some collagen types are heterotrimeric, such as type I collagen triplex consisting of two identical  $\alpha_1(\text{I})$  chains and a different one  $\alpha_2(\text{I})$  chain of over 1000 residues in length. Other types are homotrimeric, such as type III collagen,  $[\alpha_1(\text{III})_3]$ . These supramolecular structures are stabilized by cross-linking, that gives the collagen molecules a great deal of stability and strength. The main forces holding the triple helix together are hydrogen bonds within the triple helix, and covalent cross-links between molecules. The thermal stability of such a structure depends on the amino acid composition of the proteins, in particular hydroxyproline, and on the environmental conditions (concentration, pH, ionic strength, denaturing agents, etc.). The inherent nature of the parchment samples is that they contain fibrils in a wide range of orientations since the source material (skin) is a flatwork structure designed to withstand forces in the plane of the tissue.

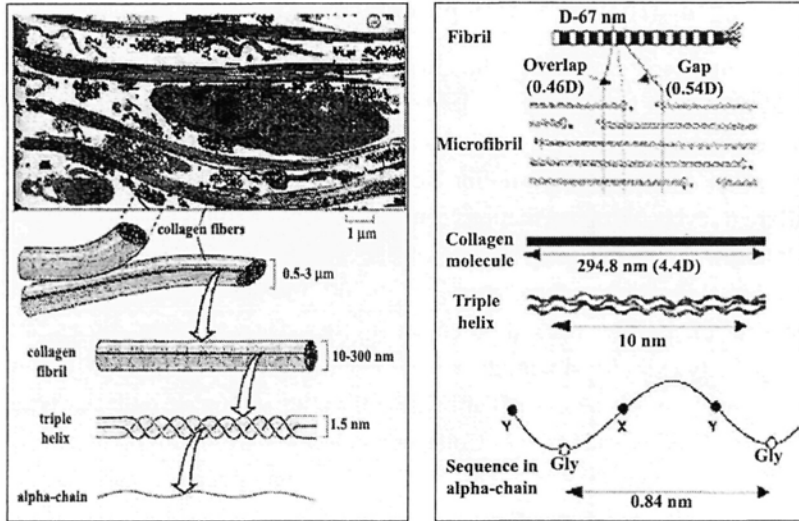


**Fig. 3:** Different levels of collagen structure (adapted from: left picture: [www.faculty.uca.edu](http://www.faculty.uca.edu), right picture: Orgel et al.).

**1.3.1. Collagen primary structure**

Typically, we distinguish between four types of defined protein structure (Figure 4):

- 1) **Primary structure:** linear sequence of amino acids that make up the polypeptide chain. This sequence is determined by the genetic code. A peptide bond is formed between two amino acids by removal of a water molecule.
- 2) **Secondary structure:** refers to the arrangement of amino acids that are close together in a chain forming a local regular pattern of twists or kinks of the polypeptide chain ( $\alpha$ -helix,  $\beta$ -sheet).
- 3) **Tertiary structure:** refers to the arrangement of amino acids that are far apart in the chain, in the folding of the entire molecule secondary structure formed by bending and twisting of the polypeptide chain (three dimensional conformation).
- 4) **Quaternary structure:** refers to the fact that some proteins contain more than one polypeptide chain, adding an additional level of structural organization - the association of the polypeptide chains.

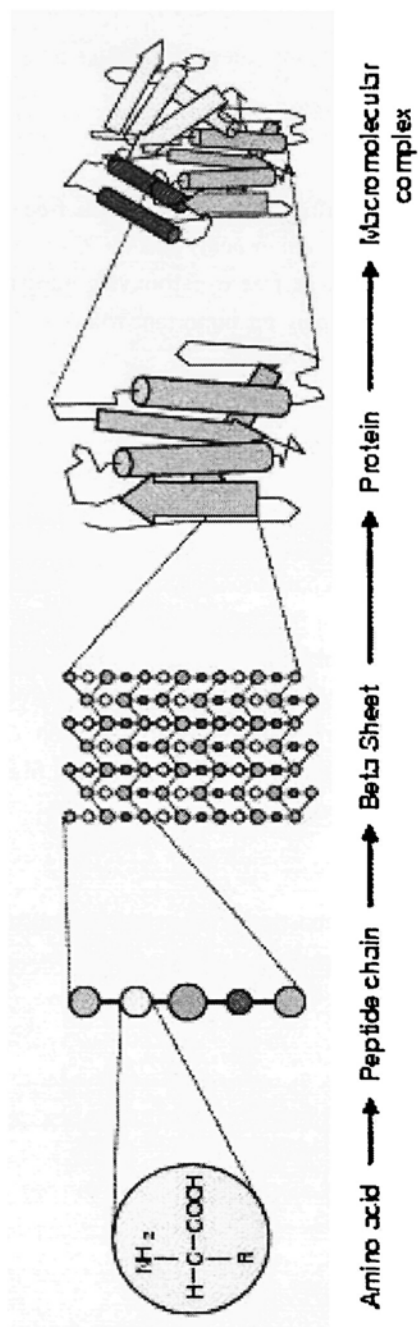


Figure 4. Types of defined protein structure from left to right: amino acid, primary, secondary, tertiary, and quaternary structures. (taken from: <http://www-users.york.ac.uk/~ma1503/common/thesis/c3.html>)

The primary structure of collagen refers to the linear combination of 1000 amino acid residues with a repeating sequence of Gly-Pr-Hyp. The structure of the interchain cross-link is the relatively complex product of a reaction involving lysine and hydroxylysine residues.

Additionally, two terminals at the ends of the polypeptide chain can be defined. The convention for the designation of the order of amino acids is that the N-terminal end (i.e. the end bearing the residue with the free  $\alpha$ -amino group) is to the left (and the number 1 amino acid) and the C-terminal end (i.e. the end with the residue containing a free  $\alpha$ -carboxyl group) is to the right. Terminals are non-helical. They play an important role in microfibril and fibril formation.

### ***1.3.2. Collagen secondary structure***

The ordered array of amino acids in a protein confers regular conformational forms upon that protein. These conformations constitute the secondary structures of a protein. The secondary structure of collagen is a helix in which glycine residues are oriented towards its center. Each of the three chains has a left-handed twist with three residues per turn [Brown]. In general proteins fold into two broad classes of structure, termed *globular proteins* or *fibrous proteins*. Globular proteins are compactly folded and coiled, whereas fibrous proteins are more filamentous or elongated. Collagen is the most abundant fibrous single protein in the body. Collagen fibers are a major portion of tendons and an important constituent of skin.

### ***1.3.3. Collagen tertiary structure***

For collagen, the tertiary structure constitutes the triple helical molecule consists of three polypeptide chains (**Figure 5**):

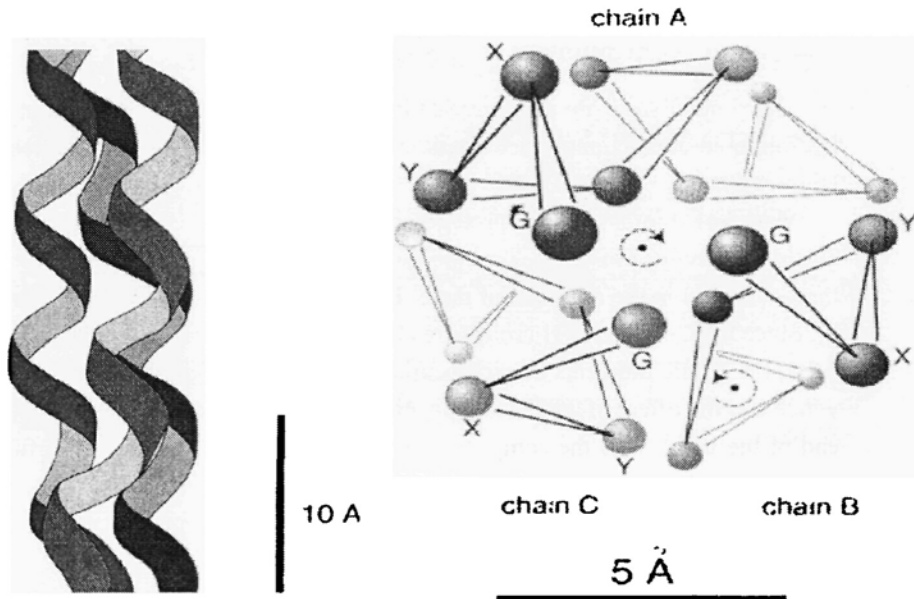


Fig. 5: Collagen tertiary structure (Beck et al.).

Collagen triple-helix has the following geometry:

- Right-handed coil
- 300 nm length
- 2.8 Å helix radius
- 1.5 nm molecular diameter
- 85.5 Å coil pitch

#### 1.3.4. Collagen quaternary structure

Many proteins contain two or more different polypeptide chains that are held in association by the same non-covalent forces that stabilize the tertiary structures of proteins. Proteins with multiple polypeptide chains are termed oligomeric proteins. The structure formed by monomer-monomer interaction in an oligomeric protein is known as quaternary structure. Oligomeric proteins can be composed of multiple identical polypeptide chains or multiple distinct polypeptide chains. To establish a quaternary structure collagen molecules align to form microfibrils, microfibrils align to form collagen fibers.

## 1.4. Factors controlling protein structure

The protein structure is controlled by several forces: hydrogen bonding, hydrophobic interactions, electrostatic interactions and van der Waals forces (Figure 6).

Many of the atoms in proteins carry partial charges due to their electronegativity. This causes a dipole moment over the peptide bond from the C=O bond in the direction of the N-H bond with a value of 3.5D (Figure 7). Since the C=O and N-H groups are aligned by hydrogen bonds in an alpha helix, the dipole moments of each peptide bond tend to align almost linearly, which has the effect of an isolated positive half unit charge at the N-terminal end of the helix, with the compensatory charge separated from it by the full length of the helix.

### 1.4.1. Hydrogen bonding

Polypeptides contain numerous proton donors and acceptors both in their backbone and in the R-groups of the amino acids. The environment in which proteins are found is rich in H-bond donors and acceptors of the water molecule. H-bonding, therefore, occurs not only within and between polypeptide chains but with the surrounding aqueous medium.

When atoms have large partial charges, electrostatic interactions are possible. In the case of hydrogen bonds a hydrogen atom with a large positive partial charge interacts with an atom with a large negative partial charge. The opposite charges attract each other and the hydrogen atom which is covalently bound to the "hydrogen bond" donor atom comes very close to the "hydrogen bond" acceptor atom with its lone pairs. In general the two partial charges are part of dipoles leading the positive hydrogen to be positioned between two negative atoms.

### 1.4.2. Hydrophobic forces

Proteins are composed of amino acids that contain either hydrophilic or hydrophobic R-groups. It is the nature of the interaction of the different R-groups with the aqueous environment that plays the major role in shaping protein structure.

Hydrophobic interactions are the most important non-covalent force that will cause the linear polypeptide to fold into a compact structure. However, it is not the interactions between side chains of hydrophobic amino acids per se (mainly van der Waals) that induce the strong interaction, but the increase in

entropy gained by the removal of hydrophobic surface area from ordered solvating water. The aggregation of the hydrophobic surfaces gives the tightly packed core of a protein. The hydrophobic interactions give a gain of 0.0-2.5 kcal mol<sup>-1</sup> per methylene group by removing approximately one-third of the ordered solvation water on formation of the secondary structure elements. On further folding into a tertiary structure another one-third of the ordered solvation water is lost.

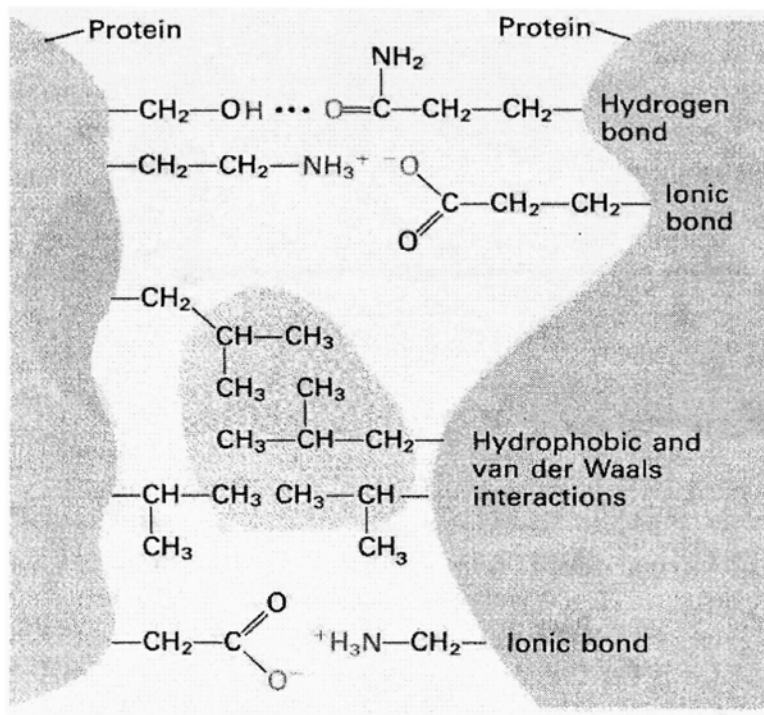


Fig. 6: Factors controlling protein structure.

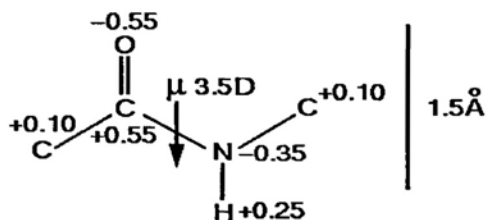


Fig. 7: Dipole moment over the peptide bond.

The hydrophobic interactions will not only be present between the amino acids with hydrophobic side chains, but between all residues depending on their total hydrophobicity. The hydrophobic residues tend to cluster in the core and the hydrophilic residues on the surface.

#### ***1.4.3. Electrostatic forces***

Electrostatic forces are mainly of three types: charge-charge, charge-dipole and dipole-dipole. Typical charge-charge interactions that favor protein folding are those between oppositely charged R-groups. A substantial component of the energy involved in protein folding is charge-dipole interactions. This refers to the interaction of ionized R-groups of amino acids with the dipole of the water molecule. The slight dipole moment that exists in the polar R-groups of amino acids also influences their interaction with water. It is, therefore, understandable that the majority of the amino acids found on the exterior surfaces of globular proteins contain charged or polar R-groups.

#### ***1.4.4. The ion pair***

The strongest electrostatic interactions are present between atoms which have a formal charge. At pH 7 the acidic and basic amino acid residues have side chain groups that are ionized, apart from the polypeptide amino and carboxyl termini. Carboxyl groups have lost a proton and carry charge -1 (which is delocalised over the two oxygen atoms), while amino groups have gained a proton and carry charge +1 (which is delocalised over the three hydrogen atoms). Electrostatic forces can be repulsive or attractive depending on the signs of the interacting charges.

The electrostatic interaction for two point charges in a homogeneous medium can be described by Coulomb's law. Although in principle the electrostatic force between two opposite charges can be relatively large, it is the dielectric constant of the medium which can largely offset this. In water, where the dielectric constant is high ( $\epsilon = 80$ ), the electrostatic interactions are much smaller than in the core of a protein, where  $\epsilon$  varies from 5-40. An ion pair in the core will therefore have considerable energy, and in fact is rarely found in this place. Residues with charged atoms are usually present on the surface of the protein, where there is interaction with water molecules in the solvent.

#### **1.4.5. Van der Waals forces**

There are both attractive and repulsive van der Waals forces that control protein folding. Attractive van der Waals forces involve the interactions among induced dipoles that arise from fluctuations in the charge densities that occur between adjacent uncharged non-bonded atoms. Repulsive van der Waals forces involve the interactions that occur when uncharged non-bonded atoms come very close together but do not induce dipoles. The repulsion is the result of the electron-electron repulsion that occurs as two clouds of electrons begin to overlap.

Although van der Waals forces are extremely weak, relative to other forces governing conformation, it is the huge number of such interactions that occur in large protein molecules that make them significant in the folding of proteins.

### **1.5. Deterioration of collagen in parchment**

The deterioration processes of collagen in parchment can be divided into two categories: the deterioration during the parchment manufacturing process and deterioration that occurs after parchment has been made. According to 'Guidelines for the conservation of leather and parchment bookbinding', the parchment preparation process causes a disorder in the collagen within the parchment; relative to natural collagen, the molecules have more ability to assume different conformations and interact with other molecules in ways that were not previously possible. The reasons for parchment deterioration are often complex, but some of the major factors can be related to a number of reasons. It can be contaminations found in the original materials, traces of chemicals remaining from the production process, chemical reactions between applied decorative materials and their substrates (e.g., pigments and binders applied to manuscripts), the influence of environmental factors: temperature, humidity, atmospheric changes and radiation levels, pollutants and microorganisms [Larsen, Della Gatta].

The deterioration may be divided into two dependent groups: chemical deterioration involves an alteration of the chemical composition of an object and physical deterioration involves any other changes in the object condition. From the moment the parchment was made, the collagen in parchment can deteriorate via a combination of several deterioration mechanisms, including oxidation, hydrolysis and gelatinization of the collagen molecules. All three

degradation paths are irreversible and will be described here based on the work of Kennedy [Kennedy et al.].

#### *Oxidation*

Oxidation is generally caused by free radicals and has an effect on the side chain amino acids by a reduction of the number of basic amino acids and an increase in the number of acidic amino acids. The level of oxidation of collagen can be determined by measuring the ratio of basic to acidic amino acids. In new collagen this ratio is 0.69 and in historic samples is 0.5 [Larsen].

The oxidation of the collagen molecules can occur in the main chain of the collagen molecule. The effect of this is cleavage of the main chain that reduces the stability of the collagen hierarchy.

#### *Hydrolysis*

Here the collagen molecule is cleaved, making smaller polypeptide molecules that disrupt the hierarchical structure of collagen matrices. Hydrolysis can be caused by acids, most commonly from atmospheric pollutants (such as SO<sub>2</sub>, NO<sub>2</sub> and water mixing to form acid).

#### *Denaturation*

Denaturation occurs when the collagen molecules break down to form gelatin. The collagen becomes structurally disorganized and no longer has a triple helical structure, but rather forms a random coil structure followed by the heavily hydrated gel matrix. The transition of collagen to gelatin on heating and in the presence of water through collagen-gelatin intermediate is presented in **Figure 8**. The final product of this conversion, gelatin, is an aqueous colloidal suspension of polypeptide chains and fragments of chains. Gelatin is strongly hydrophilic. In cold water, dried gelatin can absorb up to ten times its weight of water, forming a viscous mass.

### **1.6. Recently used methods for parchment characterization**

The creation of the extensive European research projects “Methods in the Micro-Analysis of Parchment” (MAP) and “Improved Damage Assessment of Parchment” (IDAP, 2002) that involved eight famous research partners in seven European countries highlighted the importance of the ancient

parchment characterization. The work on the projects included a complex of advanced techniques that have been used in the parchment deterioration characterization (visual damage assessment, hydrothermal, thermochemical and thermophysical properties measurements, chemical composition and structural damage evaluation). The results of these investigations were published in book form [Larsen].

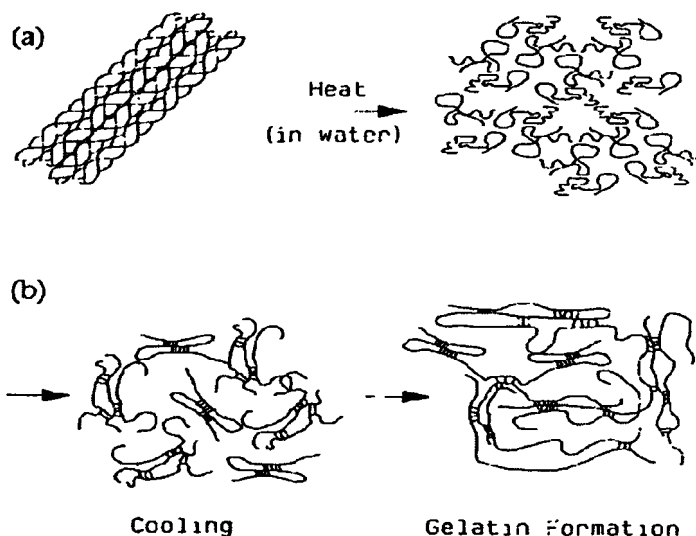


Fig. 8: Transition from the collagen to gelatin - through collagen/gelatin intermediate (taken from: [www.albumen.stanford.edu](http://www.albumen.stanford.edu)).

Moreover, our literature survey shows that the degree of parchment degradation can be assessed by several destructive methods, such as determination of the collagen/gelatin ratio [Weiner et al.], sulfur content [Larsen], thermal analysis of parchment and collagen [Chanine, Della Gatta, Bugrueac et al., Brown et al., Mannucci et al.], examining the racemization of D and L aspartic acid [Weiner et al.], small angle X-ray scattering [Larsen; Wess et al, 2001], IR spectra [Mannucci et al.] and FT-IR [Derrick]. Some investigations allow for identification of pigments, binding media and traces of preparing material, such as calcium carbonate [Edwards et al., 2001; Vandenabeele et al.].

The non-destructive characterization of archeological material has been recently demonstrated successfully using FT-Raman spectroscopy [Edwards et al, 2001]. The differences between modern and deteriorated parchments

can be seen in the “fingerprint region”, 900-1800  $\text{cm}^{-1}$ . The deterioration causes changes in characteristic amide I band near 1650  $\text{cm}^{-1}$  (reduction in intensity, broadening).

Brillouin scattering was applied for the characterization of the elastic and viscoelastic properties of intact, damaged and restored parchment [Mannucci et al.] by means of the intermediate scale between the molecular level (probed by Raman) and the microscopic level (probed by acoustic microscopy).

$^{13}\text{C}$  and  $^{15}\text{N}$  solid state NMR techniques were used to measure the historical samples [Odlyha et al., Larsen]. Scanning electron microscopy and transmission electron microscopy were applied to the parchment samples to evaluate morphological differences between the modern and historical samples [Della Gatta, Larsen, Kautek et al, 2003]. The above mentioned common methods usually provide only a few specific parameters and have serious disadvantages. As a result, until now, the monitoring of parchment parameters in real-time was impossible.

#### ***1.6.1. Disadvantages of the common methods***

All the methods mentioned above have a number of disadvantages:

- Most methods allow for estimation of one parameter only.
- None of the analytical techniques is likely to deliver the data sufficient for describing a parchment as an entire object.
- Most of the current methods are destructive and/or invasive.
- General-purpose instruments can handle limited sample size and shape.
- In many cases, the current methods are time and/or labor and/or money consuming.
- Usually, remote inspection is not possible or is difficult.

Due to these disadvantages of the currently available methods for parchment characterization, the development of fast, simple, objective and non-destructive methods is of considerable importance.

## **2. RESULTS AND DISCUSSION**

### **2.1. Parchment samples set**

A representative set of 54 real parchment samples (37 modern and 17 historical), produced from different animal skins and found at different stages

of deterioration, was assembled (Table 1). In archeological science, such a set is considered large enough, since historical samples are rare. A representative picture of the parchment samples set is shown in Figure 9.

**Table 1**  
Samples used in this study.

Sample number	Type of skin the parchment made of
1-5	modern, unknown
6-13	historical, unknown
14	historical, unknown, with painting residues
15-20	historical, unknown
21	historical, 16 century, unknown, written
22-34	modern, unknown
35-36	modern, goat
37	modern, sheep
38-42	modern, calf
43-44	modern, goat
45-47	modern, calf
48	modern, goat
49-51	modern, sheep
52-53	modern, unknown
54	historical, unknown, 2000 years old

Different physical parameters were measured for all parchment samples: thickness, water content, pH and color (using RCB imaging, for details see section 2.5 "Parchment characterization by visible imaging"). Thickness of the modern and the historical parchment samples is plotted in Figure 10. The historical samples are regularly thicker than the modern ones whilst at the same time they are less homogeneous in thickness distribution.

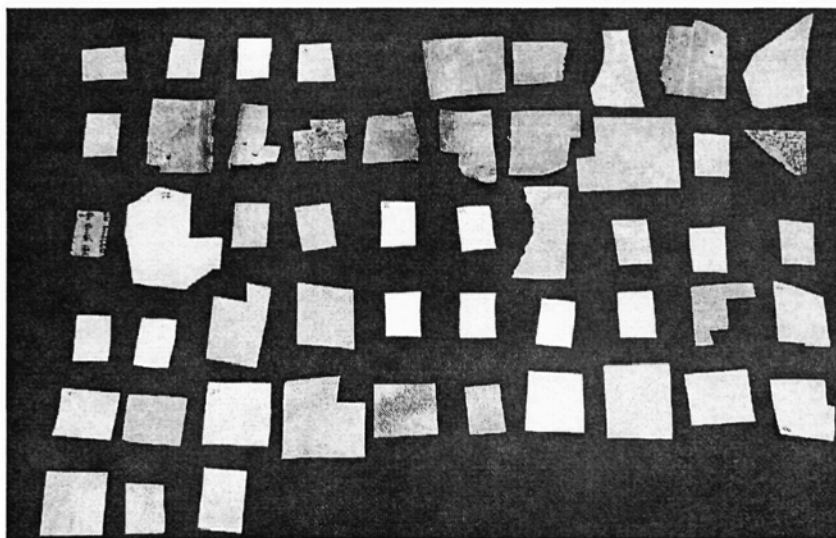


Fig. 9: Parchment samples set.

The box plot of the water content of modern and historical parchment samples is presented in **Figure 11**. The water content of the historical samples is nearly the same as that of the modern ones with a much wider distribution of the latter. The detailed discussion concerning water content is provided in the NIR chapter (2.11.4.2).

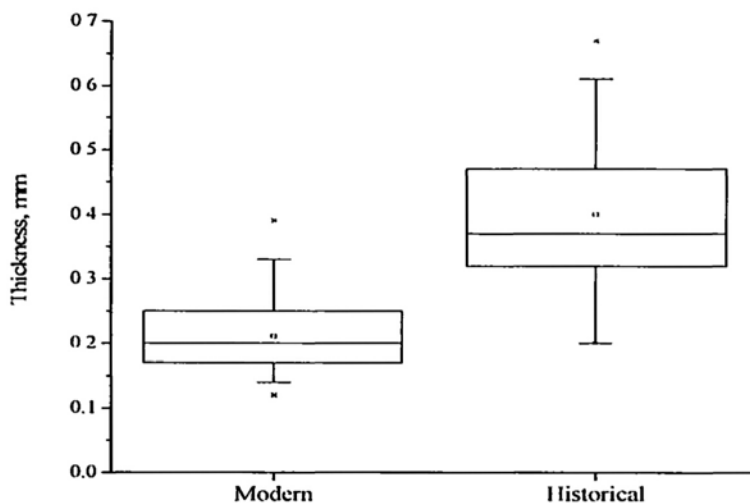


Fig. 10: Mean thickness of modern and historical parchment samples.

The box plot of the pH value of modern and historical parchment samples is presented in Figure 12. The pH was measured in solution prepared as follows: Around 25mg of parchment sample was cut into small fragments and extracted shaking at room temperature with 5 ml double distilled (18 M $\Omega$ /cm resistance) water for 24 hours. After extraction, samples were filtered through a 0.45  $\mu$ m membrane based filter. The pH mean value of historical samples is lower than that of the modern ones.

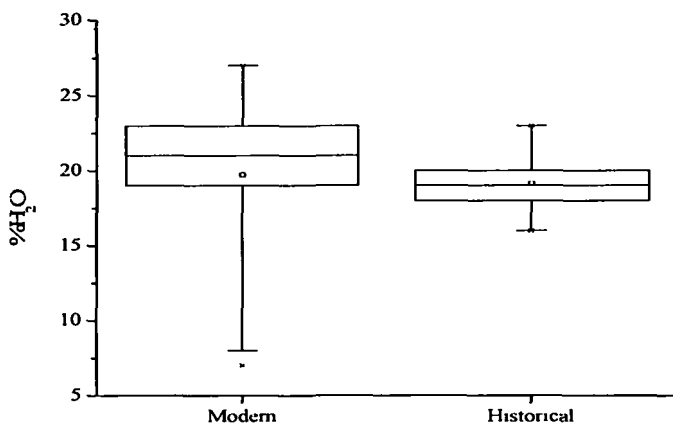


Fig. 11: Water content in modern and historical parchment samples.

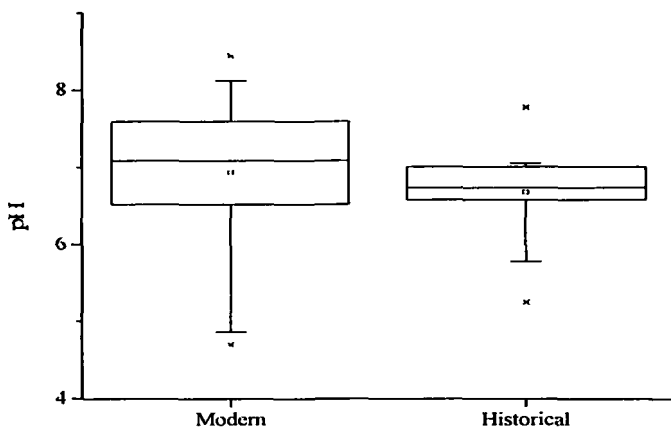


Fig. 12: The pH value of modern and historical parchment samples.

## 2.2. Methodology of parchment characterization

The main goal of the study was to characterize a given parchment sample by means of the complex analytical method. Hence, a methodology had to be developed which should be based on the measurable objective differences between the modern parchment and the historical ones. The right estimation of the correlation between the parchment deterioration stage and the factors involved may only be obtained (in proper time scale) by artificial aging of modern parchments that was carried out in order to induce deterioration under well-defined controlled conditions [Della Gatta]. The above considerations led to the following proposed strategy (**Figure 13**):

### 2.2.1. Artificial aging procedure

For the initial feasibility study of the artificial aging process on modern parchment three different parameters (UV irradiation at 254 nm, exposure to elevated temperatures and moisture treatment for various periods of time) were checked. Each parchment sample was cut into small fragments (~2×1.5 cm) and the fragments were divided into groups according to the treatment to be applied. The samples were artificially aged according to the following schemes:

- 1) *Temperature aging treatment*: samples were heated in an oven at 105-110°C for 11 days. At the end of the treatment samples were maintained in a desiccator at room temperature for at least 12 hours for equilibration before measurements were taken.
- 2) *Moisture aging treatment*: samples were maintained in a humid atmosphere for 10 days. At the end of the treatment samples were maintained in desiccator for 12 hours at room temperature and then air dried.
- 3) *UV aging treatment*: samples were illuminated using standard UV-lamp (254 nm) for 10 days. The distance between the lamp and the samples was around 10 cm. The irradiation was applied to both sides of the sample.

## **METHODOLOGY OF PARCHMENT CHARACTERIZATION**

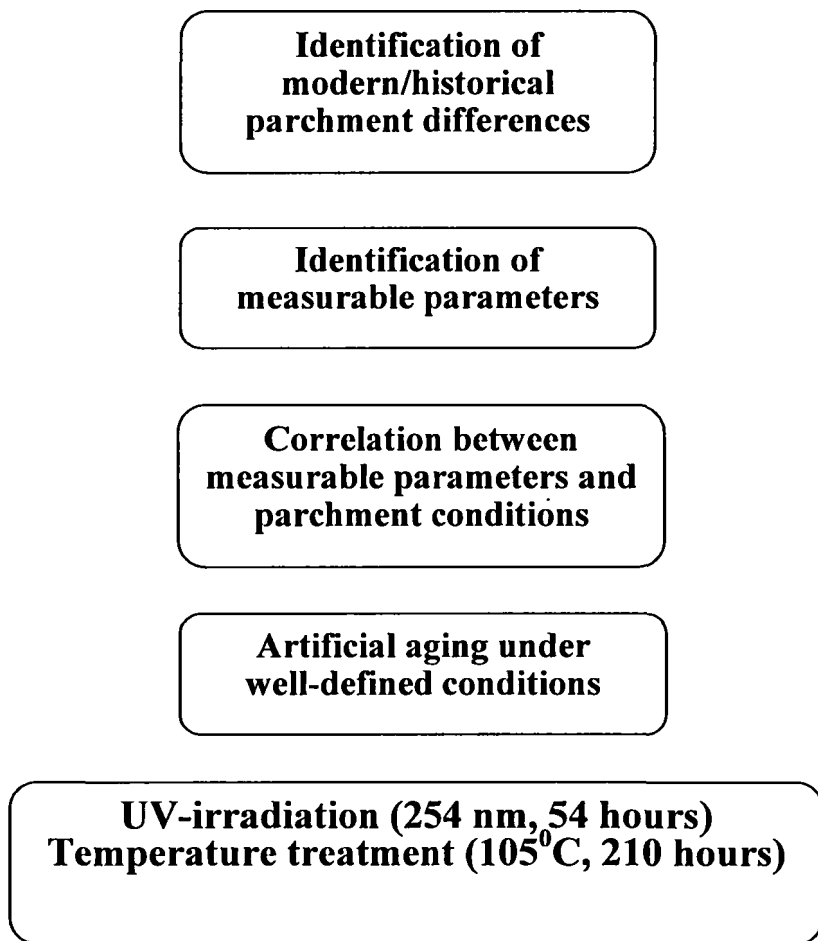


**Figure 13.** Methodology of parchment characterization.

### 2.2.2. Artificial aging observation

The detailed changes that occurred in four modern parchment samples during the appropriate treatment were observed using scanning electron microscopy technique (SEM) (Hitachi S-4000, Hitachi Inc, Japan). Modern and aged parchment samples (numbers 1-4) were examined using scanning electron microscopy. Microphotographs of the parchment surfaces were taken at three magnifications: 200  $\mu\text{m}$ , 50  $\mu\text{m}$ , and 10  $\mu\text{m}$ . The most representative results of the examination of two samples under different treatments are presented in **Figures 14-15** (the reason for choosing these specific samples is their very different thicknesses: sample number 1 is relatively thick for the modern sample – 310  $\mu\text{m}$  thickness, and sample number 4 is regular for the modern samples thickness – 170  $\mu\text{m}$ ). In the modern samples, collagen fibers are the main building block of the parchment. Depending on the portion of fibers in the sample, it can be more or less dense. As evident from the SEM images, in all the treatments the considerable structural changes occurred.

“The modern parchment displays a network of integral collagen fibers with clear contours and sharp edges. Aging causes a progressively deteriorated surface morphology, random shrinkage of fibers, formation of melt-like zones, loss of fiber network and appearance of the deep cracks, fragmentation of fibers, swelling and glass-like cross-fissuring surfaces” [Della Gatta].

### 2.2.3. Artificial aging results

The main goal of the previously described artificial aging procedure, that included three different treatments (temperature, moisture and irradiation), was to find such a combination of treatments to ensure a sufficiently high degree of deterioration. Since the largest deterioration effects in a feasibility study were found from UV irradiation and temperature, the study focused on these factors. The degree of deterioration should ideally be defined by two known “deterioration cases”. The deterioration assessed in artificially aged samples should be comparable with that in historical samples. At the same time, modern samples should be included in the deterioration range to obtain an appropriate “deterioration scale”. Therefore, the optimization of involved parameters at each specific treatment level is needed. It should be emphasized that the main goal of the artificial aging was not to provide aging, but to assess the deterioration. Therefore, the precise age of the historical samples is not relevant (and, usually, it is not known). We

correlated the observations to the conditions of artificially deteriorated samples and we added the historical samples to the set in order to show that they exhibit similar characteristics.

To develop a well defined artificial aging procedure an additional series of four modern parchment samples produced from different animals (number 35-38) was used. Firstly, the detailed study of UV irradiation effect was carried out. Samples were exposed to stepwise UV radiation (254 nm) in a specialized photochemical reactor (Rayonet, The South NE Ultraviolet CO, Connecticut, USA). They were placed in the center of the ventilated reactor, at a working distance of 12 cm from 9 mercury lamps (30W each). The radiation power was  $6\text{mW}/\text{cm}^2$ . The exposure times and the irradiation doses were comparable with data from previous available studies (for detailed description see section 2.4.3).

The irradiated samples were then treated by heating to  $105^\circ\text{C}$  in an oven, for up to 210 hours. The irradiation and heating time were sufficient to provide the maximum wanted change per each parameter checked. Final parchment samples were equilibrated at room temperature in air for at least 24 hours before analysis. As a result, a final artificial aging procedure was developed. It included two steps:

1. Irradiation at 254 nm for 54 hours.
2. Heating of the irradiated samples in an oven at  $105^\circ\text{C}$  for 210 hours.

All modern parchment samples were aged according to optimized aging procedure. The above procedure has been commonly applied for mimicking parchment deterioration [Chahine, Della Gatta et al.]. For example, the artificial aging of parchment, using visible light irradiation for 32 hours with dry heating in an oven at  $100^\circ\text{C}$  for 16 days, has been reported recently [Della Gatta et al.]. They found that samples subjected to such a treatment were heavily deteriorated and the damage affords only a partial explanation of the complex deterioration displayed in the old parchments. Miles has suggested that exposure of collagen to UV light cleaves the molecule at random points [Miles et al.].

The visual appearance of artificially aged parchment samples changes (Figure 16). Usually, the modification can be observed by the naked eye. Samples appear “tanned” like the skin under sun radiation. The degree of “tanning” for each sample is different and depends on the initial sample color and surface homogeneity. These differences can be used for parchment distinction (see chapter 2.5).

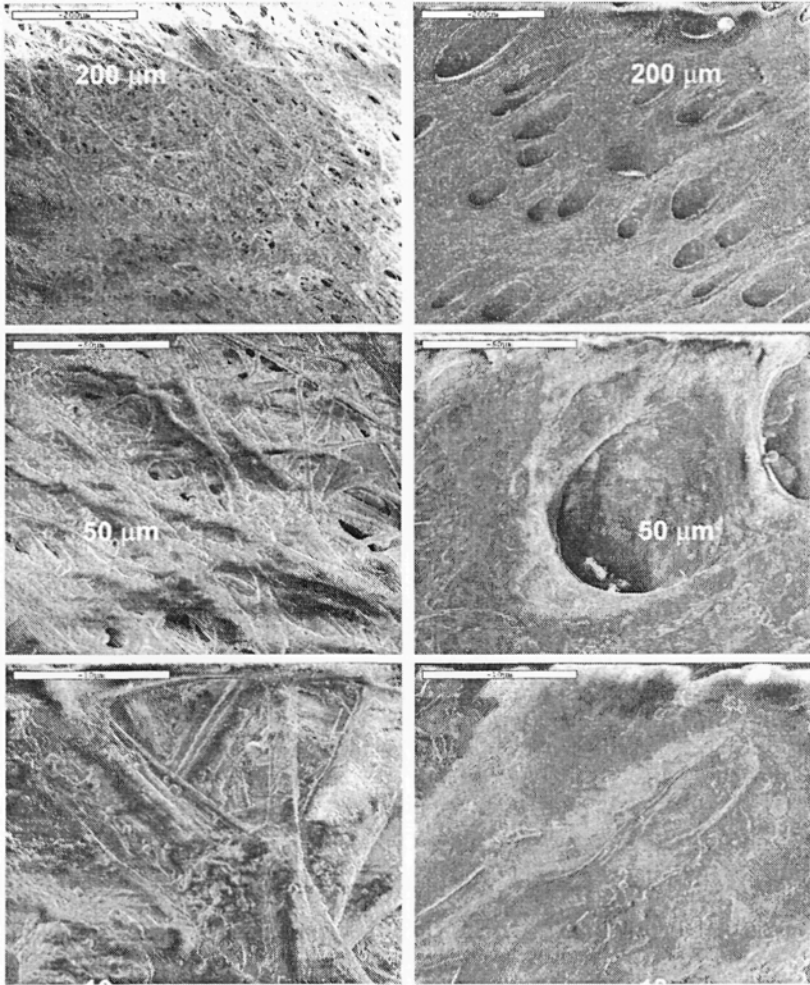


**Fig. 14;** SEM of thick modern sample before (left) and after irradiation (right).

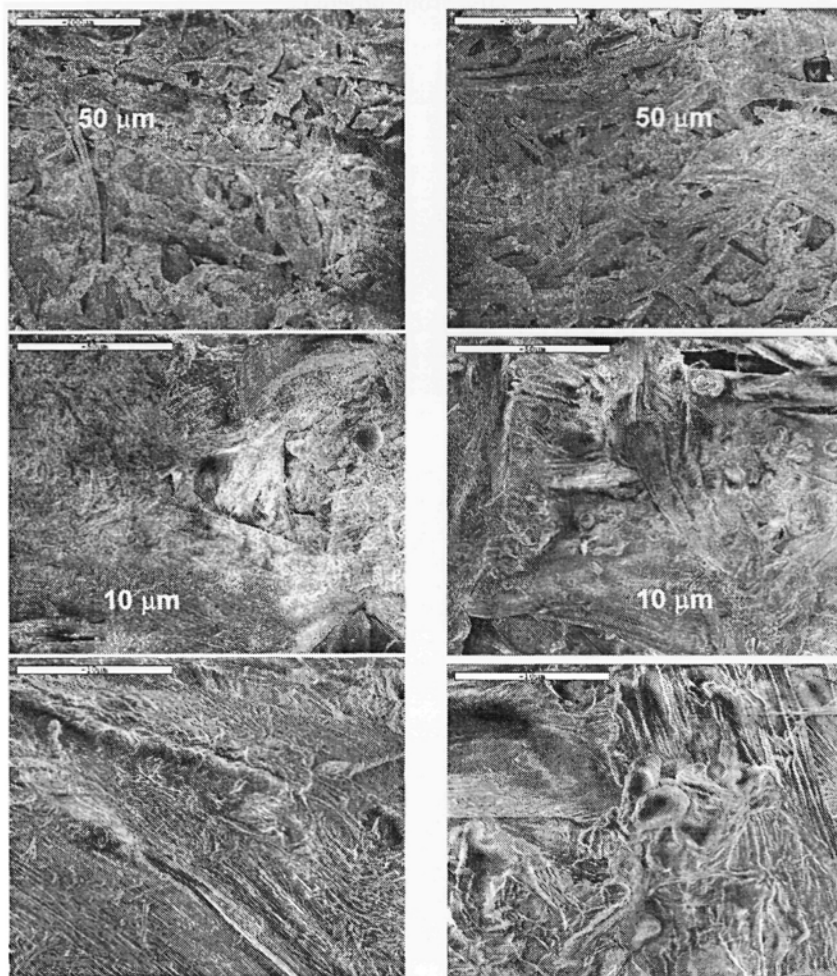


**Fig. 14 (continued):** SEM of thick modern sample after temperature treatment (left) and after moisture treatment (right).

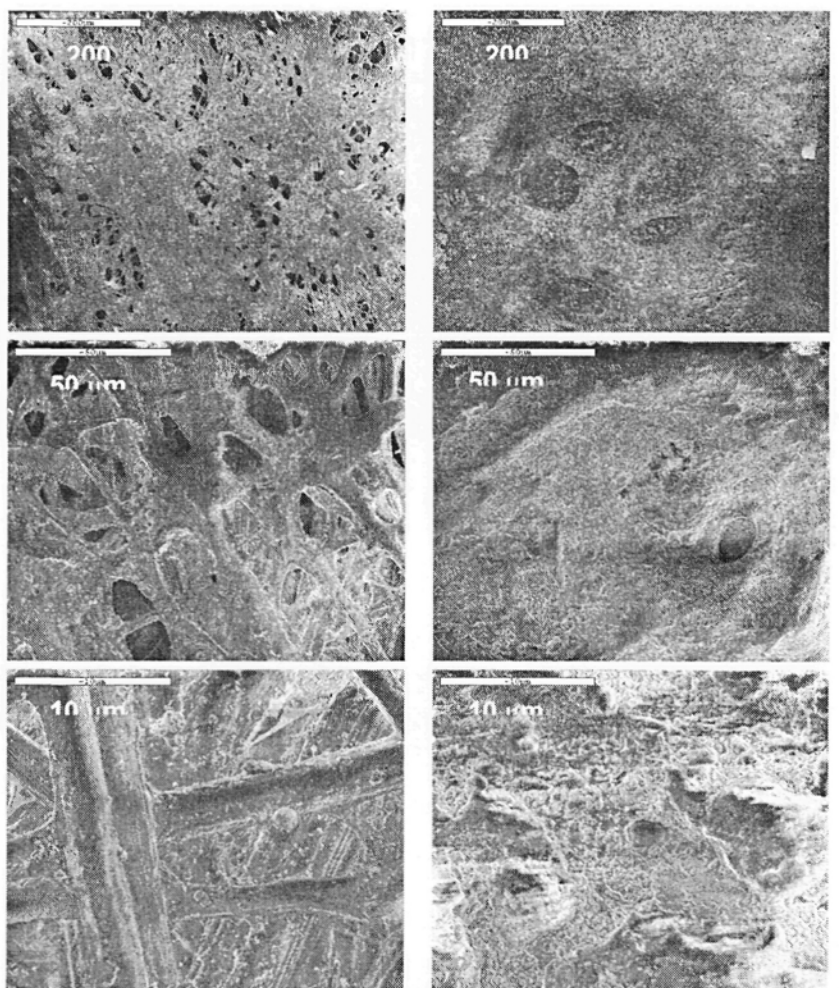


**Fig. 15:** SEM of thin modern sample before (left) and after irradiation (right).

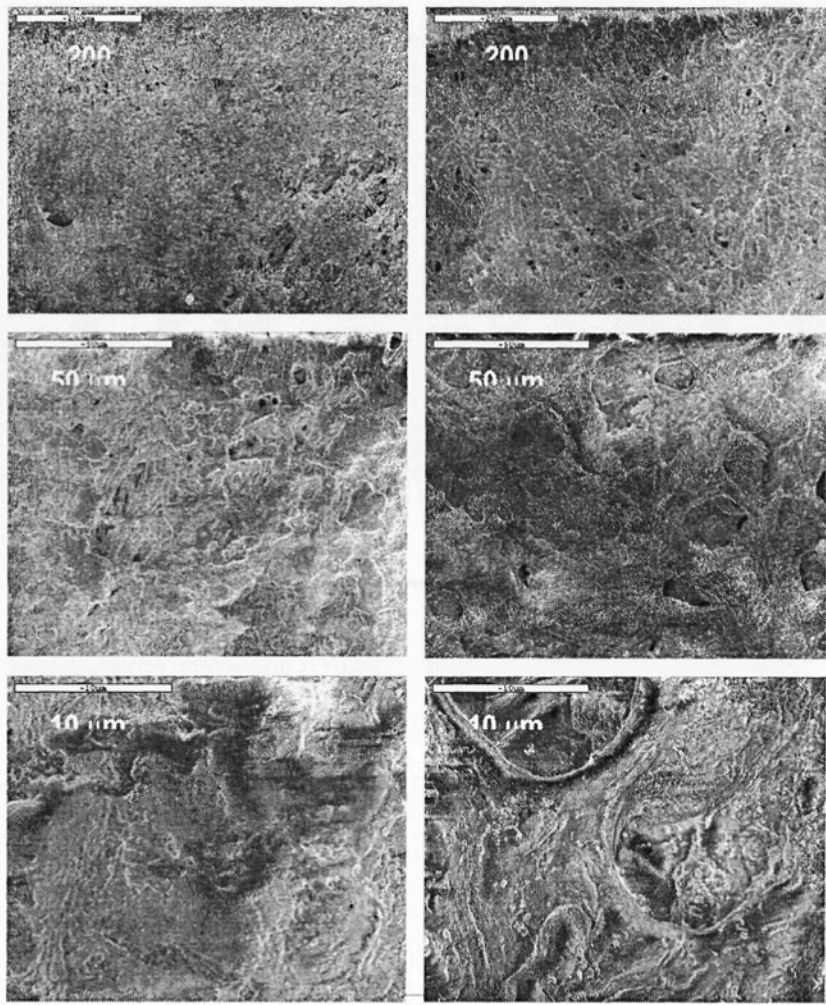


**Fig. 15 (continued).** SEM of thin modern sample after temperature treatment (left) and after moisture treatment (right).

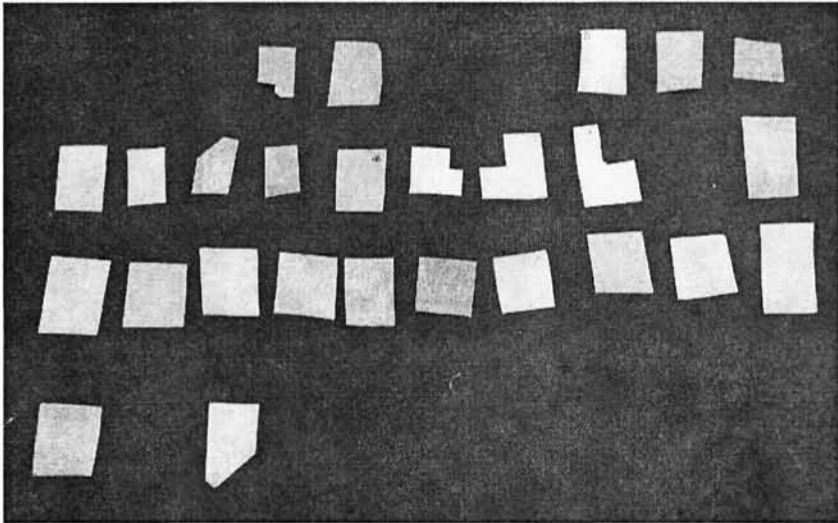


**Fig. 16:** Parchment samples' appearance after artificial aging process.

Changes in the surface structure after treatment were observed using optical microscopy (**Figure 17**). The initial sample has a hierarchical fibril structure of the surface. After the treatment the structure was completely destroyed. This analysis can serve as a non-destructive tool for rapid detection of surface morphological changes during the artificially ageing process and for investigation of historical samples.

To characterize more detailed changes in the degree of deterioration after a complete cycle of the artificial ageing, modern and aged parchments used in two artificial aging cycles (number 1-4 and 35-38) were examined using scanning electron microscopy (SEM) (Hitachi S-4000, Hitachi Inc, Japan) from both sides. Microphotographs of the parchment surfaces were taken at three scales: 200  $\mu\text{m}$ , 50  $\mu\text{m}$ , and 10  $\mu\text{m}$  (**Figure 18**). The samples examined covered a wide range of surface types, thicknesses and animal skin types.

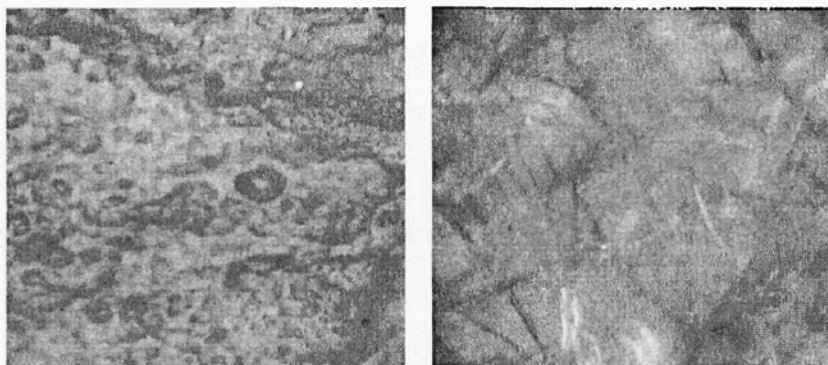


**Fig. 17:** Changes in structure of modern parchment surface (left) after aging treatment (right) obtained by optical microscopy at  $\times 200$  magnification.

SEM observations support the hypothesis that the aging process is related to destruction of the ordered internal parchment architecture. Our results are in agreement with a previous report [Della Gatta et al.], where a comparison of modern and artificially aged parchments showed the formation of crater-like spots, loss of fiber network and the appearance of cracks. It has also been found that the surface morphology of historical parchments is more varied than that of artificially aged samples. It has been concluded that the combination of SEM and another technique that measures bulk properties can be successfully applied for deterioration assessment.

### **2.2.3. Gentle artificial aging**

We also decided to examine much more gentle artificial aging treatment: irradiation at 360 nm (instead of 254 nm) for 16 hours followed by heating in an oven at 105°C for 10 hours. As a result, the influence of the gentle artificial aging process on the synchronous fluorescence properties was checked (see chapter 2.4.5).

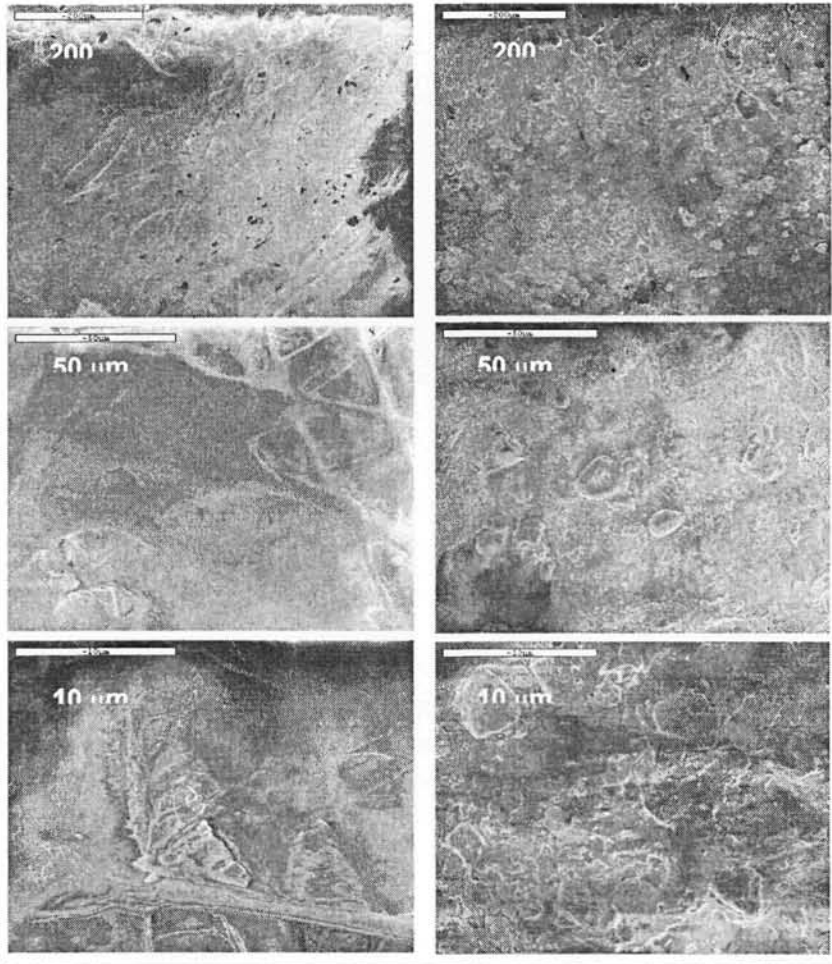


**Fig. 18:** SEM micrographs of modern (left) and aged (UV irradiation plus heating) parchment (right). The flesh side is shown, at various magnifications.

### 2.3. Methods used in the study

It was mentioned by Larsen [Larsen], that the chance of successful correlation of the physical and chemical parameters to the parchment deterioration stage is low, because the number of the historical samples acting upon the correlation is objectively small, or the number of parameters

needed to obtain significance is large. A successful outcome depends on the amount of the data available for model building and subsequent correlation analysis. It is important to apply many different techniques to a large number of samples in different stages of deterioration to get the representative parameters for the description of damage. In his opinion, the only effective way to succeed is to build a communicative network of conservators/restorers and scientists and a central database of all data available (as international database and standard parameters).

As was mentioned by Wouters, "Damage assessment involving sampling of historical objects may be performed following two approaches: simple test or sophisticated analysis. The simple tests require a low input of resources, but the risk of failure is high. This is mainly because there should be a firmly established correlation between the test procedure, its output and the real damage. The information obtained from the sophisticated analysis is more detailed and the risk of failure is low. The fact that the conservation/restoration and scientific analysis are two completely different fields is not a new notion. However, it would be wrong for people having to take active care of our cultural heritage to avoid "heavy" scientific approaches for problem solving purposes, or to prefer to replace them with a "simple" test. The goal is to produce a damage assessment that is mutually clear and understandable".

Methods used in the study can be divided into two main groups: non-destructive (or semi-destructive) and destructive methods (Table 2). The destructive methods are helpful in general parchment characterization and are used on a routine basis by the restorers/conservators. Additionally they have to be used to build the chemometrical model (as input parameters). The destructive methods may be implemented in other applications of archeological objects analysis. The non-destructive methods should supply an alternative to the regularly used destructive ones for the assessment of the measurable parameters and will be used in the model as output parameters for fast parchment characterization.

Several destructive and non-destructive methods were successfully applied in the present study for the first time to parchment samples characterization. These include: synchronous fluorescence, laser induced breakdown spectroscopy, near infrared analysis, visible reflectance spectroscopy, volt-ampere characterization, conductivity, evaluation of nitrogen content.

**Table 2**  
Methods used in the study.

Non-destructive methods	Destructive methods
Fluorescence	Inductively coupled plasma
Digital color imaging	Nitrogen content evaluation (Kjeldahl)
Optical microscopy	Water content evaluation
Laser induced breakdown spectroscopy	Electrophoresis
Near infra red analysis	Ion chromatography
Volt-ampere characteristics	Conductivity
Visible reflectance spectroscopy	pH
Multivariate analysis	Electron spin resonance
Raman	Scanning electron microscopy

#### 2.4. Fluorescence spectroscopy

Very little is known about the quantitative interaction of UV light with the solid collagen in parchment matrices. However, the photochemistry of pure collagen has been recently studied. For example, photodegradation of solid collagen type I in the ground (powder) form, caused by exposure to 254 nm UV radiation was studied [Kaminska et al., 1996, *Polymer Degradation and Stability*, 51: 15-18]. The degradation of collagen in polymer films, as well as in solution, was also studied recently [Sionkowska, 2001; Sionkowska et al., 2004; Sionkowska, 2000, *Polymer Degradation and Stability*, 68; Sionkowska, 2000, *Polymer Degradation and Stability*, 67; Sionkowska et al., 1999, Torikai et al.]. The degree of degradation depends on the presence of oxygen, the pH of solution and on UV irradiation wavelengths [Miles et al.]. These studies showed that tyrosine and phenylalanine are involved in the photochemical destruction of the collagen molecule. It has also been shown that collagen macromolecules undergo photopolymerization, under UV irradiation [Fujimori].

Fluorescence spectroscopy and its multiple applications to protein analysis are very useful in the probing of the structural features of proteins [Meyers]. The exceptional sensitivity allows routine detection of fluorescence substances on a subnanomolar scale. Fluorescence is suitable for use in

parchment characterization because of its sensitivity to small changes in the fluorophores concentration or in the local environment. As a routine procedure for assessment of parchment deterioration stage online, it is fast and simple. The main goal of this part of the study was to develop a non-destructive and non-invasive method based on fluorescence for quantitative parchment characterization and sensitive indication of its deterioration stage. For this purpose, the regular fluorescence as well as synchronous fluorescence measurements were applied. The categorization of parchment samples into groups (modern, historical and artificially aged) based on fluorescence was performed.

#### **2.4.1. Regular qualitative fluorescence measurements**

A qualitative observation of the fluorescence color using excitation in UV region was proposed as a routine analysis to inspect any alteration in the parchment preservation stage [Conserve O' Grams]. Changes in color of emitted fluorescence after the artificial aging process can be observed on parchment samples using excitation at 360 nm (high pressure mercury lamp combined with dichroic filter). The intact sample has a deep blue fluorescence. The fluorescence obtained from the artificial aged sample had a much weaker green color. The change in the fluorescence color can be observed by the naked eye, as illustrated in **Figure 19**. This resembles the inherent fluorescence of mammalian tissues, attributed to endogenous fluorophores [Gavriusinas et al.]. As a result, the color of observed fluorescence can be used as a simple primary analysis of the parchment deterioration stage. The detailed discussion on the matter of changes observed will be presented in the following sections.

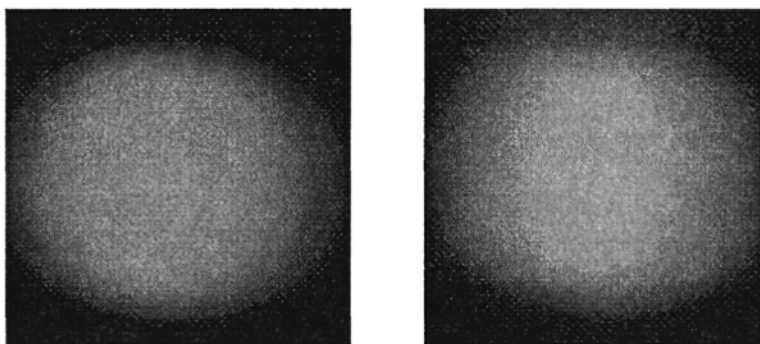


**Fig. 19:** Fluorescence of parchment sample before (left) and after (right) artificial aging under 360 nm excitation.

## 2.4.2. Regular quantitative fluorescence measurements

### 2.4.2.1. Experimental setup

The fluorescence spectra of all parchment samples were acquired from both sides (*grain* and *flesh*), using a luminescent spectrometer (Aminco Bowman Series 2, SLM-Aminco, IL, USA) equipped with a surface analysis accessory. The excitation wavelengths were 243 nm and 298 nm. The excitation and emission bandwidths were 4 nm. The angle between the excitation beam and the sample surface was  $74^{\circ}$ . This geometry results in the minimum background intensity due to specular reflection and other scattered excitation light. All spectra were recorded at room temperature.

### 2.4.2.2. Results

Firstly, the effect of aging on the fluorescence spectrum has been studied. The correlation between a parchment's condition and its fluorescence intensity was examined. For the feasibility study, three different parameters (UV irradiation at 254 nm, exposure to elevated temperatures and high humidity for various times) were checked, performing artificial aging of new parchment (for detailed procedure see section 2.2). The irradiation and temperature treatments initiated the major changes (**Figure 20**); therefore, they were taken as preferable for the final artificial aging procedure.

The fluorescence spectra of modern parchment samples are characterized by a strong and wide emission in the 260-570 nm spectral region. At least two chromophores can be found in this region. The first (chromophore-I), emits fluorescence at about 400 nm, when excited at 298 nm. The second (chromophore-II), emits at about 300 nm, when excited at 243 nm. The fluorescence measurements were performed for both types of chromophores in all parchment samples. Obviously, each sample has its own fluorescence spectrum. Moreover, each sample's side possesses specific features. However, in most cases, the differences between the samples are in the fluorescence intensity and not in the spectra shape or the main peak position. In order to perform statistical analysis and to highlight the differences, we have to compare "typical spectra" for each group of samples. For clustering the samples into groups, we have to find the characteristic peaks by their position, shape and relative intensity and to compare the tendency (increasing/decreasing of the signal). Typical fluorescence spectra of both types of chromophores are shown in **Figure 21**.

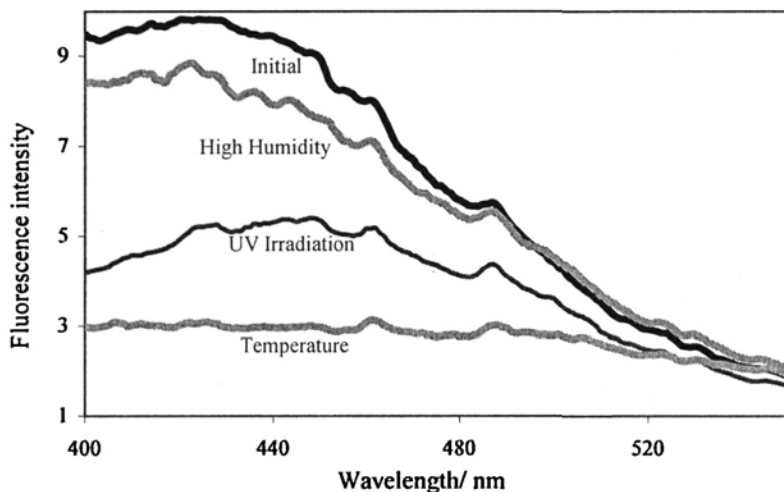


**Fig. 20:** Influence of different aging treatments on fluorescence intensity (excitation at 298 nm).

**Chromophore I:** The fluorescence spectrum of chromophore I is identical to the previously published characteristic fluorescence spectrum from type I collagen [Theodossiou et al, 2001; Theodossiou et al, 2002]. Distinct fluorescence changes were observed after UV irradiation (254 nm) of parchment samples as a first step of the artificial aging. Generally, an overall decrease in the fluorescence intensity occurred. The decay of fluorescence intensity with increasing in irradiation time is similar to the results obtained for collagen solution [Sionkowska et al., 1999; Menter et al., 1995]. The stepwise changes in the fluorescence spectra of parchment samples are shown in **Figure 22**. In this figure, the fluorescence scale has been justified, such that the spectral features can be observed in spite of the large decay of the fluorescence intensity. The data corresponding to both sides of the parchment sample are shown. The modern samples have a strong fluorescence. After UV irradiation for 35 hours the maximum change in the fluorescence intensity was achieved, but the surface appearance of some samples was not homogeneous. We decided to provide some more irradiation and after 54 hours the appearance of all samples was homogeneous.

The exposure time and irradiation dose applied to parchment samples are

presented in **Table 3**. The irradiation dose used in this study is compared to the previously examined results. The next step in the artificial aging process was heating in the oven at 105°C for 210 hours (as described in section 2.2).

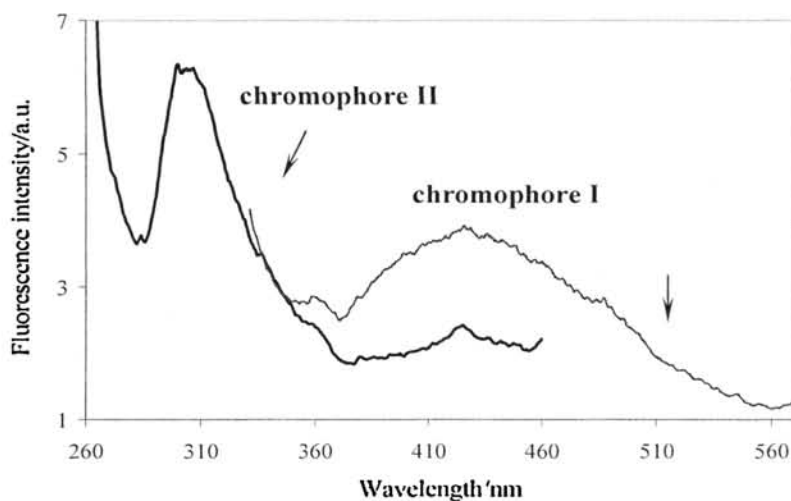


**Fig. 21:** Typical spectra of parchment chromophores.

Our detailed observations are summarized thus:

- (a) When chromophore - I is concerned, the emission peak at 400 nm decreases as a result of photochemical reactions, until it practically disappears after several hours of irradiation. This finding is in agreement with previous measurements, indicating that the integral absorbance of the collagen bands, probed by IR spectroscopy, decreased under UV irradiation [Kaminska et al., 1996]. Additionally, the progressive reduction of collagen up to 10% of its maximum value was reported after 2 hours of collagen solution irradiation [Miles et al.].
- (b) While the peak at 400 nm decreases, a new broadband peak at 450 nm emerges. The new peak clearly appears after 2 hours of irradiation. The appearance of the new intermediate state (about 60% after 1 hour irradiation) in the degradation of collagen solution to the random coils by UV irradiation was previously reported [Miles et al.]. Additionally, the shift of the absorption maximum to longer wavelengths with the increase in the irradiation time of the collagen film was reported (irradiation range  $\lambda \geq 250$  nm, irradiation time 4 hours) [Torikai et al.].
- (c) The exposure of the irradiated parchment to high temperature did not

further change the intensity of the fluorescence, but the peak was red shifted to 480 nm. This fact can be supported by the previously reported fact that there was no significant increase in absorbance of collagen solutions once the sample was denatured [Majewski et al.].

- (d) Both the peak position and intensity do not change any more after irradiating over 54 hours or heating over 210 hours.

**Table 3**

Exposure time and irradiation dose applied on parchment samples.

Exposure time	Irradiation dose, J/m <sup>2</sup>
0 min	0
30 min	$1.1 \times 10^5$
60 min	$2.2 \times 10^5$
2 hours	$4.3 \times 10^5$
3 hours	$6.5 \times 10^5$
5 hours	$1.1 \times 10^6$
7 hours	$1.5 \times 10^6$
35 hours	$7.6 \times 10^6$
54 hours	$1.2 \times 10^7$
Total irradiation dose (this study), on semi-solid matrix of collagen	$1.2 \times 10^7$
Total irradiation dose (Sionkowska, 2001) for exposure time of 5 min - 6 hours, on type I collagen solution	$1.3 \times 10^4 - 9 \times 10^5$
Total irradiation dose (Menter et al.) for exposure time of 1 hour, on collagen film	$2.6 \times 10^5$

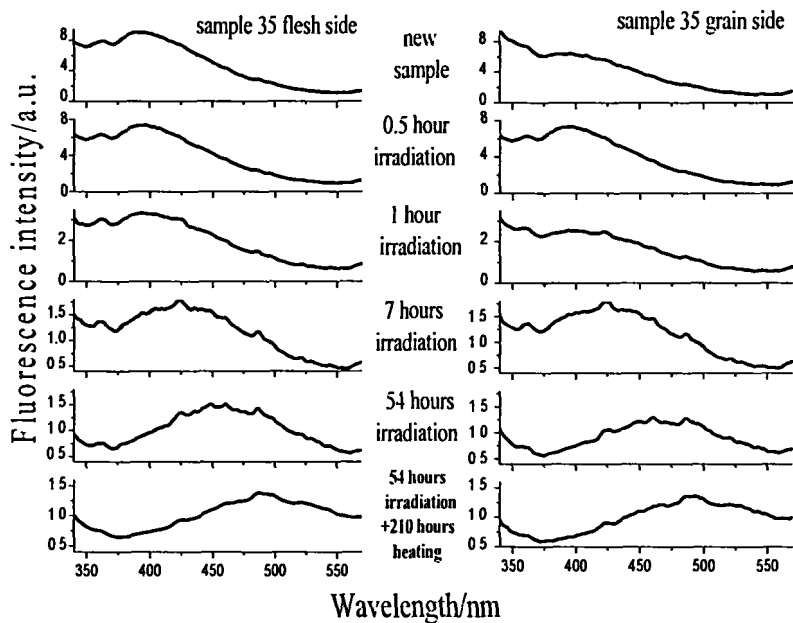


**Fig. 22:** Fluorescence intensity of modern parchment sample (number 35) at different stages of irradiation and heating treatments.

Based on the stepwise irradiation treatment data, the kinetics of the fluorescence intensity change during the aging process can be investigated. The fluorescence intensity change is plotted in **Figure 23**. The fluorescence decay cannot be described as either first or second order kinetics. Therefore, the entire aging process is interpreted as kinetically complex.

At least two different photochemical processes occur during the artificial aging process. In order to be able to extract the kinetic information from the spectra, we have to subtract the background. This procedure is reasonable because the main contribution to the background is of diffuse reflectance of the incident light on the parchment matrix that contains no useful information. The first photochemical process is relative fast decomposition of the chromophore I with the rate constant of  $33 \text{ min}^{-1}$  (**Figure 24**). The following process is much slower with the rate constant of  $3.4 \text{ min}^{-1}$ . In our opinion, the fast component describes the photochemical process on the parchment surface while the slower component is an effect of the process in deeper parchment layers. As is known, parchment consists of around 95%

collagen. Therefore, collagen fibers are the main building block of the parchment matrix. Initial parchment samples possess a finite concentration of the chromophores in their upper layer. The major chromophore here is believed to be a surface collagen. When irradiated, a hierarchical fibrillar structure of initial parchment matrix is destroyed. Collagen molecules are cleaved at random points (see Figures 14, 15, 18) and this results in a loss of fiber network. A large amount of the surface chromophores are currently concerned up to this moment. At this point, photons can penetrate into the parchment's deeper layers and the slower component starts to affect the photochemical process.

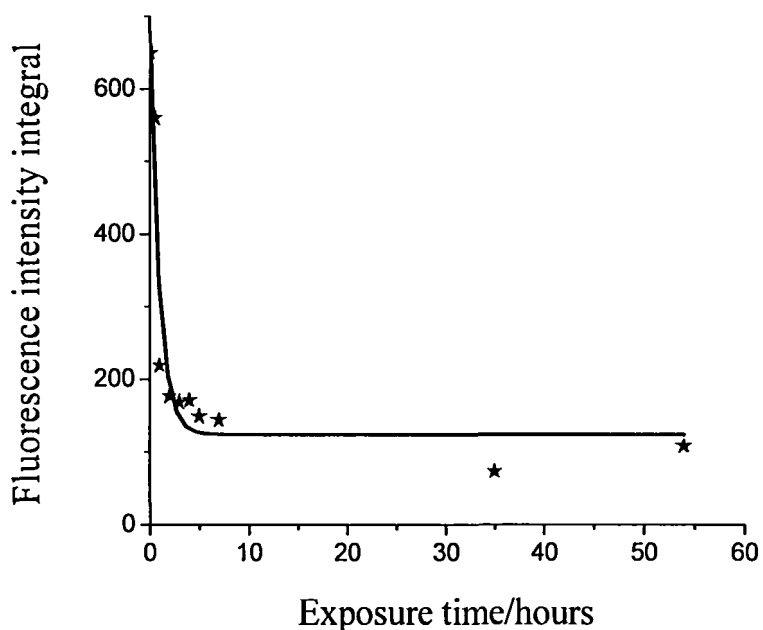
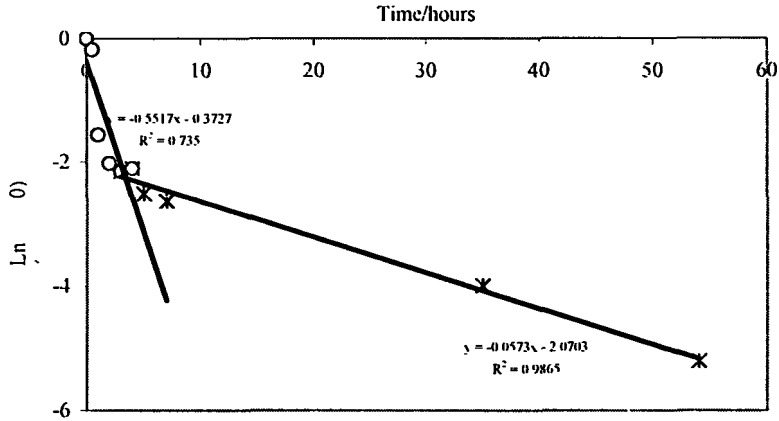


Fig. 23: Decay of the fluorescence intensity during aging process.



**Fig. 24:** Kinetics of the fluorescence intensity change during aging process (after subtraction of the background).  $X$  is the fluorescence intensity integral at given time,  $X_0$  is the initial fluorescence intensity integral.

The additional confirmation of the proposed theory may be supplied by the previously reported fact that the helix-to-unordered transition of collagen can be "characterized as a two-step process, a pre-transition followed by a more complete denaturation" [Brown]. However, we should point out that in practice, these measurements were done on dilute collagen solution and the two step nature of the process was detected by change in the circular dichroism signal. Therefore, they can serve as a complementary implement only.

**Chromophore II:** Some of the parchments possess chromophore-II (in addition to chromophore-I), which emits at 300 nm when excited at 243 nm. Such examples are shown in **Figure 25**. Upon artificial aging, irreversible fluorescence decay is observed, until the peak disappears. It should be mentioned that all the examined samples had type I chromophore, while only a few possessed chromophore II. Therefore, no change in samples without chromophores was observed. The chromophore II peak is usually observed on the *flesh* side of the parchment. Only in one sample (modern pigmented sample number 46) could chromophore II be detected on both sides. The

chemical nature of chromophore II is not clear. However, its relatively narrow fluorescence peak implies that it probably consists of a single compound. The quantification of chromophore II and understanding of its nature should be studied in the future.

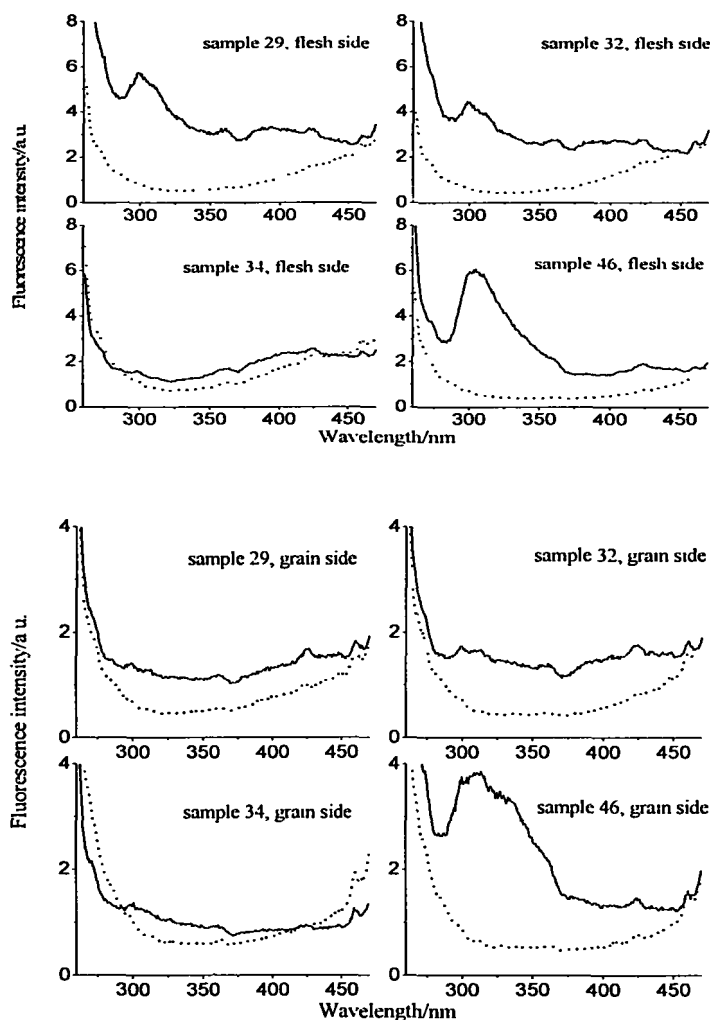


**Fig. 25:** Chromophore-II observed in some parchments samples (excitation 243 nm). The solid lines represent the modern samples and the dashed lines the aged sample.

#### 2.4.2.2.1. The nature of parchment samples' chromophores

As has been shown previously, parchment samples possess at least two different types of chromophores. The composite fluorescence pattern of a sample reflects the relative contribution of all individual chromophores. Attribution of the spectral features to specific chemical compounds would be very significant. Direct correlations to specific substances that are decomposed during the aging, and to new molecules formed in this process, are of interest. Actually, deconvolution of a fluorescence spectrum into component bands of individual fluorophores has already been reported [Na et al.]. This procedure allowed for identification of each fluorophore and provided information about their chemical degradation. This approach is broadly used for estimating various parameters of biochemical meaning in complex matrices.

In our study, we carried out peak deconvolution for modern, historical and artificially aged samples using multi-Gaussian peak fitting. Our fitting parameters included central wavelength, peak height and peak width. The fitting was performed keeping the peak position nearly constant. The results indicate that eight Gaussians are needed for a proper representation of the experimental data. The deconvolution results of typical spectra are shown in **Figure 26A, 26B, 26C** for a modern, an aged and an historical sample respectively. Our goal in this study was to understand the observed differences rather than the mechanism of the photochemical reaction. Therefore, we focused on initial (modern parchment) and final (artificially aged parchment) deterioration stages. Dealing with parchment matrix, we have to operate on the base of previous works. No data present in the literature concerning the intermediate state presented in historical samples. Some chromophores' peaks are found to be temperature dependent. Based on our experience, the kinetics of this process looks intricate and a massive series of measurements have to be carried out in order to investigate it.

It is inappropriate to explain the intermediate conditions during the artificial aging process with the smaller number of chromophores. A recently published paper demonstrates a presence of at least four photolabile fluorescent chromophores in the 300-400 nm spectral region [Theodossiou et al., 2002]. In order to simplify the picture, we decided to track the behavior of three major chromophores (those with the largest corresponding areas). The combined picture of three main chromophores in modern and aged samples is shown in **Figure 27**. Actually, during artificial aging process the

first two peaks, at 354 nm and 400 nm, disappeared, while the peak at 544 nm increased in size. According to this, formation of new chromophores at 544 nm and even at higher wavelengths seems probable.

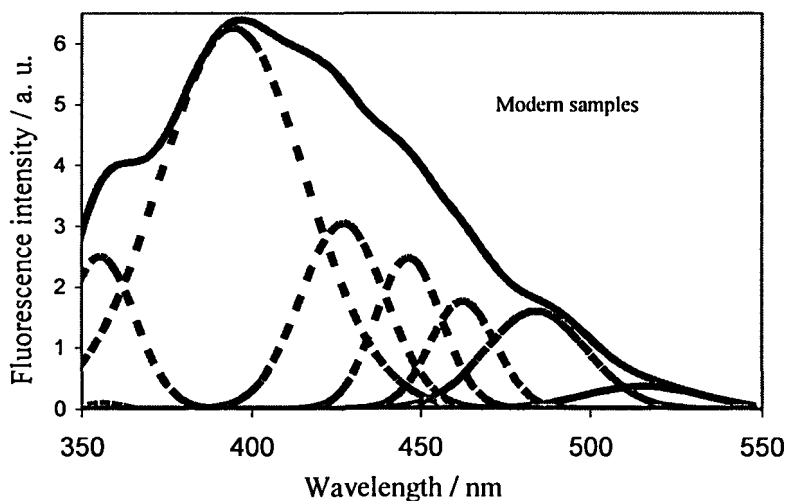


Fig. 26 (A): Chromophores found in modern samples (excitation at 298 nm).

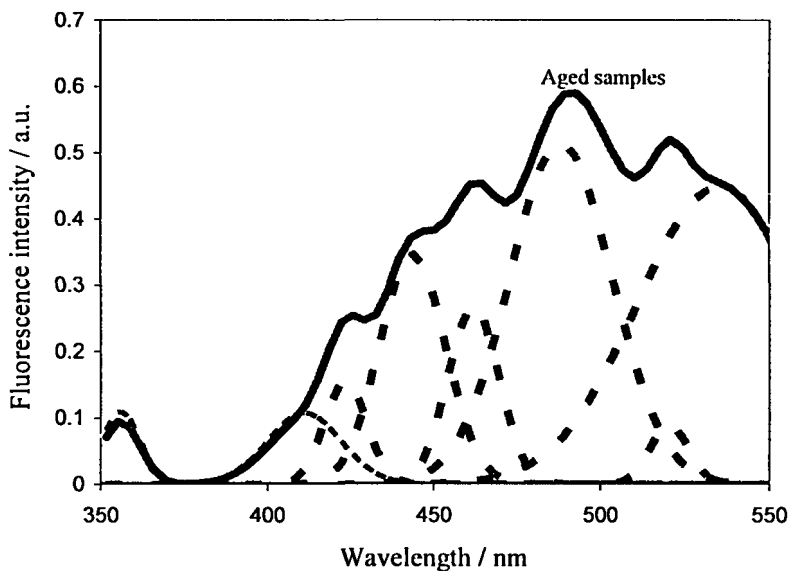


Fig. 26 (B): Chromophores found in artificially aged samples (excitation at 298 nm).

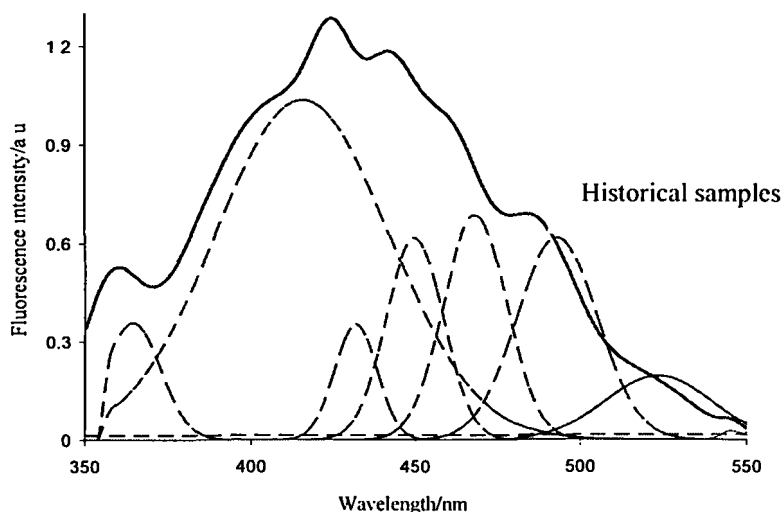


Fig. 26 (C): Chromophores found in historical samples (excitation at 298 nm).

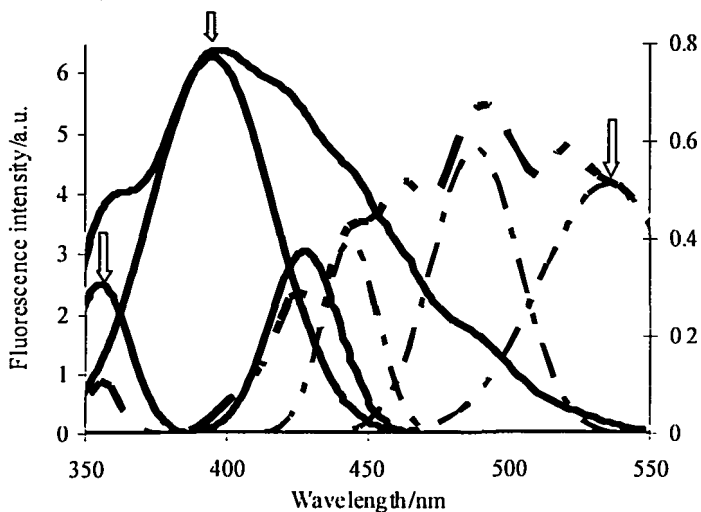


Fig. 27: Major chromophores found in modern (solid line) and artificially aged (dotted line) samples (excitation at 298 nm).

The problem of chromophore attribution to specific chemical substances is very complicated. Moreover, the effects of ultraviolet radiation even on the collagen molecule are not at the present time completely understood [Majewsky, 2001]. The classification of all the chromophores found in our

study is somewhere challenging, because of the large number of peaks found and the complexity of the matrix we are dealing with. Understanding of the unfolding processes requires a lot of routine work; therefore, this research is very time-consuming. At the present time, only the preliminary classification of chromophores in the semi-solid matrices of parchment is possible. This is based on recent studies on collagen spectroscopy [Sionkowska, 2001; Miles et al.; Fujimori; Deyl et al.; Menter et al.; Theodossiou et al., 2002]. However, "existing data is limited and in certain instances appears to be contradictory" [Majewsky]. Some collagen chromophores were isolated. The currently available information can be classified according to the excitation wavelength:

At 298 nm excitation, the parchment overall fluorescence is described by the following 8 Gaussians: 354 ( $\pm 3$ ) nm, 400 ( $\pm 12$ ) nm, 426 ( $\pm 3$ ) nm, 446 ( $\pm 3$ ) nm, 460 ( $\pm 4$ ) nm, 484 ( $\pm 3$ ) nm, 514 ( $\pm 12$ ) nm, 544 ( $\pm 7$ ) nm. Miles et al. have suggested that exposure of collagen to UV light cleaves the molecule at random points [Miles et al.]. According to Menter et al., a chromophore of emission maximum at 360 nm derives from interaction of aromatic parts in close mutual proximity. Under UV irradiation, the fluorescence peak at 360 nm disappears and a new broad weak fluorescence band of dityrosine appears at 400-420 nm (excitation at 300 nm). According to Doukas et al., the emission at 390 nm is due to the fluorescence of collagen cross-links. According to Fujimoto et al., the peak at 410 nm (observed under 325 nm excitation) corresponds to pyridinolyne, isolated from collagen, and can be attributed to cross-linked chromophore [Theodossiou et al., 2002]. The peaks at 440 nm and 460 nm are due to unknown compounds, which are accumulated with age [Menter et al.; Deyl et al.]. Taking into account the biological origin of parchment, it is possible to correlate the 410 nm and 470 nm emissions (under 337 nm excitation) to elastin and NADH (nicotinamide adenine dinucleotide) [Gavriusinas et al.].

At 243 nm excitation, the main fluorescence peak found in parchment samples is at 300 nm. The fluorescence spectra of collagen solution [Menter et al.; Sionkowska, 2001] have a peak at 300-305 nm, attributed to tyrosine (however, in these studies the excitation was at 270 nm and 275 nm, respectively). The rapid loss of tyrosine (50% in 1 hour of irradiation of collagen solution) was previously reported [Miles et al.]. During UV (254 nm) irradiation tyrosine fluorescence decreases and another broad weak band emerges, at 400-500 nm [Sionkowska, 2001]. The new product was partially contributed to photoaging of collagen.

#### 2.4.2.2. Distinction between modern and historical samples (Based on regular fluorescence measurements)

Once the effects of artificial aging on the fluorescence signal have been characterized in the previous sections, we can compare the fluorescence spectra of modern, historical and artificially aged samples. Some examples, that represent a variety of deterioration stages, are shown in Figure 26. One can clearly observe that the modern and non-deteriorated samples possess a strong fluorescence, while the fluorescence intensity of the deteriorated historical ones is much weaker. Note that the most preserved one in our set of historical parchments exhibits fluorescence intensity close to that of modern samples. The data indicates that the more the parchment is deteriorated, the less is the intensity of fluorescence. It is assumed that the decrease in fluorescence intensity under UV irradiation is a result of mononuclear reaction, Therefore, the intensity of fluorescence should be linearly correlated with collagen concentration and consequently, with the deterioration stage. Therefore, the fluorescence intensity is strongly affected by the parchment deterioration stage, and thus the fluorescence intensity can be used for characterizing the parchment deterioration stage.

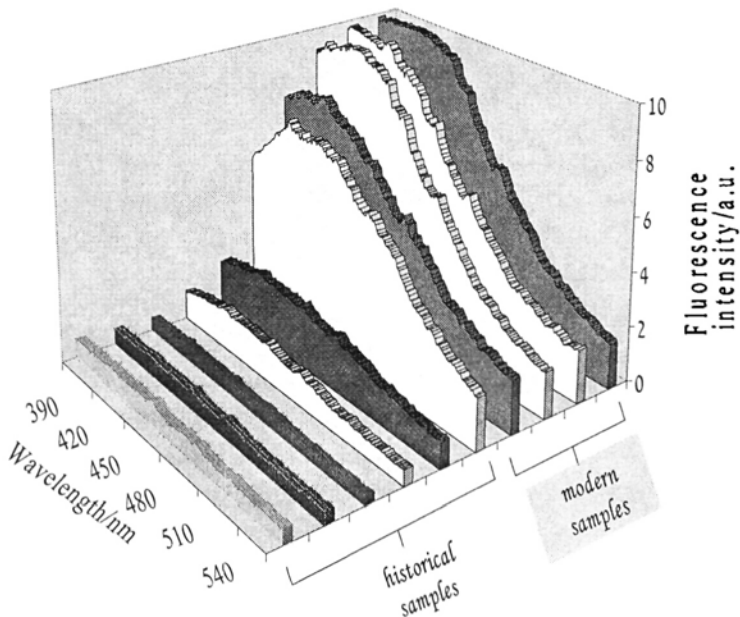


**Fig. 28:** Distinction between modern and historical samples based on regular fluorescence measurements (excitation at 298 nm).

### **2.4.3. Synchronous fluorescence**

The regular fluorescence measurements provided us with important information concerning the number of chromophores involved in the parchment fluorescence spectrum. The fluorescence peaks attribution to the specific chromophores found in collagen was in correlation with previously published data. Therefore, the results of the regular fluorescence measurements were promising, but some issues remain unresolved. The presence of a large number of chromophores, each with its specific excitation and emission characteristics, made the representation very complex. The choice of the excitation and emission wavelengths manages the way fluorophores contribute to the resulting spectrum. Accordingly, many excitation and emission combinations must be tested to determine the most useful procedure. Typical examples of three dimensional fluorescence spectra of two different parchment samples are shown in **Figures 29A, 29B**. When using the regular fluorescence measurements, this work is very time consuming and ineffectual. In fact, the same task can be completed by simply acquiring the single synchronous fluorescence (SF) spectrum. In this study, the synchronous fluorescence was applied for the first time to the measurements of parchment samples.

The SF method involves simultaneous scanning of excitation and emission wavelengths while keeping the interval between them constant. Compared with the ordinary emission spectrum, a synchronous fluorescence spectrum has more features and thus is more informative. The peaks are sharpened in the case of multicomponent analysis. The SF measurements provide greater selectivity and can be used to detect subtle differences in fluorescence. Therefore, by comparing synchronous spectra of two similar systems, it is possible to immediately identify the differences in their composition. Moreover, the SF spectrum is considered to be a characteristic “fingerprint” because it is unique for a given system [Dramićanin et al.].

#### **2.4.3.1. Experimental conditions**

Fluorescence of all parchment samples was examined quantitatively using Aminco-Bowman Series 2 spectrofluorimeter equipped with the front surface accessory (excitation and emission bandwidths 4 nm). The constant difference between excitation and emission monochromators was 70 nm. The angle between the excitation beam and the sample surface was 76°. This geometry results in the minimum background intensity due to specular

reflection and other scattered excitation light. All spectra were recorded at room temperature.

We recorded the synchronous spectra of all the samples in the study (modern, historical and artificially aged) from both sides (*flesh* and *grain*). We averaged these synchronous spectra to receive one typical spectrum for each given sample.

#### 2.4.3.2. Synchronous fluorescence during artificial aging

As mentioned above, a synchronous fluorescence spectrum is much more informative than the regular fluorescence measurements. The peaks are sharper and bandwidths narrower, thus providing higher selectivity. Then, to prove the enhanced sensitivity of SF to the parchment deterioration stage, we decided to examine additionally much more gentle irradiation at 360 nm (besides at 254 nm) followed by the temperature treatment (as described in 2.2 chapter). The choice of the irradiation wavelength based on the previously published results of Yova found that irradiation of collagen at 337 nm changed its fluorescence spectrum to be similar to that of denatured collagen [Yova et al.]. As a result, the influence of the “gentle” artificial aging process on the synchronous fluorescence properties was quantified.

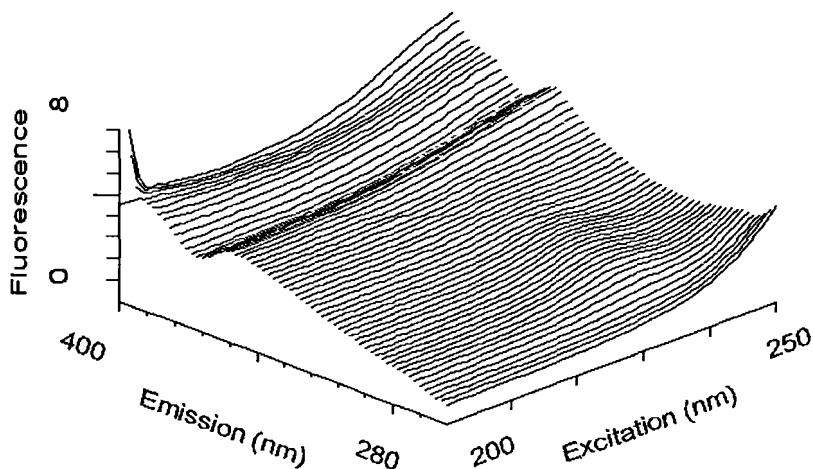
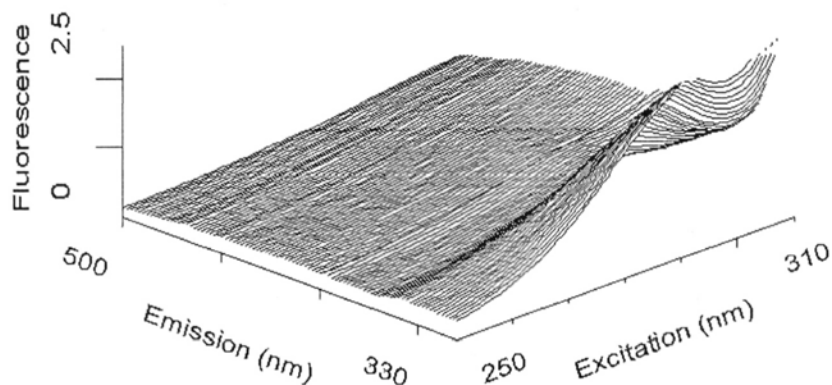


Fig. 29 (A): Three-dimensional spectra of modern parchment sample (number 3).



**Fig. 29(B):** Three dimensional spectra of pigmented modern parchment sample (number 46).

Firstly, the influence of irradiation time on synchronous fluorescence spectrum was checked. The fluorescence intensity started to decrease just after 15 min of irradiation (**Figure 30**). With the ongoing irradiation, the additional decrease as well as a change in the main peak position to higher wavelength occurs. These changes in the fluorescence spectrum are similar to the full artificial aging process case previously discussed. However, the irradiation at 360 nm caused significantly smaller deterioration in the parchment sample due to less energetic wavelength. As a result, it was concluded that the SF technique was much more sensitive than the regular fluorescence measurements.

As a final step in artificial aging process, temperature treatment was applied to the irradiated samples. Formation of the new fluorophore at high wavelengths with relatively high fluorescence intensity can be examined in the corresponding synchronous fluorescence spectra (**Figure 30**). The nature of the fluorophore involved will be discussed later.

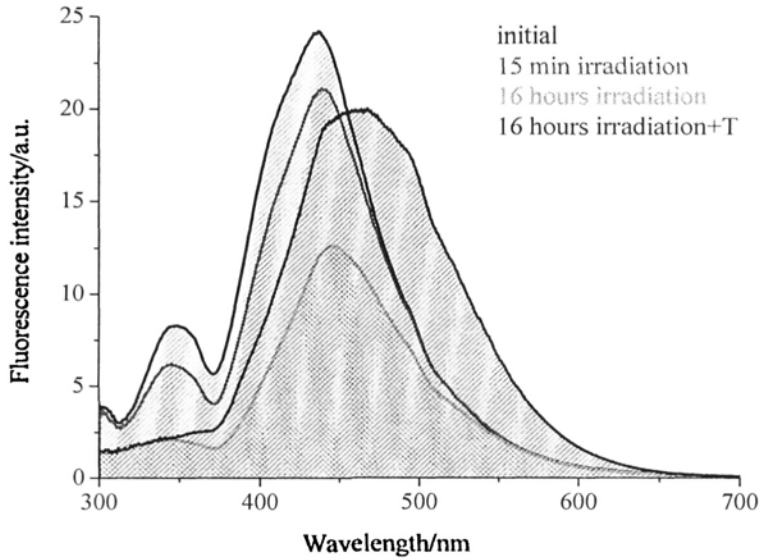


**Fig. 30:** Influence of gentle artificial aging process on synchronous fluorescence spectra. ("T" represents the temperature treatment)

The best way to highlight the changes occurring in parchment samples during the gentle artificial aging process is by using the normalized fluorescence intensity. The normalized fluorescence intensity was calculated as an intensity ratio of each specific measurement to the fluorescence intensity of the initial sample through all the spectral range. Using this procedure, formation of two new peaks was observed when comparing the initial and the final parchment sample spectra. The first new peak was found at 312 nm, and the position of the second one was treatment dependent. In the case of the temperature treatment alone it was found at 590 nm and in the case of the full gentle artificial aging cycle at 564 nm (Figure 31).

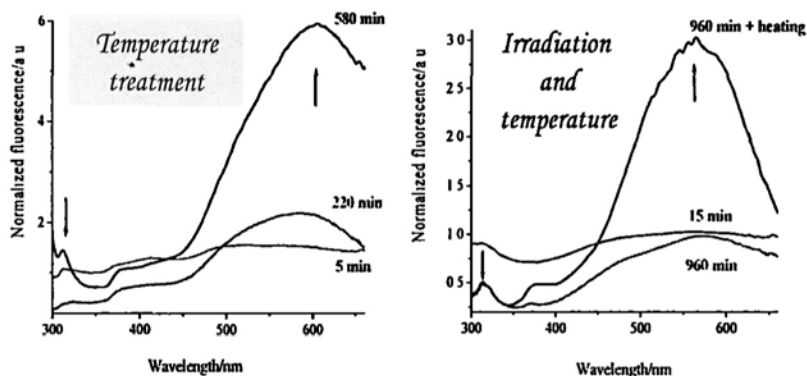


**Fig. 31:** Influence of gentle artificial aging process on synchronous fluorescence spectra. Normalized fluorescence intensity (ratio of sample fluorescence intensity to initial sample fluorescence) examination during gentle artificial aging process: temperature treatment and irradiation followed by temperature treatment.

As presented, relatively delicate artificial aging causes a noticeable change in the synchronous fluorescence spectrum. Therefore, the synchronous fluorescence serves as a sensitive tool for the parchment stage recognition. Based on this, parchment sample discrimination is possible.

#### 2.4.3.3. Differentiation of parchment samples

##### (By synchronous fluorescence)

The possibility of discrimination between parchment groups based on synchronous fluorescence measurements has now to be proved quantitatively. As was previously mentioned, even a relatively delicate artificial aging causes a noticeable change in the synchronous fluorescence spectrum. Therefore, a regular artificial aging process (much more vigorous) should result in considerable changes in the SF spectra. **Figure 32** shows typical synchronous fluorescence spectra of the modern, historical and fully artificially aged parchments. Dealing with SF data, we will present “typical spectra” for each group of samples (as in regular fluorescence measurements) due to the same reasons (for detailed description see p.37-38).

Two main differences between the three parchment groups can be clearly observed when examining the synchronous fluorescence spectra (**Figure 32**). The first one can be observed when examining the 270-370 nm spectral

region. The appearance of two noticeable peaks at 305 nm and 346 nm was detected in modern samples only. This fact can serve as a qualitative indicator for the preliminary parchment characterization.

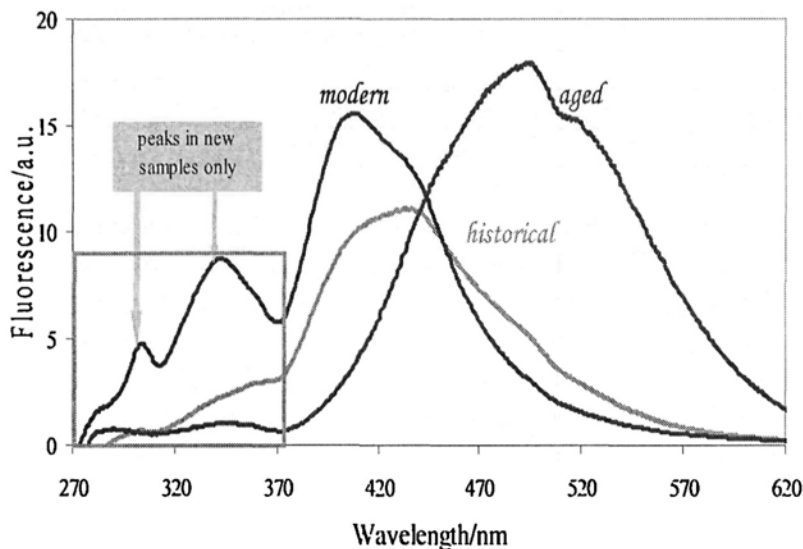


**Fig. 32:** Synchronous fluorescence spectra of modern, historical and artificially aged parchments.

To quantify the observed differences and to investigate whether they are suitable for parchment discrimination, we calculated the spectral intensity integral over the 270-370 nm region. The results are listed in Table 4. We performed null hypothesis testing on all spectral properties using ANOVA and statistical power analysis to see if there are statistically significant differences between spectral properties of the modern, historical and aged samples. The null hypothesis was that the parchment conditions had no effect on the intensity integral as well as on the main peak position, taking a probability value of 0.01. Then,  $t$  values ( $t$  value is defined as the ratio of group means to the variability of the groups) and statistical powers,  $P$ , were calculated. Statistical analysis reveals that two statistically significant spectral differences exist between the groups, namely the fluorescence intensity integral and the main peak position. These features can be used for the statistically based quantitative discrimination between parchment groups.

**Table 4**  
Intensity integral and main peak position for modern,  
historical and aged parchment samples.

	Intensity integral, a.u.	Main peak position, nm
Modern samples	$322 \pm 22$	346 pm 1
Historical samples	$66 \pm 9$	$336 \pm 11$
Aged samples	$25 \pm 5$	$292 \pm 6$

The **second region** of interest was the 370-700 nm spectral region. The main peak position in this region was different for the modern, historical and aged samples. In modern samples, the peak was found at 410 nm, in artificially aged samples at 438 nm and in historical samples at 496 nm. It is worth mentioning the main peak in historical samples is positioned between that of the modern and that of the artificially aged samples. Its position supports the logical assumption that the historical samples are found in the "intermediate" deterioration stage. Their conditions are neither as good as modern samples nor as poor as artificially aged ones when probed by synchronous fluorescence.

The main peak shape in the 370-700 nm spectral region indicates the existence of a number of chromophores. The multi-Gaussian peak fitting was used to represent the experimental data. Out fitting parameters included the central wavelength, peak height and width and baseline position. The fitting was performed keeping the peak position nearly constant. The results indicated that the peak consists of at least eight different chromophores. The main chromophores presented in this region are at 400 nm, 435 nm, 450 nm, 470 nm, 495 nm, 522 nm, 540 nm and 623 nm. The aged and historical samples have a larger relative proportion of chromophores at the higher wavelength than the modern ones (**Figure 33**). 93% of modern samples chromophores are found between 435 nm and 450 nm, whereas the distribution of historical samples chromophores is much wider (from 435 nm to 540 nm). The main portion of the artificially aged samples chromophores are found in 495-540 nm spectral range. Based on chromophores emission wavelength, the differentiation of parchment samples is available. The reason for differences in chromophores distribution is found in the relative proportion of collagen and gelatin content in a specific parchment sample. The detailed discussion is provided in the next chapter.

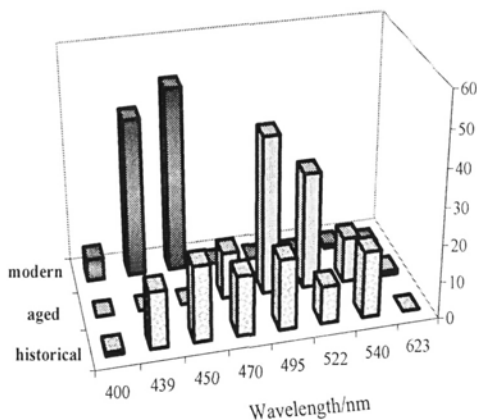


**Fig. 33:** Relative proportion (% of intensity integral) of chromophores in modern, historical and artificially aged parchment samples.

#### 2.4.3.4. Collagen-to-gelatin ratio calculations

##### (Based on synchronous fluorescence)

The attribution of synchronous fluorescence peaks to specific chemical substance/s is of particular interest. The synchronous fluorescence intensity,  $I_s$ , is directly related to the concentration of the analyte,  $c$ , as:

$$I_s = KcbE_{ex}(\lambda_{ex})E_{em}(\lambda_{ex} + \Delta\lambda) \quad (1)$$

where  $E_{ex}$  is the excitation wave function at a given wavelength;  $E_{em}$  is the emission wave function at a given wavelength;  $b$  is the thickness of the sample;  $K$  is the instrumental geometry and related parameters [Patra et al.].

The multiplication of two Gaussians ( $E_{ex}$  and  $E_{em}$ ) results in narrower spectral peaks. In particular, the overlapped peaks of conventional fluorescent spectra could become separated in synchronous fluorescence performed using a suitable wavelength interval [Xia et al.]. The SF measurements can be used to detect subtle differences in fluorescence. In our study, the fluorescence spectra are a complicated mixture of fluorescence signals from a large number of chromophores. Thus, the goal is to identify the differences in composition of the similar systems. In fact, the synchronous fluorescence spectroscopy may offer other advantages. These include enhanced selectivity

due to spectral simplification, decreased measurement time in multi-component analysis, improved spectral resolution, and elimination of the Rayleigh scattering peak [Wang et al.]. Therefore, the synchronous fluorescence method is a best choice for our complicated matrix.

In order to be able to attribute a certain peak to a specific chromophore, we decided to examine the synchronous fluorescence spectra of the pure substances: collagen and gelatin. The modern and the historical parchment synchronous fluorescence spectra were compared to the pure collagen and the pure gelatin synchronous fluorescence spectra respectively. It is assumed that modern parchment consists of ~95% of collagen, which is lost during deterioration process when the peptide bonds are broken. Therefore, the collagen content in historical samples is lower.

While inspecting the synchronous fluorescence spectrum, the peaks in the 270-370 nm spectral range were attributed to pure collagen, whereas the biggest fluorophore peak in a higher wavelength region (370-700 nm) was a superposition of pure collagen and pure gelatin peaks. Initially, the modern samples exhibited spectra identical to pure collagen, but as the parchment deterioration progressed, the fluorescence intensity signal in the relevant region of collagen fluorescence decreased, as presented in **Figure 34**. The presence of the pure gelatin features in the synchronous fluorescence spectrum of the historical samples can be explained by the fact that the gelatinization is considerable in these samples, based on the collagen-to-gelatin ratio measured in a previously published study [Weiner et al.]. Laser-induced fluorescence was applied to collagen and gelatin in an earlier study [Theodossiou et al., 2002] to illustrate reversible and irreversible changes in collagen fluorescence due to heating. Additionally, it was reported that on heating or irradiation, the triple collagen helix in solution unfolds to produce random chains of gelatin [Miles et al.].

In washed and dried collagen (from rat tail tendon) the collagen to gelatin (C/G) ratio was reported to be 10.2, when in denaturated rat tail tendon (mainly, gelatin) the C/G ratio was 0.7 [Weiner et al.]. It was claimed that the unfolding of collagen to gelatin is one of the major chemical changes the parchment have undergone. In our study, in modern parchments C/G ratio was 9.8-12.5, and in historical parchments 0.6-7.6, respectively.

Synchronous fluorescence was used as a non-destructive technique to estimate the collagen to gelatin ratio. The spectral resolution was insufficient

for extracting the pure components; therefore, direct calculations of C/G ratio could not be provided. Instead, peak deconvolution applying multi-peak Gaussian fitting was carried out. The fitting was performed keeping the peak position nearly constant. The results of the deconvolution are presented in **Figure 35**.

Let us examine each case in detail. The spectrum of collagen consists of two well-defined peaks at 305 nm and 343 nm and an additional broad band with a maximum at 440 nm. Similarly, the spectrum of gelatin has small maxima at 305 nm and 343 nm, but the peak at 440 nm has an enhanced intensity comparable to that of the collagen peak. The percentage of collagen in each sample was calculated according to the following formula:

$$\% \text{ collagen} = \frac{10x_i}{y_i \times z} \times 100\% \quad (2)$$

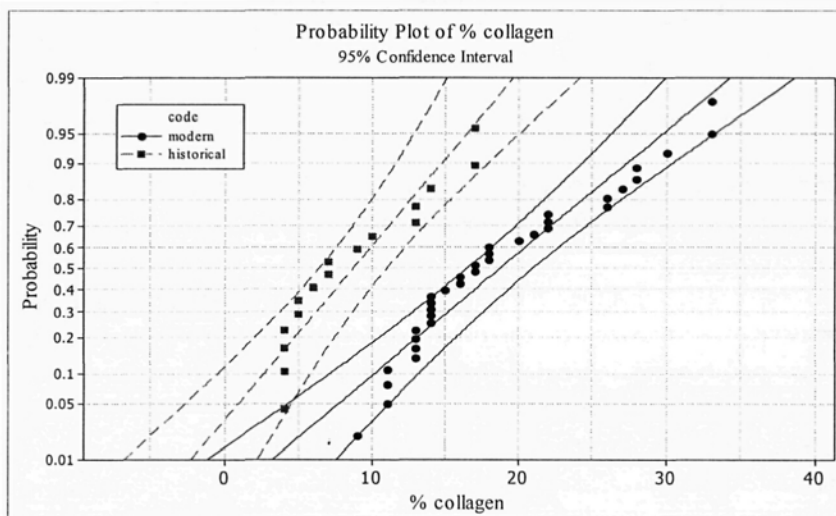
where  $x_i$ - the height of the deconvoluted peak at 343 nm,  $y_i$ - the height of the deconvoluted peak at 440 nm,  $z$ -the percent of collagen calculated from the pure collagen spectra.

Accordingly, when the C/G ratio was examined, a statistically significant difference was observed between the calculated percent of collagen found in modern and historical samples (**Table 5**). The calculated data show good agreement with the previously cited results [Weiner et al.]. The probability plot of calculated percentage of collagen in the modern and historical samples is presented in **Figure 36**, clearly showing the differences. The C/G ratio was not examined in artificially aged samples because the correspondent peaks of collagen at 305 nm and 343 nm are missing (collagen was destroyed during artificial aging process) and the entire parchment matrix of these samples is a non-homogeneous mixture of gelatins.

In summary, we have shown that the synchronous fluorescence spectrum is very sensitive to the conformational changes in the parchment environment and deterioration stage and is a helpful technique for the measurement of parchment conditions. The advantage of this method is that it does not require sample preparation; it is non-destructive, simple, reliable and fast.

**Table 5**  
 Calculated percent of collagen found in modern and historical samples.

	Mean % collagen $\pm$ SE of the mean
Pure collagen	100
Pure gelatin	4
Modern samples	18.7 $\pm$ 1.2
Historical samples	8.7 $\pm$ 1.2



**Fig, 36:** Probability plot of collagen content in modern and historical samples.

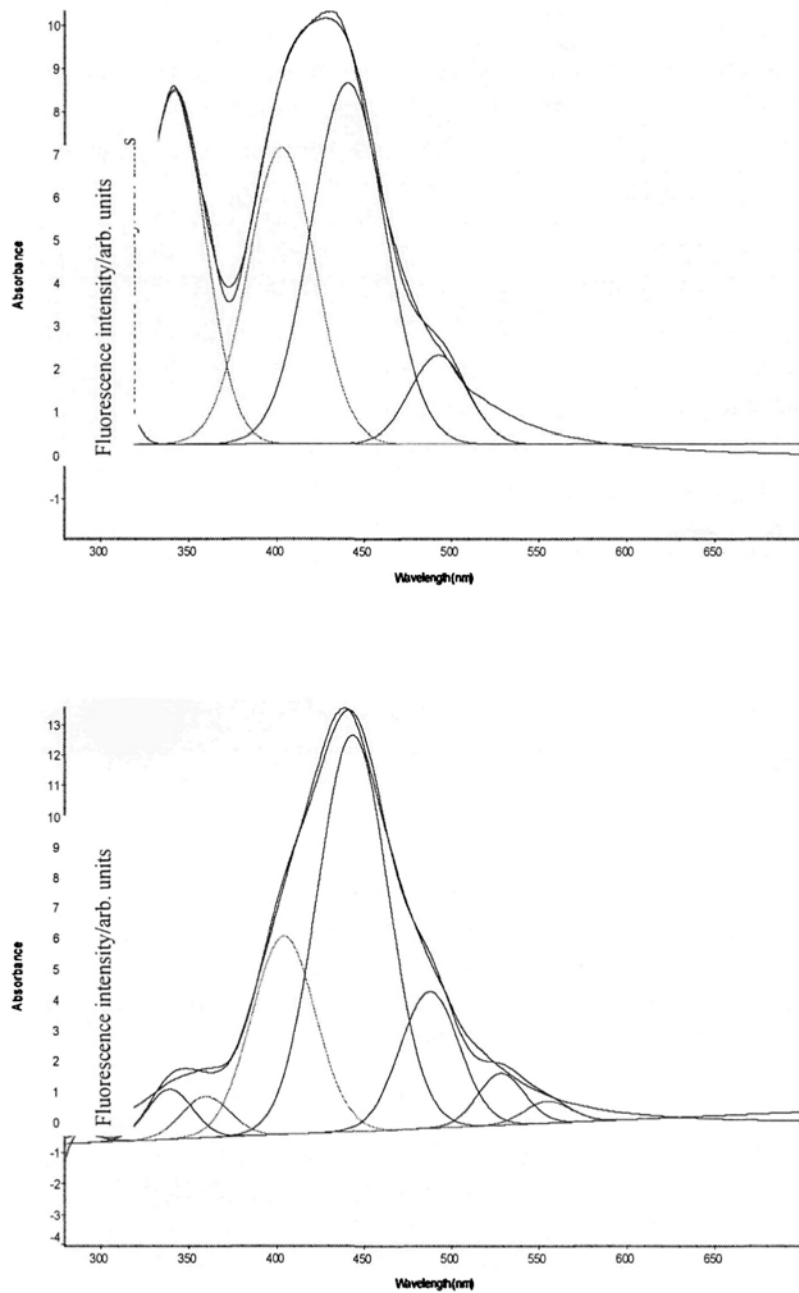


**Fig. 35:** Examples of deconvolution of modern (top) and historical (bottom) parchment samples.

#### 2.4.3.5. Concept of layer-resolved profiling of parchment

Parchment has a multilayered structure, therefore depth-resolved measurements are crucial in understanding the nature of fluorophores in each distinct layer. These investigations may solve a dilemma of chromophore distribution mapping, which is difficult to obtain by other techniques due to morphological complexity and inhomogeneous optical properties of parchment layers.

The layer-resolved profiling of parchment was obtained by application of a series of ongoing laser shots (Nd:YAG laser operating at its fundamental wavelength (1064 nm, 7ns pulse duration, 1Hz repetition rate) to the parchment surface. The laser beam was focused on the sample surface with a quartz cylindrical lens ( $f=100$  mm, beam focus size  $10\text{mm}\times 70\mu\text{m}$ ). The pulse energy was adjusted to 310mJ/pulse. Layer-resolved profiling was achieved moving horizontally from the left to the right side of the parchment sample by  $\sim 50$   $\mu\text{m}$  steps. Vertical axis probing was performed by removal of 3-5  $\mu\text{m}$  layers to obtain interference free layered-resolved synchronous fluorescence analysis. Consequently, the number of layers obtained depended on the parchment sample thickness.

The synchronous fluorescence of every single sample layer was acquired according to the previously described procedure (chapter 2.4.2). The results of this experiment are shown in **Figure 37**. The measured fluorescence intensity is a mixture of fluorescence signals from the upper layer and a few layers below. Each spectrum provides the change in peak intensity and position at different continuously increasing depths. The depths were estimated by optical microscopy taking a difference while focusing on the surface and the crater, correspondently. Such estimations are not very accurate; therefore, we prefer to present the number of shots (or normalized depth) in the following figures and not the “real coordinates”.

Additionally, each layer was examined by optical microscopy. As evident from **Figure 38**, firstly, the removal of pigmented upper layer occurred. Then, the fibrils of hierarchically structured collagen layers were imaged. Finally, the single collagen fibers were clearly seen. These observations can be supported by the previously reported [Xiao et al.] fail of structural integrity of collagen fibers during laser ablation of the soft tissues.

Let us examine the detailed changes in synchronous fluorescence spectrum performing layer-resolved profiling. Generally, spectral characteristics of the bulk fluorescence are strongly affected by the variation

in the layers' thicknesses, because the bulk fluorescence is a mixture of the fluorescence from the different parchment layers.

The layer-resolved study of synchronous fluorescence was performed on modern, historical and artificially aged samples. As a representative sample, the artificially aged one was chosen for discussion here due to its having the highest degree of deterioration (i.e. maximal change in synchronous fluorescence expected). The grain side was examined.

The synchronous fluorescence of the upper layer from surface to a depth of around 5  $\mu\text{m}$  is typical for the artificially aged samples and peaked mostly at 495 and 525 nm (after deconvolution). Based on previously reported results (Chapter 2.4.3.3), the main peaks position gives an impression of a high degree of upper layer deterioration. Consequently, a strong fluorescence peak at this region confirms the existence of age-related cross-linking substances. The additional argument to support this assumption originates in the fact that the synchronous fluorescence spectrum measured at  $\sim 10$   $\mu\text{m}$  depth shows a change in the peaks position to the lower wavelength (475 nm and 495 nm) with simultaneous fluorescence intensity increase. Therefore, we can conclude that our artificial aging process results in a high degree of deterioration of 10  $\mu\text{m}$  thick layer at least.

The synchronous fluorescence spectrum measured at  $\sim 30$   $\mu\text{m}$  depth shows a shift in peaks position to 440 nm and 475 nm respectively with a simultaneous fluorescence intensity decrease. In particular, the contribution of age-related substances to total fluorescence decreased rapidly with thickness indicating the existence of a transition zone at the depth range of 20-70  $\mu\text{m}$ .

When sampling depth is continuously increased up to a half-thickness, the main fluorescence peak further decreases. Considering the fluorescence signal from the layers approximately at half-thickness, a significant increase in the measured signal observed and the main peaks was found at 415 and 434 nm, as in the modern parchment samples. At this point, the majority of the fluorescence signal is the superposition of native chromophores localized within these layers with only a negligible portion contributing to the real origin of the parchment sample being aged.

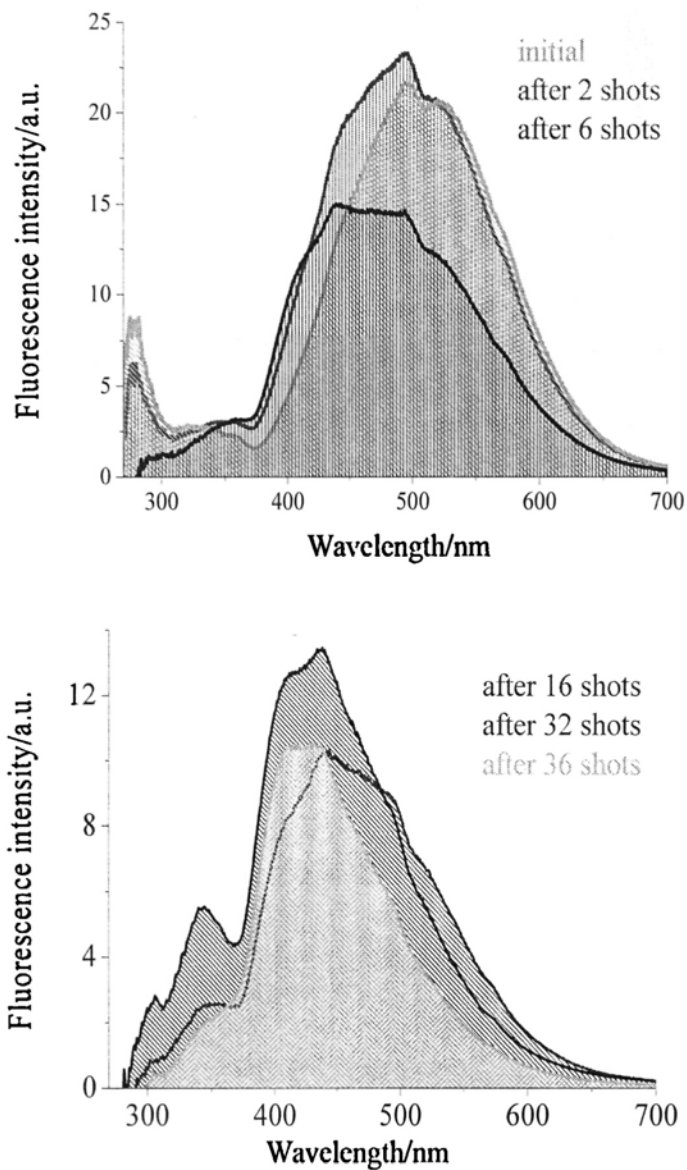
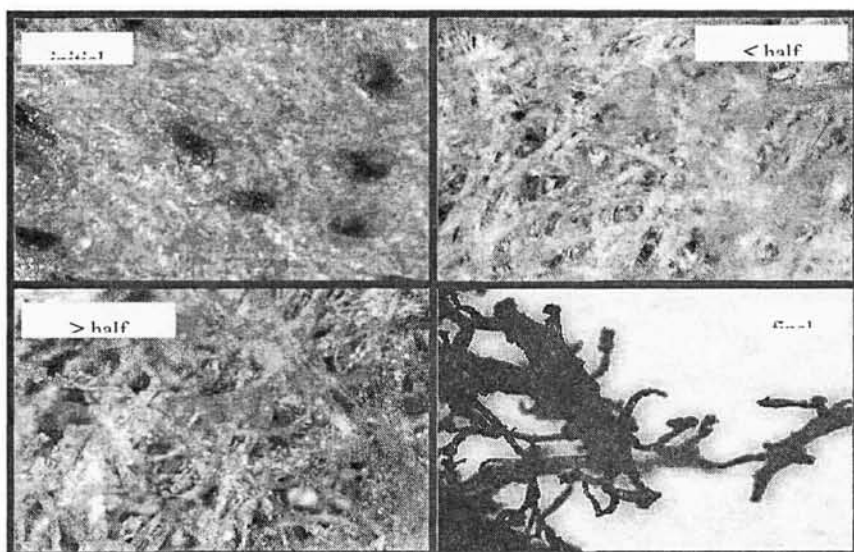


Fig. 37: Layer-resolved synchronous fluorescence of artificially aged parchment sample.



**Fig. 38:** Layer-resolved optical microscopy of artificially aged parchment sample.

Finally, the fluorescence spectra taken from a few bottom layers looks actually like the opposite (flesh) sample side (**Figure 39**). It means that the fluorescent emission of the dominant fluorophore in the few last layers obtained is identical to that of the flesh side. This fact proves the capability of layer-resolved synchronous fluorescence to pick out the presence of individual chromophores besides the potential to map the sample surface according to its local deterioration stage.

To examine the relative differences in layer-resolved profiling of parchment samples, four various representative examples (modern and pigmented modern, historical and aged parchment samples) were examined. The correspondent spectral profiling is presented in **Figures 40-42**. To highlight the variations, the normalized integral of synchronous fluorescence intensity as a function of normalized layers depth was calculated (**Figure 43**). As expected, the depth resolved profile of normalized integral behavior is different for each sample group.

The fluorescence integral of modern non-pigmented samples demonstrated the most temperate and understandable functioning: it increased slightly near the half thickness and then declined a little. The analysis was started from the grain side. The value of fluorescence integral at

the final layers approached was close to 1, but a little bit higher, which means that fluorescence of the flesh side is higher. It is in fact the situation when inspecting the respective synchronous fluorescence spectra.

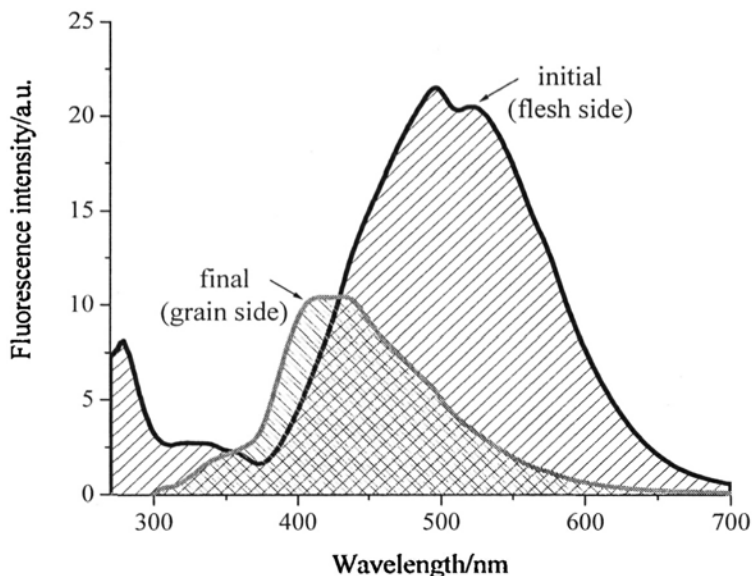


**Fig. 39:** Synchronous fluorescence of initial and final samples' layers of aged parchment.

In modern pigmented samples, the fluorescence increased after a few first layers ablation occurred. This enhancement in fluorescence signal is due to removal of the pigmented layers which are weakly fluorescent. The following ablation of the deeper layers results are similar to modern non-pigmented sample synchronous fluorescence spectrum.

The fluorescence of the artificially aged parchment increased very fast after the first layers ablation. Most likely, the exterior of collagen, which chromophores are strongly fluorescing, can explain this effect. Then, the synchronous fluorescence signal had a minimum when half of the artificially aged sample thickness was ablated. The rationale for the existence of this minimum is not clear.

The behavior of the layer-resolved fluorescence of the historical samples is quite different. The normalized integral of synchronous fluorescence

intensity of these samples decreased steadily from the first few layers, and after half-thickness achievement, it gives the impression of being a superposition of modern and artificial aged samples signals.

Overall, the information derived from the depth-resolved spectra indicates that the parchment has layered structure when the dominant fluorophore in the upper layer (grain side) is different from that in the lower layer (flesh side). Most importantly, it possesses the ability to quantify the contribution of each chromophore in each given layer to the whole picture.

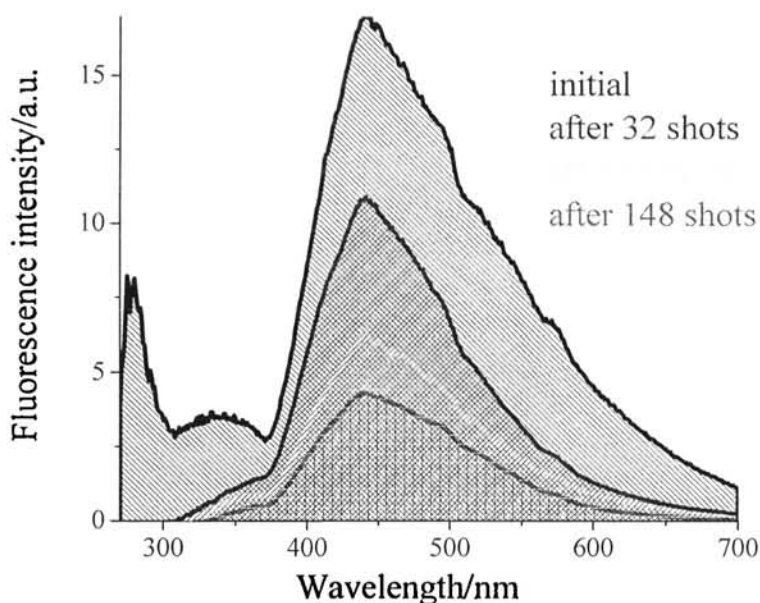


**Fig. 40:** Layer-resolved synchronous fluorescence of historical sample.

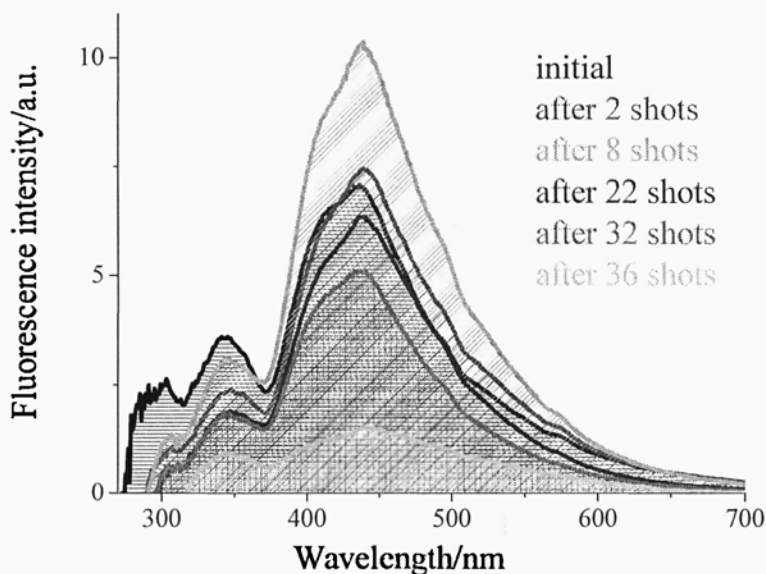


**Fig. 41:** Layer-resolved synchronous fluorescence of pigmented modern sample.

## 2.5. Parchment characterization by visible imaging

As previously shown, fluorescence spectroscopy is sensitive to the conformational changes in parchment environment and deterioration stage. Providing morphological imaging of a given parchment section is of special interest, since the deterioration processes may not be homogeneously distributed. Therefore, mapping the parchment surface using visible imaging may be useful for determination of local deterioration.

### 2.5.1. Visible color (RGB) imaging

Color RGB imaging, using digital photography, is much more reliable, faster and cheaper than the simple examination of the parchment surface by the naked eye or by using complicated techniques. RGB imaging was successfully used in digital processing of Dead Sea Scrolls [Knox et al.]. Optionally, it can be used on line for parchment conservation monitoring in museums. Libraries containing photographs of each parchment at specific preservation stage can be very helpful in this area.

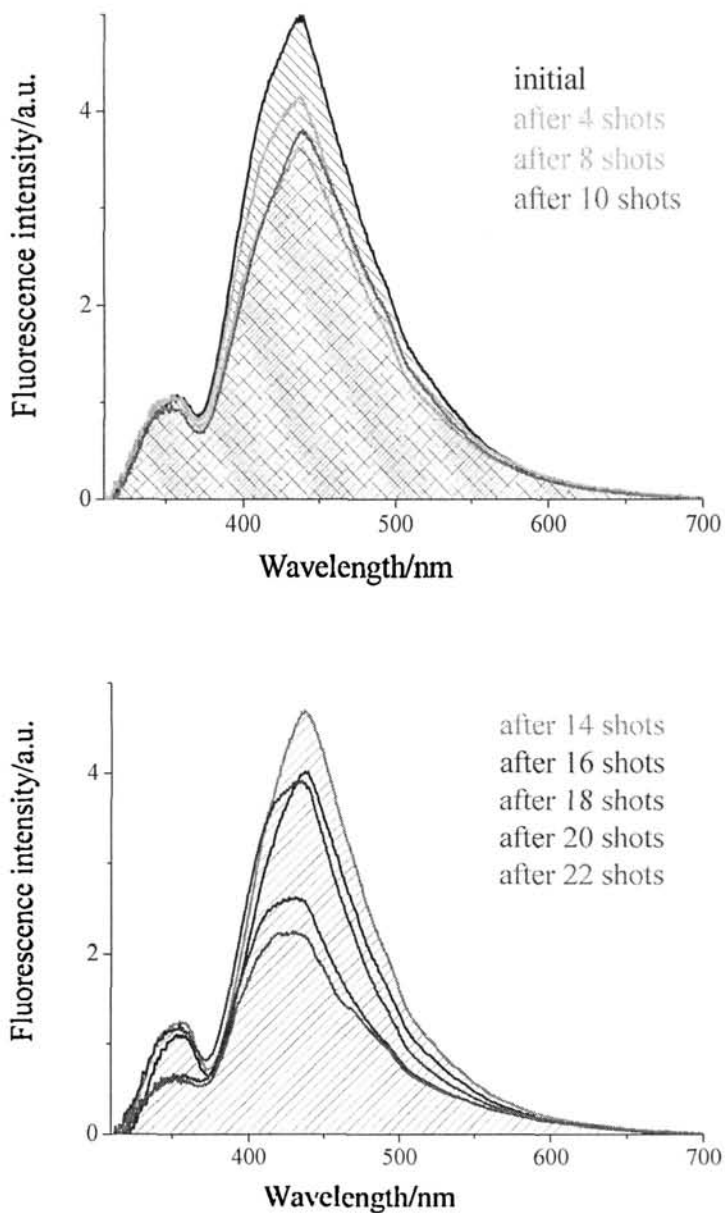
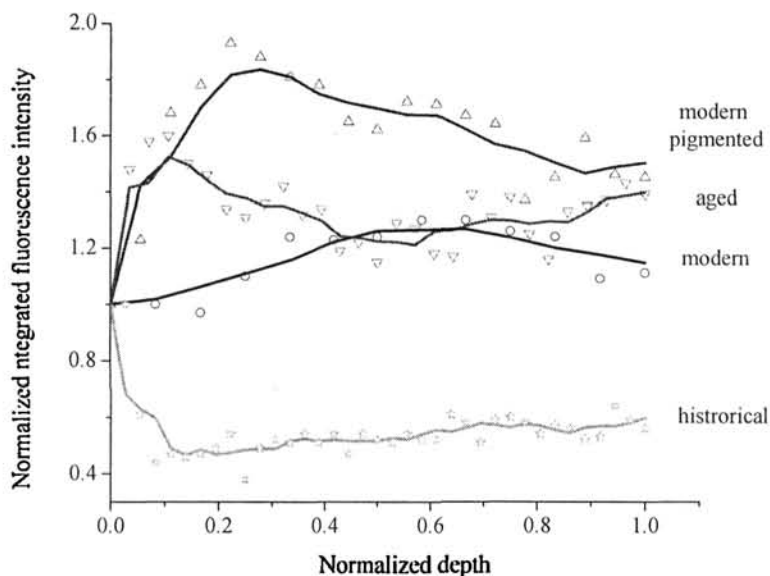


Fig. 42. Layer-resolved synchronous fluorescence of modern sample.



**Fig. 43:** Normalized integrated synchronous fluorescence of modern, modern pigmented, artificially aged and historical parchment samples.

#### 2.5.1.1. Experimental procedure

Digital photographs of the modern, historical and artificially aged parchments were acquired using a digital camera (Olympus C720UZ, with auto white balance). RGB imaging analysis was performed using Adobe Photoshop 6.0 software, providing the luminosity value and red, green and blue counts. The intensity scale for each color was from 0 to 255 (8 bit), where the maximum value corresponded to the pure colored pixels. At least  $100 \times 100$  pixels in each picture were used for analysis. All the counts were normalized to the correspondent luminosity value. Since no color calibration has been carried out, the absolute RGB values are not significant. However, normalization to luminosity allowed for appropriate comparison of the samples at the same conditions.

#### 2.5.1.2. Parchment characterization by color imaging

The colored picture (image) of the object is produced, actually

summarizing the correspondent reflection spectra from the whole inspected surface. In all cases studied, we analyzed the *grain* side of the parchments, since in our preliminary study it was found to be more sensitive to changes during artificial aging process. The absolute distribution of basic colors (red, green and blue) was changed after the artificial aging treatment in all samples examined. As an example, the changes presented in **Figure 44** deals with four samples with different thickness and surface structure (modern and artificially aged samples number 1-4). The blue color intensity decreased dramatically (in absolute number scale), while other colors remained nearly the same.

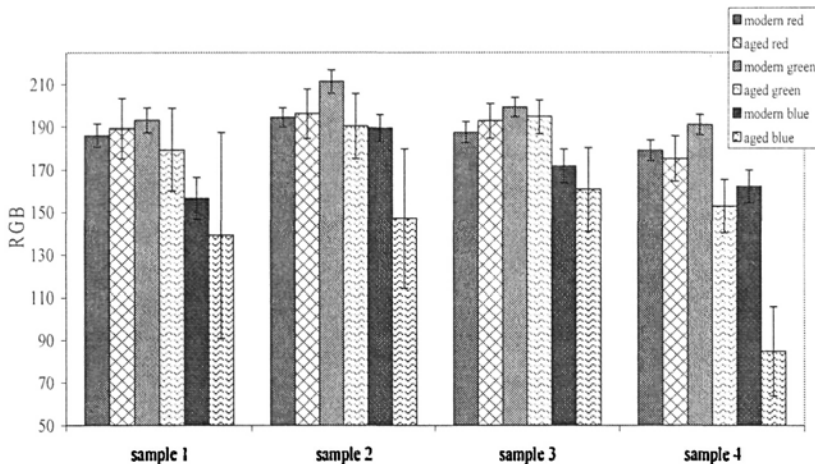


**Fig. 44:** Distribution of basic colors in modern and artificially aged parchment samples.

To standardize the intensity scale for all samples, a normalized value was calculated for each color as described in experimental part of this section. A statistically significant difference was found between initial and artificially aged samples when examining the same normalized color (**Figure 45**).

When the normalized RGB counts were plotted as a three-dimensional RGB plot, three clearly separated groups of samples were observed, as shown in **Figure 46**. The distinction between the new, aged and historical samples based on 3D RGB plot is then unmistakable. These data indicate that fast mapping of parchment deterioration is possible using RGB imaging. Additionally, it seems to us possible to determine where the real historical samples are when compared to the artificially aged ones. The statistical

distinction requires the examination of additional historical samples dated before the 16th century.

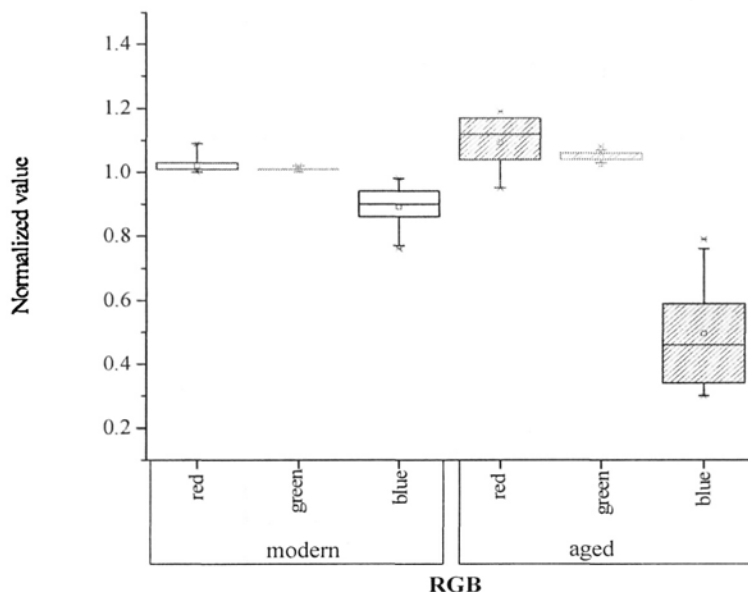


**Fig. 45:** Normalized values of basic colors for parchment samples.

This hypothesis was validated by the real historical samples. The results are shown in **Figure 47**. The RGB counts of the historical samples are presented. The samples are plotted according to decreasing RGB counts. The most non-deteriorated historical sample (number 19) has the highest overall counts and the most deteriorated one (number 20) has the smallest overall counts. It also seems that the separate RGB counts contains significant information, however, more detailed investigation of this point is required for resolving this issue. The discrimination among three parchment groups: modern, historical and aged sample, based on the normalized blue counts, is available taking into account a 95% confidence interval. The correspondent probability plot is shown in **Figure 48**. Therefore, the digital color imaging is capable of the fast discrimination of parchment deterioration stage.

The considerable decrease of the blue counts in reflected light may be attributed to the shift of the absorption maximum from UV to visible spectral range [Torikai et al.].

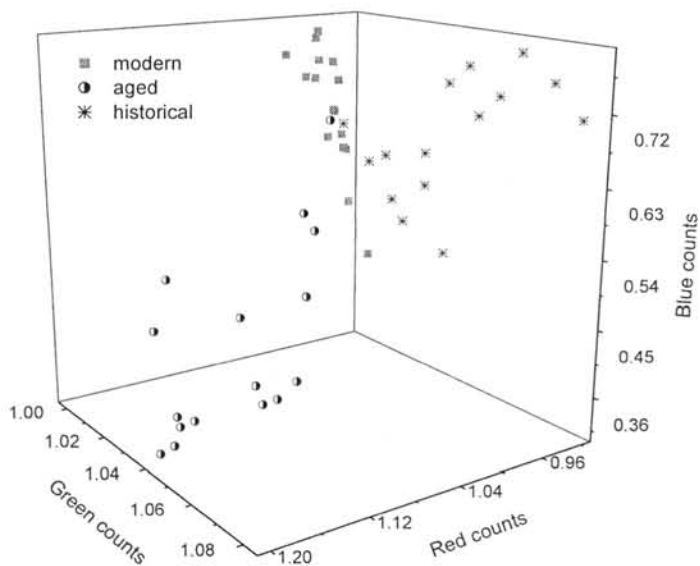


**Fig. 46:** Three-dimensional plot of normalized basic colors for different parchment groups.

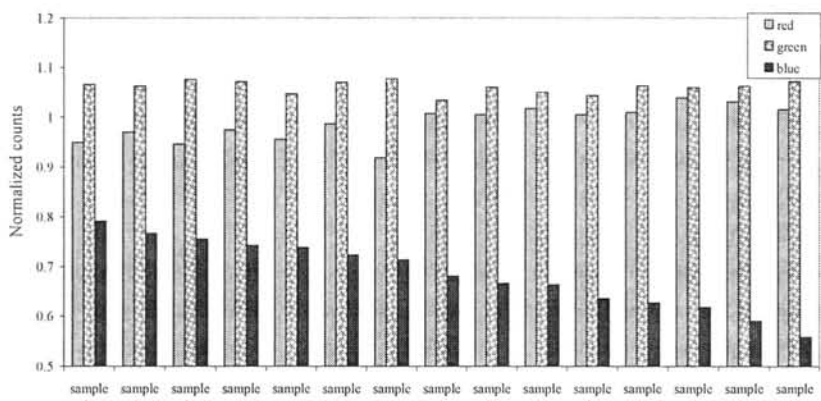


**Fig. 47:** Normalized counts of basic colors for historical samples.

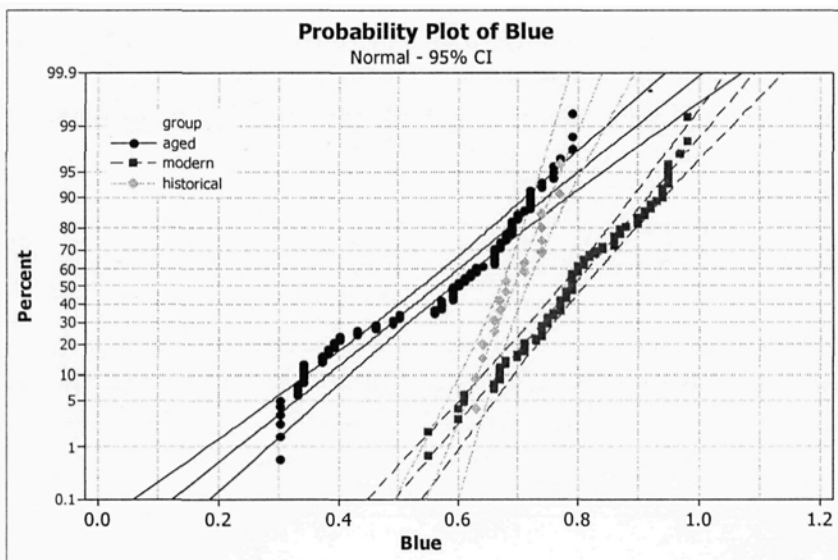


**Fig. 48:** Probability plot of the blue color for modern, historical and artificially aged samples.

### 2.5.2. Visible reflectance spectroscopy

Another simple and fast imaging technique is based on acquiring the reflection spectra of the parchment surface in the visible spectral region using an appropriate instrument. We used an NIR instrument with a wide spectral region (400-2500 nm) for this analysis.

#### 2.5.2.1. Experimental setup

Visible reflectance measurements of parchment samples were made using a FOSS grating spectrometer model 6500 (FOSS NIRSystems, Silver Springs, MD, USA). The spectral acquisition and the data treatment were performed using WinISI version 1.50 (developed by Infracsoft International<sup>®</sup>) software. A NIR diffuse reflectance spectrum was recorded as  $\text{Log}_{10}(1/R)$  (where R is diffuse reflectance) for each side of each sample as the average of 32 scans, over the wavelength range 400 - 2498 nm, at 2 nm increments (1050 data points). A standard ceramic was applied as a reference before each measurement. An averaged value of both sample sides at 470 nm was taken as a result for a comparison procedure.

### 2.5.2.2. Parchment characterization by visible reflectance imaging

The relationship between diffusively reflected spectral values involving the scattering of solid particles can be evaluated by means of the Kubelka-Munk mathematical transformation:

$$F(R) = \frac{(1-R)^2}{2R} = \frac{K}{S} \quad (3)$$

where  $K$  is the absorption coefficient,  $R$  is diffuse reflectance and  $S$  is the scattering coefficient. The scattering coefficient depends on the number, size, shape and refractivity of particles, while absorption coefficient depends on the absorbing species and the wavelength [Szalay et al.]. It may be stated that the diffuse reflectance ( $R$ ) is a function of  $K/S$  ratio. Smaller particles have a smaller  $K/S$  ratio, a lower absorbance, and hence a higher diffuse reflectance [Szalay et al.].

The mean value of visible reflectance from the parchment surface at 470 nm is presented in **Figure 49** for the modern, historical and artificially aged parchment samples. The deterioration changes the absorption and scatter properties of the parchment samples, in particular on the surface. During artificial aging, collagen molecules undergo cleavage into smaller fragments. As a parallel process, the color of the sample changes. The artificially aged samples have the highest value of  $\log(1/R)$  that is in correlation with previously cited findings. The modern samples demonstrate the smallest  $\log(1/R)$  value, thus, they should have the maximal particle size. Actually, the position of historical samples between the modern and the artificially aged samples is reasonable because the artificial aging makes the most of available deterioration and produces heavily deteriorated samples.

The statistically significant differences were found between parchment groups applying ANOVA at  $p=0.05$  value. Therefore, a visible reflectance from the parchment surface at 470 nm can serve as non-invasive, simple on-line method for parchment distinction. The fact that the single wavelength is sufficient for entire parchment characterization can lead to the development of a commercially available specialized NIR instrument. Additionally, an option of particle size estimation is relevant. The only thing needed is the proper calibration of the instrument with the standard size particles.

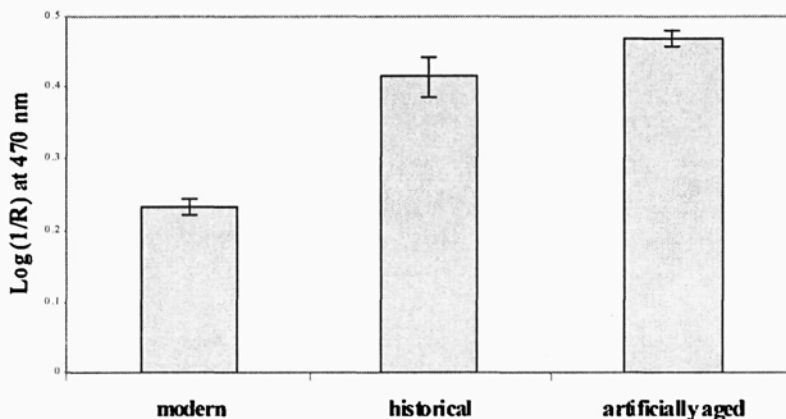


**Fig. 49:** Visible reflectance from the parchment surface at 470 nm for the modern, historical and artificially aged parchment samples.

## 2.6. Parchment characterization by Laser Induced Breakdown Spectroscopy and Inductively Coupled Plasma

Laser induced breakdown spectroscopy (LIBS) has been widely used in the microanalysis of various archeological samples: pigments in paintings, icons, ceramics and metals [Melessanaki et al.]. Recently, applications to biological aerosols [Hybl et al.; Morel et al.; Boyain-Goitia et al.] and to various tissues [Samck et al.; Corsi et al.; Akshaya et al.] have also been developed. LIBS was also applied for pattern classification [Hybl et al.; Sattmann et al.]. Cleaning of parchments and other organic fibrous materials by laser ablation has also been reported [Strli\_ et al.; Kautek et al., 1998; Kautek et al., 2000; Sportun et al.; Kollia et al; Cefalas et al.; Ali et al.]

The main advantages of LIBS are its portability and relative simplicity, low operational cost, short analysis time and no need for sample preparation. Therefore, LIBS is suitable for routine classification, where a large number of samples have to be analyzed. Moreover, when concerning precious samples (such as historical parchments), LIBS is preferred since it is practically non-destructive. It ablates only a few nanograms and the damage caused to the artifact is practically invisible.

The main goal of this research was to find a simple and reliable method for fast identification of historical parchment. Additionally, the possibility of classifying the animal from which the parchment was made is of interest. The

LIBS results have been compared to a standard laboratory technique - inductively coupled plasma spectroscopy (ICP) data.

### 2.6.1. Experimental procedure

#### 2.6.1.1. Clean parchment matrices preparation

Clean parchment matrices were prepared according to the following procedure: small pieces of parchment were placed in 10 ml double distilled water and shaken at room temperature for 24 hours. Two additional cycles were applied using fresh portions of water. The cleaned matrix samples were then dried in air at room temperature for 24 hours.

#### 2.6.1.2. LIBS measurements

The beam of Nd:YAG laser (Contium, Powerlite-8010, USA) operating at its fundamental wavelength (1064 nm, 7ns pulse duration, 1Hz repetition rate) was focused on the sample surface with a quartz lens ( $f=150$  mm). The laser energy was adjusted to 20mJ/pulse. The focused beam intensity was  $2.3 \cdot 10^9$  W cm<sup>-2</sup>. The emission of the plume was collected by a quartz optical fiber bundle and delivered to the entrance slit of monochromator (SpectraPro-500i, Acton Research Corporation, Acton, MS) coupled with a gated intensified CCD (ICCD) (Princeton Instruments, Trenton, NJ). Spectral resolution better than 0.2 nm was achieved using a 1200 grooves/mm grating. The effective wavelength range viewed by detector was about 40 nm. Atomic spectral lines used for identification of the elements are presented in **Table 6**.

**Table 6**  
Atomic spectral lines used for LIBS elemental analysis.

Element	Spectral line
Ca	429.90 (I)
Na	589.59 (I)
K	766.49 (I)
Mg	285.21 (I)
Fe	438.35 (I)
Cu	324.75 (I)
Mn	403.08 (I)

The detector was for a fixed time in order to eliminate the intense continuum emission immediately after the plasma formation. The delay between the laser pulse and the exposure was 1.5  $\mu\text{s}$  and the integration time was 2.0  $\mu\text{s}$  - 5.0  $\mu\text{s}$  (depending on the specific emission line of interest).

The sample was positioned 6 mm before the focal point of the lens. The spot diameter was smaller than 0.4 mm, and its exact size dependent upon the specific ablation characteristics of the parchment. The scheme of the analysis using LIBS is presented in **Figure 50**.

The detector was for a fixed time in order to eliminate the intense continuum emission immediately after the plasma formation. The delay between the laser pulse and the exposure was 1.5  $\mu\text{s}$  and the integration time was 2.0  $\mu\text{s}$  - 5.0  $\mu\text{s}$  (depending on the specific emission line of interest).

The sample was positioned 6 mm before the focal point of the lens. The spot diameter was smaller than 0.4 mm, and its exact size dependent upon the specific ablation characteristics of the parchment. The scheme of the analysis using LIBS is presented in **Figure 50**.

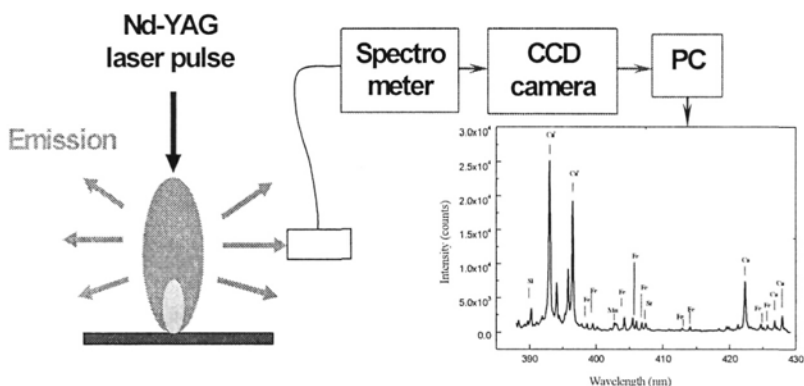


**Fig. 50:** Laser Induced Breakdown Spectroscopy setup.

Analysis was performed on 5 different spots, in order to average over local sample inhomogeneity. No difference was found in the homogeneity and reproducibility within a sample. However note that most of the samples (especially, the historical ones) were relatively small ( $\sim 5 \text{ cm}^2$ ).

*Depth profiling* was obtained by application of a series of laser shots to the same location. The pulse energy for depth profiling was 30mJ and the

focused beam intensity was  $3.5 \cdot 10^9 \text{ W} \cdot \text{cm}^{-2}$ . The ICCD gate width was  $10.0 \mu\text{s}$  for Fe, Mg, Cu, K, Mn and  $2.0 \mu\text{s}$  for Ca and Na. The number of laser pulses needed for depth profiling depends on the sample thickness (range of the samples thickness  $120\text{-}670 \mu\text{m}$ ) and color and varies from 100 to 270 shots.

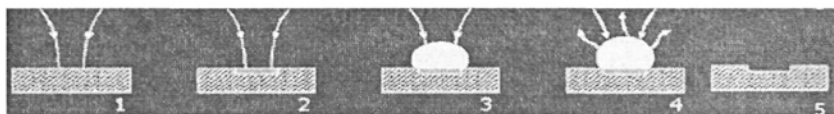


**Fig. 51:** Principle of Laser Induced Breakdown Spectroscopy: 1. Focusing of a pulsed laser beam on the sample surface; 2. heating; 3. material ablation; 4. plasma emission; 5. crater formation.

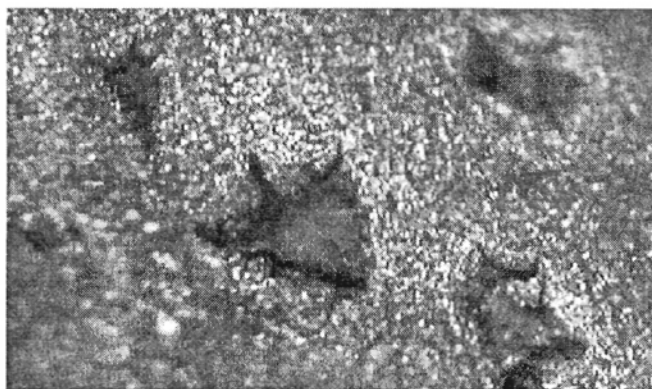


**Fig. 52:** Craters obtained in parchment samples during LIBS measurements.



**Fig. 53:** Principle of depth profiling using LIBS.

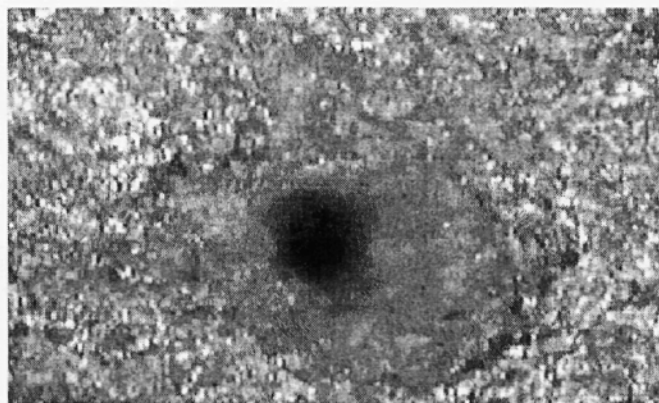


**Fig. 54:** Crater obtained in parchment samples during depth profiling LIBS measurements.

The etching process was examined first. Microscopic inspection of a crater produced by laser showed an almost cylindrical shape. No ablated/sputtered material was found on the crater bottom, indicating a clean ablation process. The etching process was also monitored microscopically as a function of the number of laser shots (**Figure 55**). For both modern and historical samples the crater depth was found to be linearly dependent on the number of shots applied.

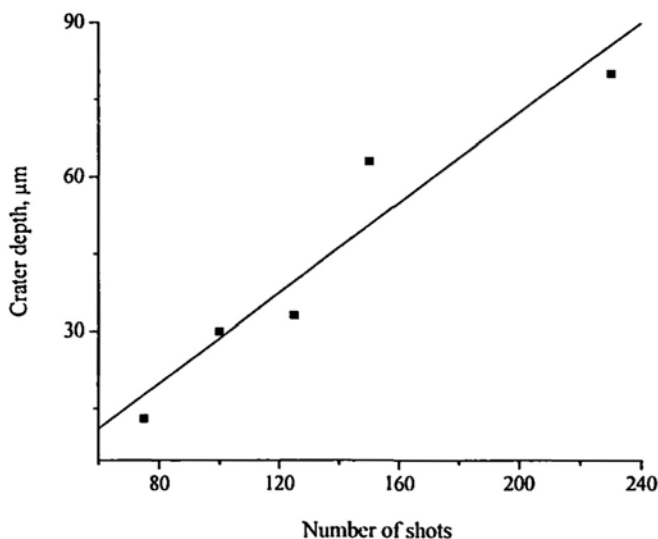


**Fig. 55:** The crater depth during LIBS profiling of parchment samples.

### 2.6.1.3. ICP measurements

Inductively Coupled Plasma Optical Emission Spectroscopy (ICP-OES) (Perkin Elmer Optima model 3000V) served as a reference technique for elemental analysis. Around 30 mg (dry weight) of parchment was ashed at 600°C. The ash was taken up in 10% (v/v) nitric acid (65%, Suprapur, Merck, Darmstadt, Germany) and dissolved completely. The total final volume was 10 ml and the total final concentration of the nitric acid was 2% (v/v). Multielemental standards (Exaxol Chemical Corporation, USA) were used for calibration at appropriate dilution.

## 2.6.2. Results and Discussion

### 2.6.2.1. Comparison to ICP analysis

It is well known that LIBS performance improves with the square root of the number of laser shots applied to the sample. However, in this study, we are concerned with characterization of precious parchments; therefore, we limited the analysis to no more than five laser shots of a relatively low laser power. As a result, data were acquired almost instantaneously and the damage was not observable by the naked eye.

ICP was used as reference, due to its high accuracy. Elemental analyses of parchments obtained by ICP have already been established, and it has been stated that the concentrations are directly correlated to the global parchment characteristics. However, there are substantial differences between these two methods, therefore, it is not clear that LIBS data can provide the same precise parchment characterization. The differences between ICP and LIBS which affect parchment characterization are discussed below.

LIBS provides *relative* detection limits in the low numbers of the ppm range, while ICP performs well in the low ppb. However, the *absolute* detection limits of LIBS, which are in the pg to ng range, are much better than obtained by ICP analysis. The main reason is related to the tiny amount of material ablated by a laser shot in most LIBS setups. Moreover, the best relative LODs in LIBS are obtained only when averaging over a large number of laser shots, which is not allowed when non-destructive analysis is required.

In this regard it should also be mentioned that while ICP requires time-consuming sample preparation and is relatively free of matrix effects, LIBS is an on-line method but its signal is matrix dependent. When dealing with parchment analysis, considerable matrix effects, related to sample color and

absorptivity, are experienced.

Moreover, while LIBS measures the surface elemental concentration, ICP provides the bulk concentrations. This could result in considerable discrepancies, since the elemental composition might depend on the sampling depth. On the other hand, LIBS is capable of examining full depth profiling (such data will be provided below).

In view of the aforementioned considerations, one cannot expect to obtain good elemental concentrations using single-shot LIBS, however, a statistical correlation between the ICP and LIBS signals is essential for developing a reliable marker. In order to examine the correlation between ICP and single-shot LIBS obtained from parchments, 7 minor and trace elements (Na, K, Mg, Ca, Fe, Cu and Mn) were analyzed in all our 54 parchment samples, by both methods. For the initial validation purpose, LIBS was applied to 5 different locations on the *grain* and on the *flesh* sample sides and the average signal was calculated.

Usually, the LIBS data must be properly calibrated (e.g., using an internal or added standard) in order to extract elemental concentrations. However, in our case, we were interested in the spectral intensities rather than in the actual elemental concentrations, therefore, the traditional calibration was not necessary. The reason is that the final goal was to correlate a simply measurable quantity (LIBS spectrum) to the parchment condition. Since the elemental concentrations are not important, the internal calibration may introduce unnecessary errors. On the other hand, comparison of the LIBS and ICP data requires a proper compensation for the LIBS instrumental function. For this purpose, the average LIBS values were scaled by a constant factor  $k$  ( $k$  minimized the function:

$$F(x_i, y_i) = \sum_{i=1}^n (x_i - ky_i)^2 \quad (4)$$

where  $x_i$  are the LIBS values and  $y_i$  are the corresponding ICP values).

The reason for the scaling procedure was the performance of the measurements in different spectral frames without taking into account the difference in the wavelength dependence of the ICCD sensitivity. The scaled LIBS values were compared to the corresponding ICP data using the paired  $t$ -test at 0.01 significance level and the resulting two-tail  $p$  values are reported in **Table 7**. It means that there is a 99.9% probability that the null hypothesis,

which states that there is no difference between the results obtained by the two methods, (other than that which can be attributed to random variations) can be retained. The results in **Table 7** indicate that this is valid for all examined elements besides Cu. A good correlation obtained between the LIBS and ICP mean values can be observed in **Figure 56**.

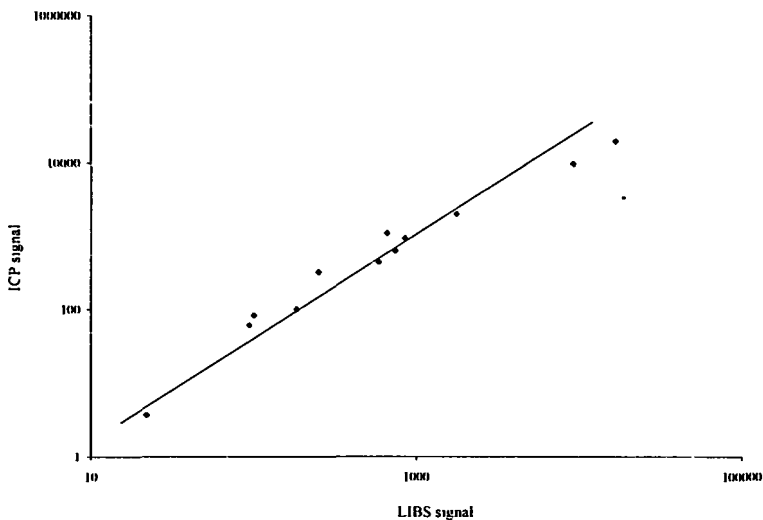


**Fig. 56:** Correlation between LIBS and ICP signals.

**Table 7**  
Correlation between single-shot LIBS and ICP data

Element	$p( t  \geq t_{critical})$ (two-tailed)
Fe	0.82
K	0.70
Mg	0.70
Na	0.63
Mn	0.54
Ca	0.20
Cu	<0.01

### 2.6.2.2. Animal type identification

It is known that sheep skin contains statistically significant more manganese than goat skin [Onwuka et al.]. The same is true also for iron. However the reported differences were not statistically significant. The reasons for these differences are unclear and are presumably related to animals' metabolism and nutrition. Since identification of the animal type is often required for parchment restoration procedures, a simple marker would be useful.

**Table 8**  
Results of modern parchment analysis according to animal type.

Element	Method	Mean Concentration ( $\mu\text{g/g}$ ) $\pm$ SD of the mean		
		Calf (8 samples)	Goat (5 samples)	Sheep (4 samples)
Ca	ICP	4459 $\pm$ 835	5955 $\pm$ 1905	10652 $\pm$ 3053
	LIBS	4791 $\pm$ 1261	5402 $\pm$ 1778	11915 $\pm$ 3851
Na	ICP	314 $\pm$ 45	292 $\pm$ 50	267 $\pm$ 34
	LIBS	474 $\pm$ 61	454 $\pm$ 89	759 $\pm$ 255
K	ICP	62 $\pm$ 10	69 $\pm$ 17	53 $\pm$ 17
	LIBS	144 $\pm$ 20	102 $\pm$ 17	269 $\pm$ 102
Mg	ICP	355 $\pm$ 54	422 $\pm$ 169	488 $\pm$ 71
	LIBS**	516 $\pm$ 53	802 $\pm$ 112	1088 $\pm$ 142
Fe	ICP	44 $\pm$ 7	41 $\pm$ 4	59 $\pm$ 18
	LIBS**	53 $\pm$ 6	81 $\pm$ 13	107 $\pm$ 11
Cu	ICP	1.1 $\pm$ 0.4	0.3 $\pm$ 0.2	not detected
	LIBS	26 $\pm$ 7	15 $\pm$ 3	21 $\pm$ 4
Mn	ICP	1.3 $\pm$ 0.2	2.5 $\pm$ 0.6	3.5 $\pm$ 1.3
	LIBS	1.9 $\pm$ 0.3	3.5 $\pm$ 1.3	4.6 $\pm$ 1.4
(Fe/Mn)	ICP**	35 $\pm$ 3	22 $\pm$ 6	18 $\pm$ 9
	LIBS	32 $\pm$ 7	40 $\pm$ 17	35 $\pm$ 11
(Mg/Cu)	LIBS*	29 $\pm$ 9	61 $\pm$ 15	54 $\pm$ 11

The difference between groups is significant at  $p = 0.01$ (\*\*) and  $p = 0.05$  (\*)level.

**Table 8** presents the elemental distribution in parchments derived from different animals: calf, goat and sheep. Both ICP and LIBS data are provided. Applying ANOVA, statistically significant differentiation between the

groups, at  $p = 0.01$  level, was obtained for the Mg and Fe LIBS signals. By applying statistical evaluations, we found that the (Fe/Mn) ratio is a useful linear marker for rapid identification of the animal type in parchment characterization by ICP. When using the LIBS data, the intensity ratio of (Mg/Cu) was found as the most significant marker at  $p = 0.05$  level for the animal type recognition.

### 2.6.2.3. Markers for identifying ancient specimens

Generally, it has already been recognized that the elemental composition of parchments may be indicative of their age [Larsen]. The explanation is not clear, but this could be attributed to the production procedures, to the chemicals used for skin processing, or even to variations in animal nutrition. Therefore, the possibility of applying LIBS to fast identification or verification of historical parchments should be feasible. We looked for possible markers for identifying the ancient parchment specimens.

Several elemental signals, or combinations of signals, can be examined for providing the required differentiation between ancient and modern parchments, therefore statistical evaluation is required. For this purpose we applied the *t*-test for comparison of the two groups, assuming unequal variances. We only considered such markers that are statistically significant at significance levels of 0.01 (or 0.05), i.e. reject the null hypothesis that there is no difference between the groups (rather than that which can be attributed to random variations). It means that we look for such markers that may be false with a probability lower than 1% (or 5%). We provide more detailed information on the various elemental signals below. The LIBS results for ancient and modern samples are presented in **Table 9** and the corresponding ICP data in **Table 10**.

Let us examine the data in detail:

*Na, K:* One can clearly distinguish between modern and ancient samples, when measured by the ICP method, since ancient parchments are considerably richer in these elements. Similar results are obtained from the corresponding LIBS intensities. However, the distinction is less significant than that obtained by the ICP. It is interesting to note that the LIBS intensities of elemental K provide a better marker than the ICP concentrations (significance level of 0.01 for LIBS and 0.05 for ICP). This can be attributed to the fact that LIBS signals are subjected to considerable matrix effects, which, in turn, are related to sample's conditions.

**Table 9**  
LIBS markers for ancient/modern samples.

Element	Mean LIBS intensity $\pm$ SD of the mean	
	Modern samples	Historical samples
Ca**	9302 $\pm$ 1113	16803 $\pm$ 1921
Na**	585 $\pm$ 51	1777 $\pm$ 180
K**	183 $\pm$ 19	849 $\pm$ 153
Mg	740 $\pm$ 47	658 $\pm$ 93
Fe**	98 $\pm$ 10	249 $\pm$ 40
Cu*	22 $\pm$ 2	92 $\pm$ 38
Mn**	4 $\pm$ 1	18 $\pm$ 3

\* - The difference between modern and historical samples is significant at  $p = 0.05$

\*\* -  $p = 0.01$ ) level.

**Table 10**  
Concentration (ICP-OES) makers for ancient/modern samples.

Element	Concentration ( $\mu\text{g/g}$ ) $\pm$ SD of the mean	
	Modern samples	Ancient samples
Ca**	9508 $\pm$ 996	19329 $\pm$ 2068
Na**	432 $\pm$ 56	2012 $\pm$ 393
K*	100 $\pm$ 14	912 $\pm$ 342
Fe	82 $\pm$ 10	319 $\pm$ 151
Mg	617 $\pm$ 68	1065 $\pm$ 328
Cu	4 $\pm$ 2	61 $\pm$ 47
Mn**	3.1 $\pm$ 0.3	28 $\pm$ 7

\* - The difference between modern and historical samples is significant at  $p = 0.05$  level.

\*\* - The difference between modern and historical samples is significant at  $p = 0.01$  level.

Ca: The Ca concentration is also expected to provide good parchment characterization, since its manufacturing involves treatment with calcium containing chemicals (CaO, CaSO<sub>4</sub>, CaCO<sub>3</sub>). We found that the Ca

concentration in ancient samples, measured by both methods, is higher than in the modern ones. This seems to be attributed to the ancient technology that enriched the parchment matrix in calcium. This finding correlates well with previously reported results [Larsen, Mannucci et al.]. Ca concentration is a statistically significant marker (at  $p < 0.01$  level) for the difference between modern and ancient samples in both techniques.

*Cu*: The trace amount of Cu found in our parchments correlates well with the values reported in previous publications [Larsen]. A statistically significant difference (at  $p = 0.05$  level) was found between the LIBS signals of Cu in ancient and modern samples, however the ICP data is a much less significant marker. In the statistical evaluation, sample 14 (the one containing painting residues) was an outlier with very high Cu concentration. This is attributed to the painting pigments (e.g., azurite, malachite, emerald green, etc.) that contain copper [Anglos].

*Fe*: The mean Fe concentration in the modern samples was smaller than in the ancient samples. The highest concentration was found in sample number 21 (written parchment from the 16th century), due to the gall ink that contains iron. The statistical evaluation indicates a significant difference (at  $p = 0.01$  level) between the Fe LIBS-signals in ancient and modern samples.

*Mn*: Ancient parchments are richer in manganese, due to the abundance of this element in natural calcite [Larsen]. A statistically significant difference (at  $p = 0.01$  level) was found between the signals of Mn in ancient and modern samples for both LIBS and ICP.

*Mg*: The magnesium signals provide no significant correlation to the parchment's age.

*Markers*: In view of the above findings, each of the statistically different elements acts as a simple marker that can be used for the fast identification of ancient parchments that was required. Graphic presentation of the differences observed in the modern and historical parchment samples is shown in **Figure 57**. In fact, each of the elements Ca, Na, K, Fe and Mn can serve as such markers.

#### 2.6.2.4. Discriminant analysis based on LIBS

Discriminant analysis based on the three elements (Ca, Fe, Mg) calculating Euclidian distance was performed. The ratio of the LIBS integral intensity to the background was used, and the resulted discriminant groups are shown in **Figure 58**. A clear distinction between the two groups of the

modern and historical parchments is observed. The detailed explanation concerning principles of discriminant analysis is provided in chapter 2.11.4.1.

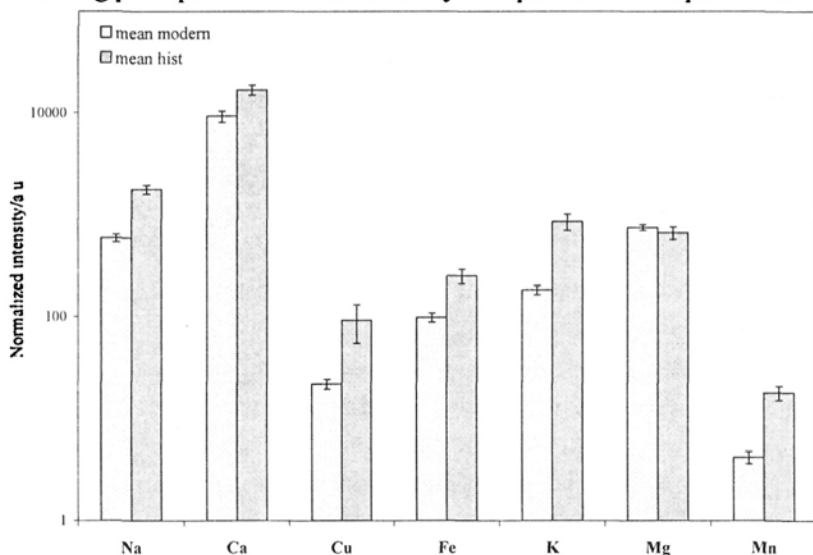


**Fig. 57:** Differences observed in normalized LIBS signal in modern and historical parchment samples.

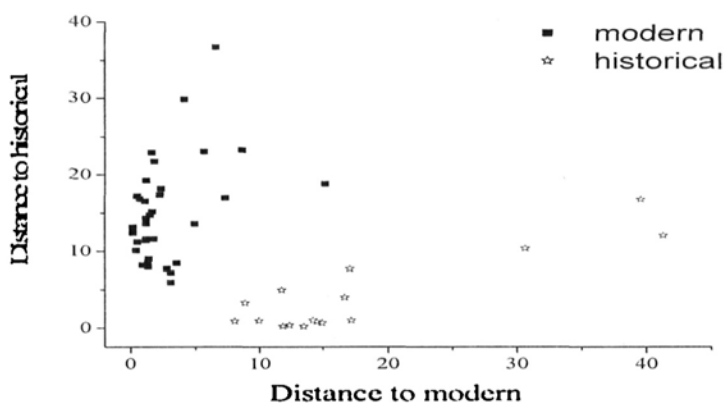


**Fig. 58:** Parchment samples grouping according to discriminant analysis results.

#### 2.6.2.5. Depth profiling

The LIBS method allows depth profiling, by repeatedly probing the same spot by the laser. Then, the signals provide relative concentrations of various

elements of interest as a function of probing depth. Two factors contribute to the actual depth profile of a given element: (a) the core composition, which is most probably related to the animal skin origin, and (b) the material added to the parchment during its processing and the later occasional contaminations.

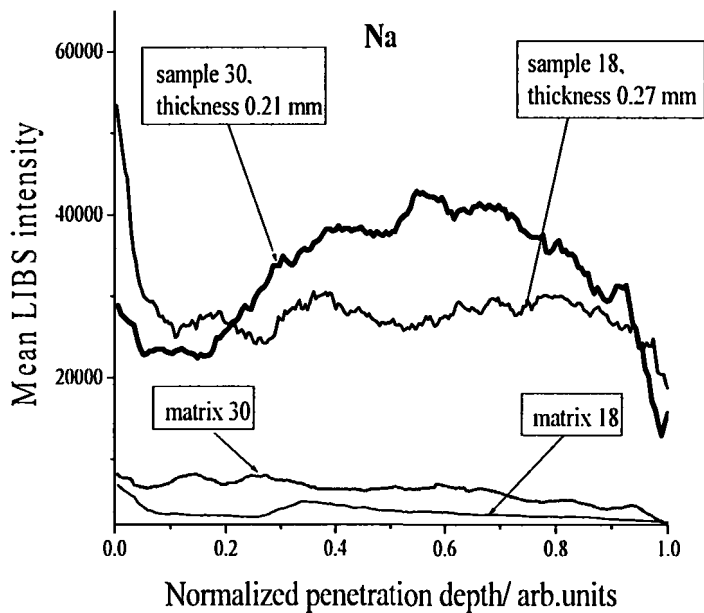
The discrimination among these two components is essential for the restoration and preservation. No commonly used method was found for the parchment matrix in literature. Therefore, we developed an experimental procedure for this purpose, by washing the samples as described in the experimental session. Thus the washed samples will be referred as the “clean matrix”. This concept of preparation, if successful, additionally permits self-made reference material preparation. Having a reference material for such a complicated matrix as the parchment can really improve the accuracy of analysis. The reasons for that are: 1) The analyte used can be fitted for the purpose; 2) It can be used for the preparation of different analyte concentrations (calibration curve) in a matrix similar to the routine analysis matrix.

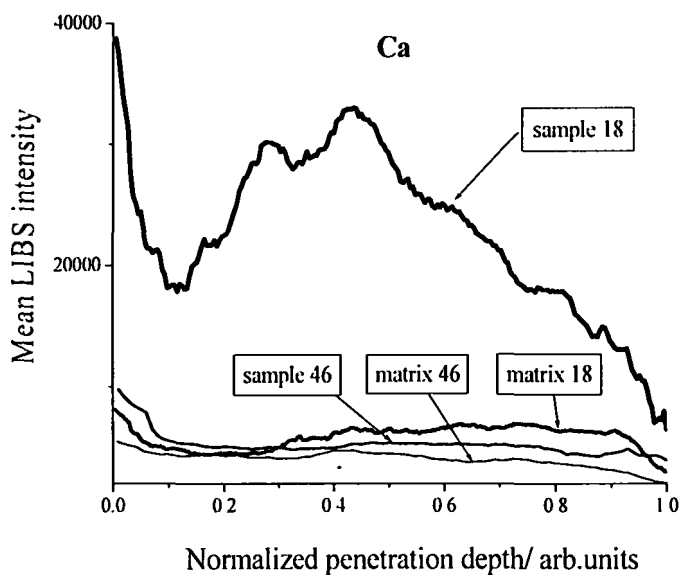
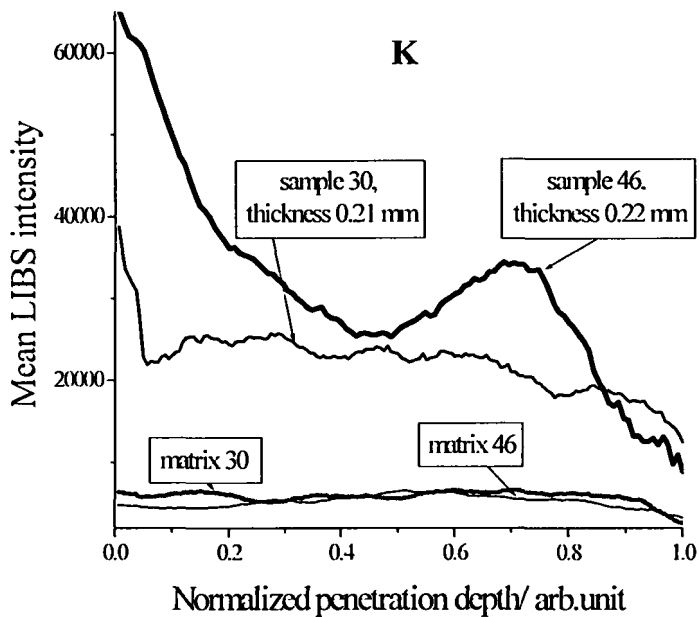
Some results of the parchment depth profiling are presented in **Figures 59**. As was expected, the concentration of the checked elements in the original samples is significantly higher than in the clean matrix. Especially, surface elemental content is much higher than in the core. Elemental distribution in a clean matrix is much more homogeneous than that of original samples. Ca content in historical samples is much higher than in the modern ones. This fact correlates with our surface measurements and previously published works discussed earlier. The experimental curves of depth profiling are non-symmetrical due to matter ablation from the opposite side of the examined sample during the experiment.

Interestingly, Cu and Fe concentrations through depth profile do not change (besides for the thin surface layer), neither for original samples nor for the clean matrix. Since the collagen three-dimensional structure contains no metal atoms in its internal structure, we may conclude that the penetration of Cu and Fe into the parchment matrix took place by diffusion from the surface. Transference of Cu and Fe to the surface over the lifetime of the artifact is probably related to the presence of these elements in atmospheric dust.

The measurements of magnesium depth profile indicate that it may be correlated to the animal type from which the the parchment is made. Five different types of depth profile can be observed in **Figure 60**, relating to

different animals. In this respect, note that the Mg LIBS signals from the surface also provide statistically significant characterization of the animal type. A future work including a larger set of parchment samples of known animal type can be provided to prove our assumption.





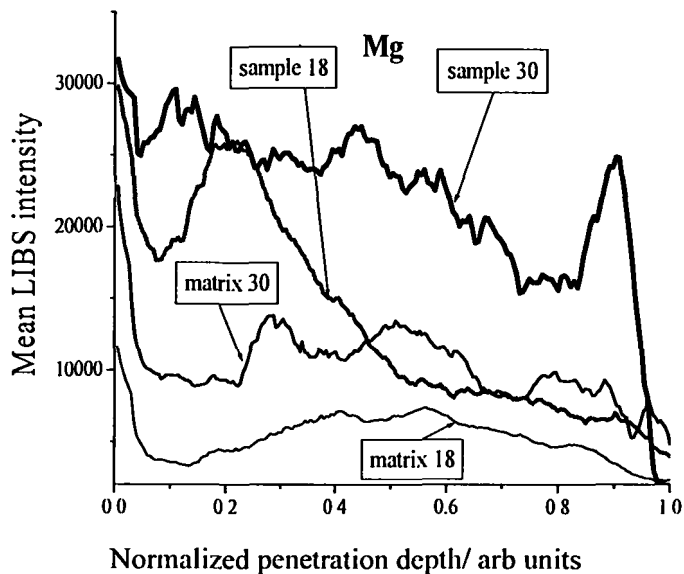


**Fig. 59:** Depth profile of the original parchment samples and the corresponding clean matrices (sodium, potassium, calcium, magnesium).

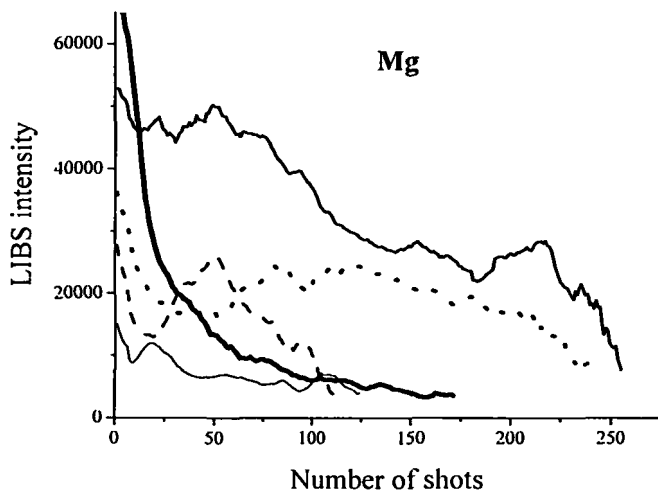


**Fig. 60:** Magnesium depth profiles of modern and historical parchment samples.

### 2.6.2.6. Additional ICP measurements

ICP was successfully applied for the detection of some additional elements in parchment samples. Statistically significant differences (at 95% confidence level) between the modern and historical samples were found (see Table 11). The manufacturing process as well as the animal's nutrition is responsible for the presence of the specific elements in parchment samples.

**Table 11**  
Additional ICP measurements.

	Mean Concentration ( $\mu\text{g/g}$ ) $\pm$ SD of the mean	
	Modern	Historical
Pb	5 $\pm$ 1	47 $\pm$ 22
Th	13 $\pm$ 2	7 $\pm$ 1
Sb	5.1 $\pm$ 1.1	2.2 $\pm$ 0.3
Mo, As, V	not detected	detected

### 2.7. Ion chromatography

During manufacturing, parchment is processed with different solutions containing organic and inorganic substances, therefore, different salts can be found on a parchment surface. Additionally, the environmental pollutants (for example, SO<sub>2</sub>, NO<sub>2</sub>, CO<sub>2</sub>) reacting with a parchment surface in a humid atmosphere may contribute to contamination producing acids. These acids cause water-soluble salts to form from the insoluble ones. Thus, the soluble salts can penetrate deeper into the porous parchment surface and later recrystallize on or just under the surface of the artifact causing damage. In the worst cases, a large area of an artifact can be deteriorated. To stop salt deterioration, once it has begun, a conservator should develop a preservation strategy that takes into account the parchment matrix and the concentration of particular salts causing the deterioration.

Ion chromatography is a useful technique for measurement of cations and anions concentration in solution at part-per-billion level. The use of ion chromatography in detection of some ions (chloride, nitrate, sulfate) on the surface of parchment samples was successfully applied [Larsen]. In this cited

study, the difference in calcium as well as chloride content between the modern and the historical samples was found.

In our study, parchment samples were analyzed using ion chromatography for the Li<sup>+</sup>, Na<sup>+</sup>, K<sup>+</sup>, Ca<sup>2+</sup>, Mg<sup>2+</sup>, N (in the NH<sub>4</sub><sup>+</sup>, NO<sub>3</sub><sup>-</sup>, NO<sub>2</sub><sup>-</sup> form), Cl<sup>-</sup>, Br<sup>-</sup>, CH<sub>3</sub>COO<sup>-</sup>, C<sub>2</sub>O<sub>4</sub><sup>2-</sup>, SO<sub>4</sub><sup>2-</sup>, PO<sub>4</sub><sup>3-</sup> content. The results have been compared to conductivity measurements and good correlations were obtained. Discriminant analysis has been applied to ion chromatography data and a chemometrical model for ancient samples distinction was developed. Additionally, identification of the animal type from which the parchment is made is possible based on ion chromatography data.

### 2.7.1. Experimental procedure

Conductivity ( $k$ ) is inversely proportional to resistance and measured in a standard cell with electrodes of 1 cm<sup>2</sup> area held 1 cm apart. The conductivity can be measured by multiplying the conductance value (1/R) by the conductivity cell constant  $K$ :

$$k = K \cdot \frac{1}{R} \quad (5)$$

Concentration can then be calculated from Kohlrausch's Law, which states that the total conductivity of a solution is the sum of the individual conductivities of its ionic constituents, multiplied by each ion's ionic limiting equivalent conductivity  $C^\circ$ :

$$k = \frac{\sum_i \lambda^\circ_i c_i}{1000} \quad (6)$$

Chromatographic detection of ions follows five steps: injection, separation, suppression, detection and recording. An aqueous solution is injected into a stream of mobile phase. The ions to be detected are separated on the basis of their affinity for the resins functional groups within the guard and analytical column. The guard column is used to prevent undesired and damaging impurities from penetrating to the analytical column. During the suppression step, a conductivity suppressor is used to decrease the background conductivity of the eluent while increasing the conductivity of

the analyte. A detector measures the conductivity of the analyte against that of the eluent, and records it in terms of retention time and conductivity.

#### **2.7.1.1. Parchment samples**

Around 25 mg of each parchment sample was cut into small fragments, weighted and extracted shaking at room temperature with 5 ml double distilled (18 M $\Omega$ /cm resistance) water for 24 hours. After extraction, the supernatant was filtered through a 0.45  $\mu$ m membrane based filter to avoid blockages or damage to connecting tubing, column end frits. Samples were injected into the ion chromatograph after appropriate dilution.

#### **2.7.1.2. Chromatographic setup**

The instrument used was a Dionex model DX-100. The system consisted of: GP50 Gradient Pump, LC20 Chromatography Enclosure with a rheodyne injection valve, ED50A Electrochemical Detector and Chromeleon<sup>®</sup> Chromatography Workstation.

The separation of anions was performed at a flow rate of 2mL/min using the IonPac AS4A-SC, 250 x 4 mm column, 1.8 mM Sodium carbonate/ 1.7 mM Sodium bicarbonate eluent and suppressed conductivity detection at self-regenerating mode (applied current 27 mA). System backpressure was 1280 psi and background conductance was 14  $\mu$ S. All the anions were well resolved within a total run time of less than 10 min.

The separation of cations was performed at 1mL/min flow rate using the IonPac CS12A, 250 x 4 mm column, 18mM methanesulfonic acid eluent and suppressed conductivity detection at self-regenerating mode (applied current 75 mA). System backpressure was 1350 psi and background conductance was 3  $\mu$ S. All the cations are well resolved within a total run time of less than 15 min.

The injection volume for cations and anions determination was 25  $\mu$ L. The calibration was performed using commercially available standards (Exaxol Chemical Corporation, USA) after appropriate dilution. The method linearity was determined for all ions over a five-point calibration range. At least two repeat injections of each sample were performed for quantification (RSD<2%). The typical chromatograms for the separation of the standard solutions of cations and anions as well as modern and historical parchment samples are shown in **Figures 61 -66**.

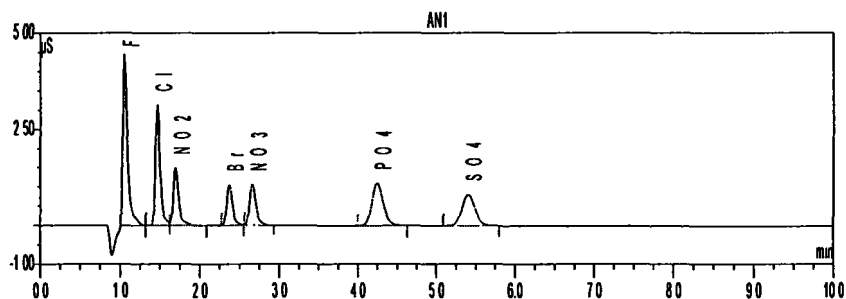


**Fig. 61:** Separation of anions standard solution. Conditions: column, Dionex® IonPac® AS4A-SC, 4 x 250 mm column, eluent 1.8 mM Sodium carbonate/ 1.7 mM Sodium bicarbonate eluent and suppressed conductivity detection at self-regenerating mode (applied current 27 mA), injection volume, 25 µL; solutes, 1) fluoride (2 ppm), 2) chloride (2 ppm), 3) nitrite (2 ppm), 4) bromide (2 ppm), 5) nitrate (2 ppm), 6) phosphate (6 ppm), 7) sulfate (2 ppm).

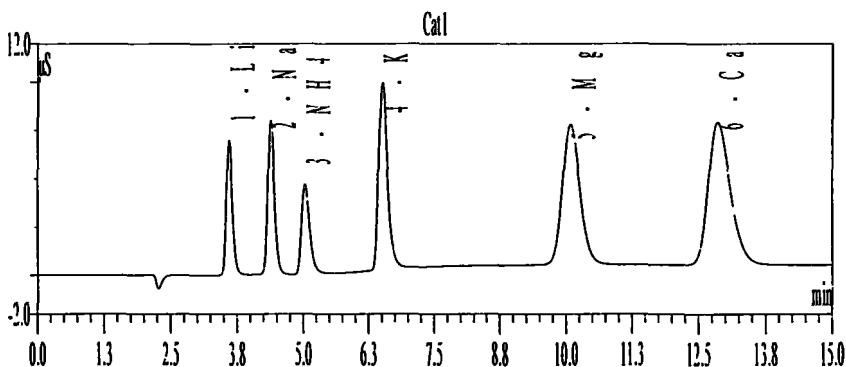


**Fig. 62:** Separation of cations standard solution. Conditions: column, Dionex® IonPac® CS12A; eluent, 18mM methanesulfonic acid; flow rate, 1.0mL/min; detection, suppressed conductivity with a cation self-regenerating suppressor (CSRS) operated at 75mA in self-regenerating mode; injection volume, 25 µL; solutes, 1) lithium (1 ppm), 2) sodium (4 ppm), 3) ammonia (5 ppm), 4) potassium (10 ppm), 5) magnesium (5 ppm), 6) calcium (10 ppm).

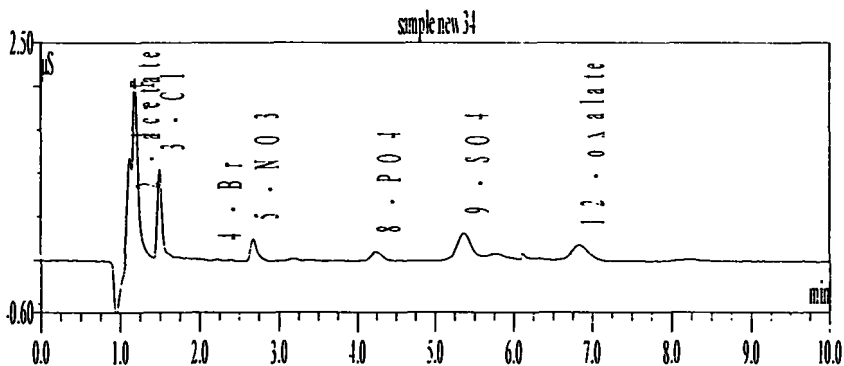


**Fig. 63:** Separation of anions in solution of modern sample. Conditions: column, Dionex® IonPac® AS4A-SC, 4 x 250 mm column, eluent 1.8 mM Sodium carbonate/ 1.7 mM Sodium bicarbonate eluent and suppressed conductivity detection at self-regenerating mode (applied current 27 mA), injection volume, 25 µL; solutes, 1) fluoride, 2) acetate, 3) chloride, 4) bromide, 5) nitrate, 8) phosphate, 9) sulfate, 12) oxalate.

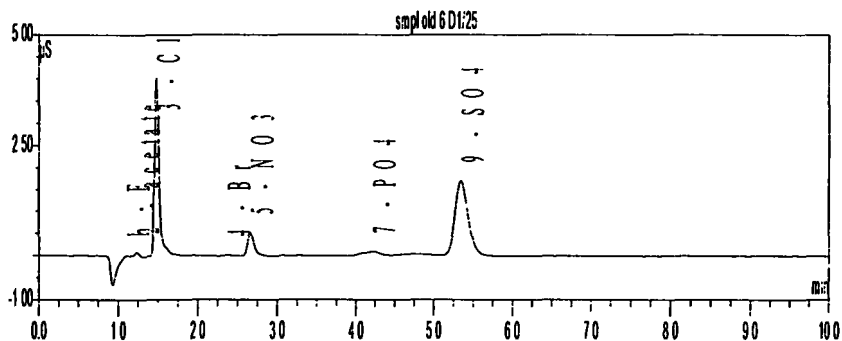


**Fig. 64:** Separation of anions in solution of historical sample. Conditions: column, Dionex® IonPac® AS4A-SC, 4 x 250 mm column, eluent 1.8 mM Sodium carbonate/ 1.7 mM Sodium bicarbonate eluent and suppressed conductivity detection at self-regenerating mode (applied current 27 mA), injection volume, 25 µL; solutes, 1) fluoride, 2) acetate, 3) chloride, 4) bromide, 5) nitrate, 7) phosphate, 9) sulfate.

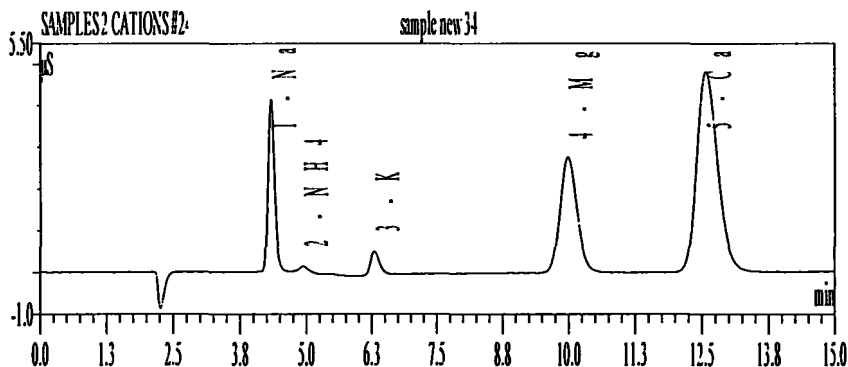


**Figure 65.** Separation of cations in solution of modern sample. Conditions: column, Dionex® IonPac® CS12A; eluent, 18mM methanesulfonic acid; flow rate, 1.0mL/min; detection, suppressed conductivity with a cation self-regenerating suppressor (CSRS) operated at 75mA in self-regenerating mode; injection volume, 25 µL; solutes, 1) sodium, 2) ammonia), 3)potassium, 4) magnesium, 5) calcium.

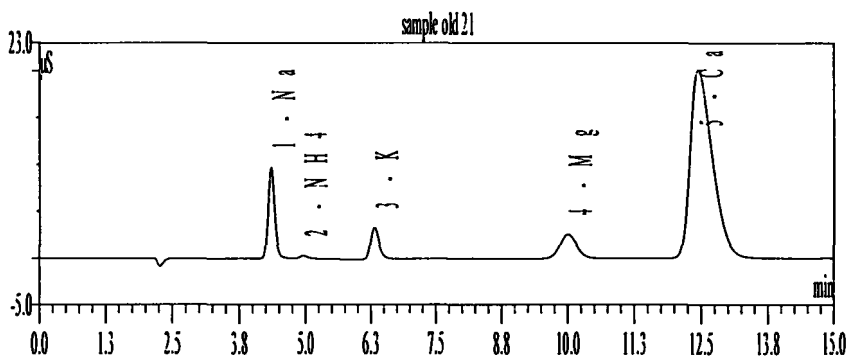


**Figure 66.** Separation of cations in solution of historical sample. Conditions: column, Dionex® IonPac® CS12A; eluent, 18mM methanesulfonic acid; flow rate, 1.0mL/min; detection, suppressed conductivity with a cation self-regenerating suppressor (CSRS) operated at 75mA in self-regenerating mode; injection volume, 25 µL; solutes, 1) sodium, 2) ammonia), 3)potassium, 4) magnesium, 5) calcium.

### 2.7.2. Parchment characterization by ion chromatography

The detection of several ions in parchment samples was performed using ion chromatography. Statistically significant differences between modern and historical parchment samples were found in cations ( $\text{Na}^+$ ,  $\text{K}^+$ ,  $\text{Ca}^+$ , total cations) as well as anions ( $\text{Cl}^-$ ,  $\text{NO}_2^-$ ,  $\text{Br}^-$ ,  $\text{NO}_3^-$ ,  $\text{SO}_4^{2-}$ ,  $\text{PO}_4^{3-}$ , total anions) content (Table 12). Additionally, fast evaluation of damage from the specific environmental or other pollutants is possible based on the ion chromatographic separation.

**Table 12**

Ion content in modern and historical parchment samples.  
**Bold font** indicates the statistically significant difference between modern and historical samples at  $p = 0.01$  level.

Ion	Mean concentration ( $\mu\text{eq/g}$ ) $\pm$ SD of the mean	
	Modern samples	Historical samples
<b>Cations</b>		
$\text{Li}^+$	N.D.	N.D.
$\text{Na}^+$	16 $\pm$ 1	84 $\pm$ 15
$\text{NH}_4^+$	16 $\pm$ 4	28 $\pm$ 10
$\text{K}^+$	3.7 $\pm$ 0.5	26.9 $\pm$ 4.5
$\text{Mg}^{2+}$	21 $\pm$ 2	32 $\pm$ 6
$\text{Ca}^{2+}$	98 $\pm$ 7	404 $\pm$ 49
<b>Total cations</b>	155 $\pm$ 10	575 $\pm$ 67
<b>Anions</b>		
$\text{F}^-$	5 $\pm$ 1	9 $\pm$ 2
$\text{CH}_3\text{COO}^-$	74 $\pm$ 11	79 $\pm$ 20
$\text{Cl}^-$	18 $\pm$ 6	144 $\pm$ 28
$\text{NO}_2^-$	1.2 $\pm$ 0.2	0.6 $\pm$ 0.4
$\text{Br}^-$	0.04 $\pm$ 0.01	1.06 $\pm$ 0.15
$\text{NO}_3^-$	5 $\pm$ 1	120 $\pm$ 29
$\text{PO}_4^{3-}$	5 $\pm$ 1	75 $\pm$ 30
$\text{SO}_4^{2-}$	7 $\pm$ 1	152 $\pm$ 46
$\text{C}_2\text{O}_4^{2-}$	1.9 $\pm$ 0.3	2.5 $\pm$ 0.2
<b>Total anions</b>	118 $\pm$ 12	583 $\pm$ 72

The manufacturing process is mainly responsible for the presence of ions on parchment surface. The ancient and modern parchment manufacturing processes use practically the same methods of treatment. Similarly, tools and equipment are virtually the same; the main difference being in the chemicals used. In order to highlight the differences in ion content, we will examine the data in detail, starting with cations:

*Li*: The presence of lithium in parchment samples is not expected. It was not detected in all examined samples.

*Na, K*: The presence of these elements at high concentration is expected. Firstly, table salt containing sodium is used regularly for drying the skin during the manufacturing process. Potassium is an abundant element in the earth's crust. One can clearly distinguish between modern and historical samples using sodium and potassium content, since historical parchments are considerably richer in these elements. Na and K concentration is a statistically significant marker (at  $p < 0.01$  level) for differentiation between modern and historical samples.

*NH<sub>4</sub>*: Ammonia is sometimes used in cleaning out acids after the tanning process and in the permanent discoloring of pigments, therefore, it presented in high concentration in both modern and historical samples, and no statistically significant difference was found between them. Note that the concentration in historical samples is somewhat higher than in the modern ones.

*Ca*: The calcium concentration was also expected to provide good parchment characterization, since the manufacture involves treatment with calcium containing chemicals (CaO, CaSO<sub>4</sub>, CaCO<sub>3</sub>). We found that the Ca concentration in historical samples was higher than in the modern ones. This seems to be attributed to the ancient technology that enriched the parchment matrix in calcium. This finding correlates well with previously reported results [Larsen]. Ca concentration is a statistically significant marker (at  $p < 0.01$  level) for the difference between modern and historical samples.

*Mg*: Magnesium is a relatively abundant element in the earth's crust and hence a common constituent of natural water. Grease spots are treated with magnesium oxide during the parchment manufacturing; moreover, its presence can be explained by the animal's nutrition. No statistically significant difference was found between modern and historical samples (at  $p < 0.01$  level), other than the concentration in historical samples was higher than in the modern ones.

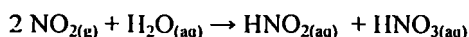
We continue with the examination of anions:

*F*: Fluoride presented in a small amount in both modern and historical parchment samples, and no statistically significant difference between them was found.

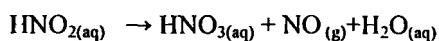
*Acetate*: The presence of acetate in the parchment samples was in surprisingly considerable amounts, and its origin is unclear. No statistically significant difference was found between modern and historical samples.

*Cl, Br*: The presence of chloride and bromide ions in a parchment sample is predictable because table salt contains chloride ions, used for drying and disinfection of skin and both chloride and bromide ions are present in sea water, used for washing the skin in the parchment manufacturing process instead of urban water due to its relatively high cost. The higher chloride and bromide content in historical samples can be explained by the fact that today the regular urban water is used for washing the skin in the manufacturing process.

*NO<sub>2</sub>, NO<sub>3</sub>*: The air pollutant NO<sub>2</sub> can undergo reactions on parchment surface, leading to formation of the nitrous and nitric acids:



Nitrous acid is an intermediate stage in the nitrogen cycle; it is unstable in solution and decomposes rapidly according to the following reaction:



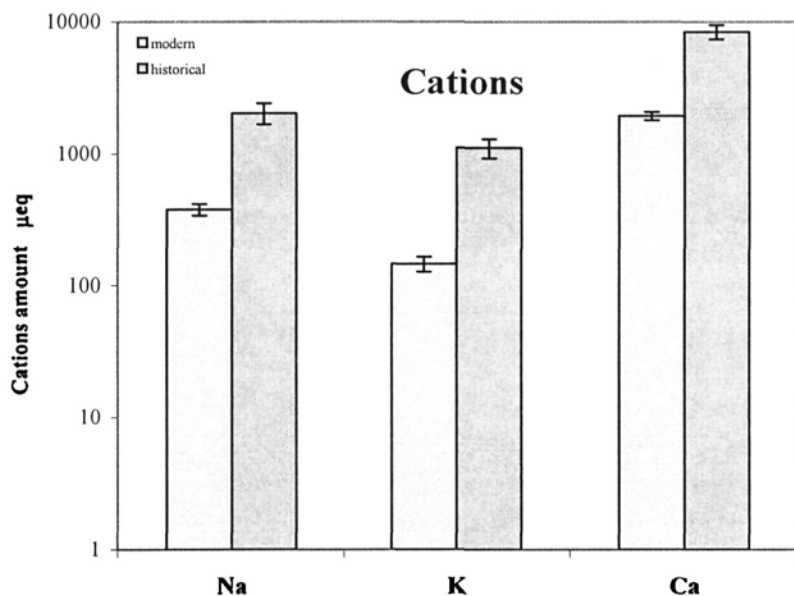
Therefore, nitrite is present in a sufficient amount in modern samples only, and the amount of nitrate on parchment surface is much higher for the historical samples. Nitrate and nitrite are statistically significant markers (at  $p < 0.01$  level) for distinction between modern and historical samples.

*SO<sub>2</sub>*: Sulphurous chemicals are used in the manufacturing process and later are converted to sulphuric acid. Sulphuric acid reacts with calcium carbonate present on the parchment surface to produce calcium sulphate. Sulfate is present in higher amounts in historical samples and can serve as a marker for distinction between parchment samples. This finding correlates well with previously reported results [Larsen].

*PO<sub>4</sub>*: Phosphate is present in higher amounts in historical samples and can serve as a marker for distinction between parchment samples.

**Oxalate:** Impurities and pigmentation on the parchment surface is often bleached with oxalic acid. Therefore, it can be present in considerable amounts in both modern and historical samples. The historical samples contain more oxalate than the modern ones, other than that in general no statistically significant difference was found between modern and historical samples.

In view of the above findings, each of the statistically different elements can be used as a simple marker for fast identification of ancient parchments. In fact, each of the cations  $\text{Na}^+$ ,  $\text{K}^+$ ,  $\text{Ca}^+$  as well as anions ( $\text{Cl}^-$ ,  $\text{NO}_2^-$ ,  $\text{Br}^-$ ,  $\text{NO}_3^-$ ,  $\text{SO}_4^{2-}$ ,  $\text{PO}_4^{3-}$ ) can serve as such markers (Figure 67). Additionally, the total amounts of cations and anions can be used for the same purpose.



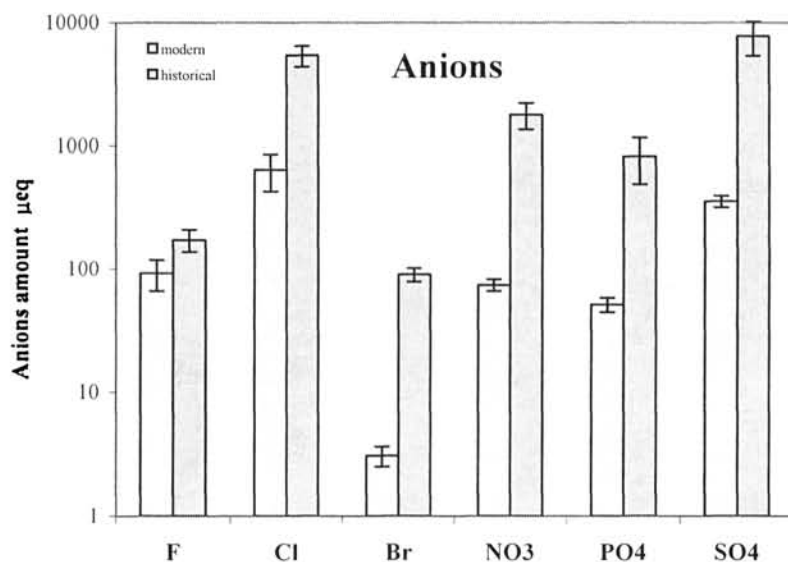


Fig. 67: Markers for fast identification of ancient parchment.

#### 2.7.2.1. Chemometrical model for parchment discrimination

Multivariate analysis (see chapter 2.11) is a powerful tool when dealing with multi-component systems. The model for parchment discrimination was built applying principal component analysis (PCA) and discriminant analysis (DA) to four ions (magnesium, bromide, nitrate, phosphate). At the first step, principal component analysis was applied to the original data set to extract the principal components. For each component, the variable with the highest loading was retained and the resulting new set of variables was used in discriminant analysis based on calculating Euclidian distance. The characteristics of eigenanalysis and the appropriate variables are presented in **Table 13**. We decided to use scores of the first two principal components in the discriminant analysis model. The classification performed with cross-validation gives 98.1% of correct classification. The resulted discriminant groups are shown in **Figure 68**. A clear distinction between two groups of the modern and historical parchments is observed. The detailed explanation concerning principles of discriminant analysis is provided in Chapter 2.11, subchapter "NIR model".

**Table 13**  
Multivariate analysis based on ion chromatography data.

Eigenanalysis of the Correlation Matrix				
Eigenvalue	2.11	1.01	0.53	0.35
Proportion	0.53	0.25	0.13	0.09
Cumulative	0.53	0.78	0.91	1.00

Principal Component Analysis		
Original Variable	Loadings	
	PC <sub>1</sub>	PC <sub>2</sub>
Magnesium	0.467	-0.528
Bromide	0.577	-0.013
Nitrate	0.606	0.022
Phosphate	0.284	0.849

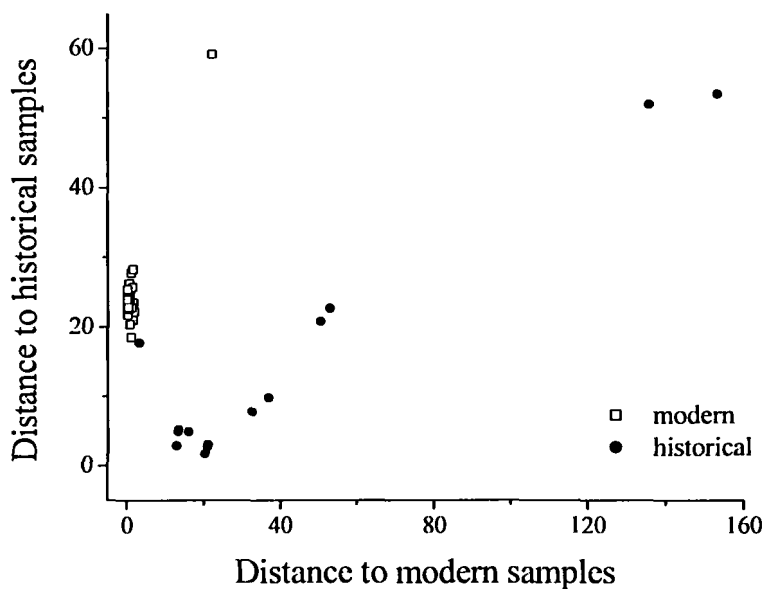


**Fig. 68:** Discriminant analysis of the parchment samples based in ion chromatographic measurements.

### 2.7.3. Animal type identification

Parchment is made from the skins of calves, goats and sheep. Identification of the animal type is of specific interest during the restoration process. Usually the classification is based on the visual appearance of the parchment and the subjective experience of the restorer. When contaminated and deteriorated historical samples are examined, such a classification may be somewhat problematic. More objective and reliable tools are needed to provide an accurate test. To prove the ability of ion chromatography for animal type classification, a statistical test (ANOVA) was done with the three available animal types: calf, goat and sheep. Identification of the animal type is possible based on cation (calcium) and/or anion (nitrate) content (Table 14). The difference in ion content is statistically significant at  $P=0.05$  level and can be used as a marker for animal type distinction. At the present, commercially available sets for express calcium and nitrate determination makes this finding extremely vital for the restoration process.

**Table 14**  
Marker ions for animal type identification.

	Calf	Goat	Sheep
Ion	Concentration [meq/g] $\pm$ SE of the mean		
Ca <sup>2+</sup>	2 $\pm$ 1	4 $\pm$ 1	9 $\pm$ 3
NO <sub>3</sub> <sup>-</sup>	59 $\pm$ 7	76 $\pm$ 5	119 $\pm$ 23

### 2.7.4. Electrical Conductivity

Electrical conductivity is a numerical expression of the ability of an aqueous solution to carry an electric current. This ability depends on the presence of ions, their total concentration, mobility, valence, and on the temperature of the solution. As previously seen, this type of data is obtainable by applying ion chromatography. However this analysis may be expensive, unavailable or time consuming. Thus, an alternative of using a simple conductivity measurement for parchment discrimination was checked. Based on an excellent achieved correlation between the corrected conductivity and

normalized total ion amount, a fast characterization of parchment surface was found to be possible.

#### 2.7.4.1. Experimental procedure

Around 25mg of a parchment sample was cut to small fragments, weighted and extracted shaking at room temperature with 5 ml double distilled (18 M $\Omega$ /cm resistance) water for 24 hours. After extraction, supernatants were filtered through a 0.45  $\mu$ m membrane based filter to avoid blockages or damage to connecting tubing, column end frits. This stock solution was used for pH measurements. Then, the stock solution was diluted (1/25) with double distilled (18 M $\Omega$ /cm resistance) water. The conductivity of the diluted parchment samples solution was measured. The corrected values of conductivity and total ions concentration were calculated according to the following formulas:

$$\text{Total ion concentration} = \text{concentration of cations} + \text{concentration of anions} \quad (7)$$

$$\text{Corrected conductivity} = \frac{\text{measured conductivity}}{\text{sample weight}} \times \text{dilution} \quad (8)$$

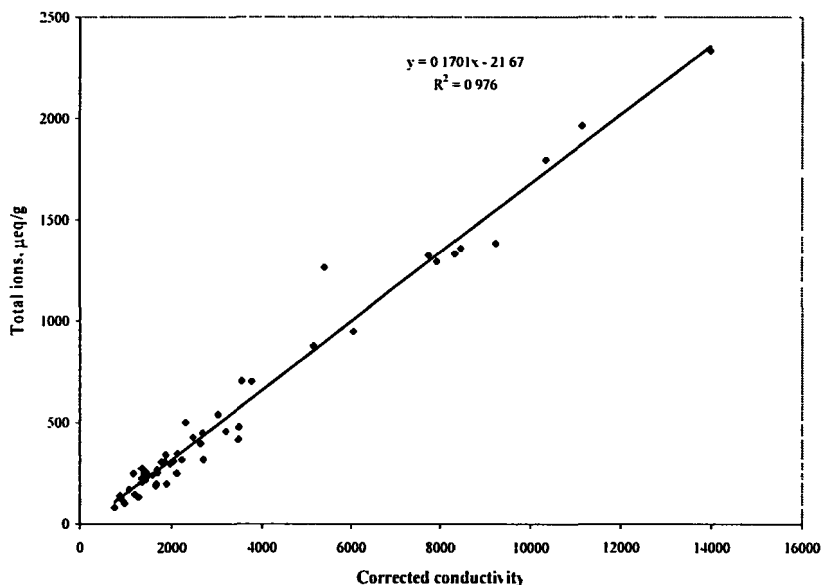


Figure 69. Correlation between conductivity and total ions concentration.

#### 2.7.4.2. Parchment characterization measuring conductivity

An excellent correlation between the corrected conductivity and total ion concentration was found (Figure 69). Thus, in order to characterize the total ion concentration in a specific parchment sample we needed only to perform a conductivity measurement which is simple and fast. Based on the conductivity data only, a statistically based discrimination among the modern and historical parchment groups is available, giving an outstanding on-line solution for difficulties in the restoration process.

#### 2.7.5. Ionic balance

It is well known that the stable solutions are electroneutral, therefore, the full ionic balance in the following calculations should be zero:

$$\text{Ionic balance} = \frac{\text{total cation concentration} - \text{total anion concentration}}{\text{total cation concentration} + \text{total anion concentration}} * 100\% \quad (9)$$

In historical samples, the difference is relatively low. However, a considerable difference was found for the ionic balance of the modern samples (Table 15). As presented in Figure 70, the biggest differences are observed at pH of parchment measured according to procedure (chapter 2.7.4.1) higher than 7 only. The exact reason for this finding has not been identified at the moment but the fact that the same manufacturer produced all these samples may be of great importance. The dependence of the difference on pH seems to be correlated with the carbonate/bicarbonate presence in solution. The modification of the applied method is needed for quantitative determination and can be the goal of future study.

**Table 15**  
Ionic balance in parchment samples.

	Ionic balance, % difference	
	Modern samples	Historical samples
Mean ± SD of the mean	22±3	8±2

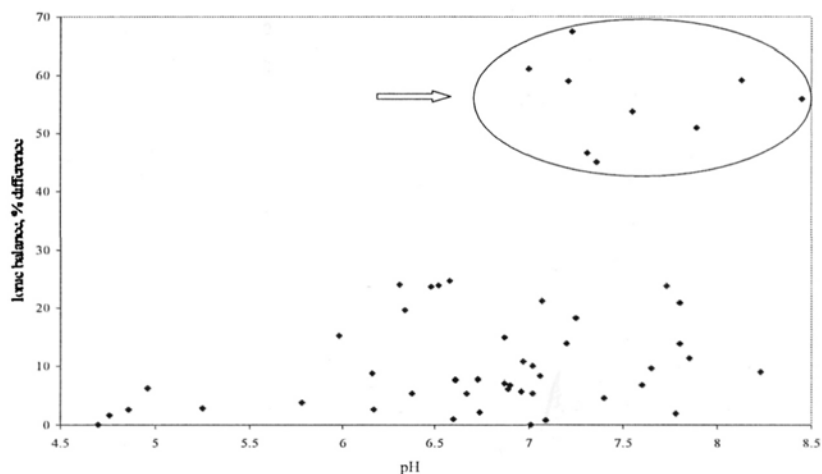


**Fig. 70:** Ionic balance in parchment samples as a function of pH.

## 2.8. Volt-ampere characterization of parchment

Volt-ampere characterization of parchment may be of importance in assessing the nature of water and salts interaction in the surface layer. Some researchers have used techniques of applying electrical current on human skin [Danielsen et al., Vanbever et al.], generally for the pharmaceutical purposes. A literature survey indicated that it might be appropriate to extend the study using current to another collagen consisting matter - parchment.

### 2.8.1. Experimental setup

The measurements were performed using the 237 Source-Measure unit (Keithley Instruments, Inc., Cleveland, Ohio) capable of sourcing voltage and measuring current, or vice versa. It can measure voltage from  $10\mu\text{V}$  to  $1100\text{V}$  and current from  $10\text{fA}$  to  $100\text{mA}$ . The current was a monitored parameter in our case.

The pieces of parchment samples were attached to a PMMA holder to keep the sample flat and to insure the same area of contact over the sample (Figure 71). The conductive area on the sample was  $150\text{ mm}^2$  per sample. Stainless steel electrodes (effective area  $204\text{ mm}^2$ ) were attached to the sample. The electrodes were rigorously cleaned before measurements to avoid any interference from contaminations. The equivalent scheme used for the measurements is shown in Figure 72.

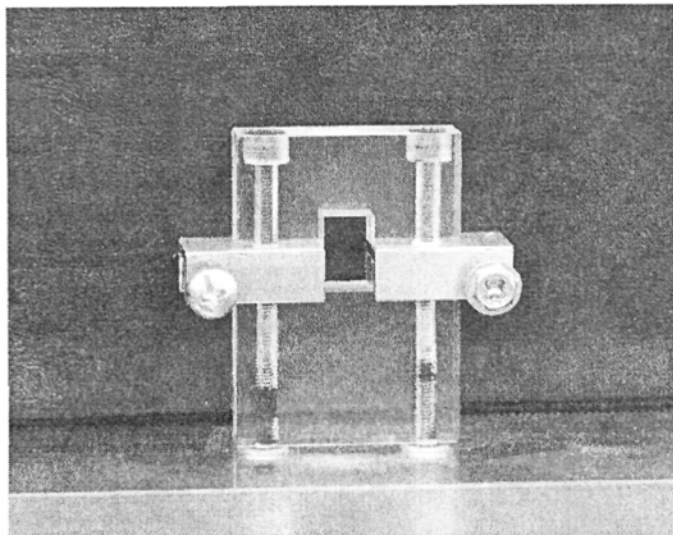


Fig. 71: Sample holder and electrodes used in the measurements of current.

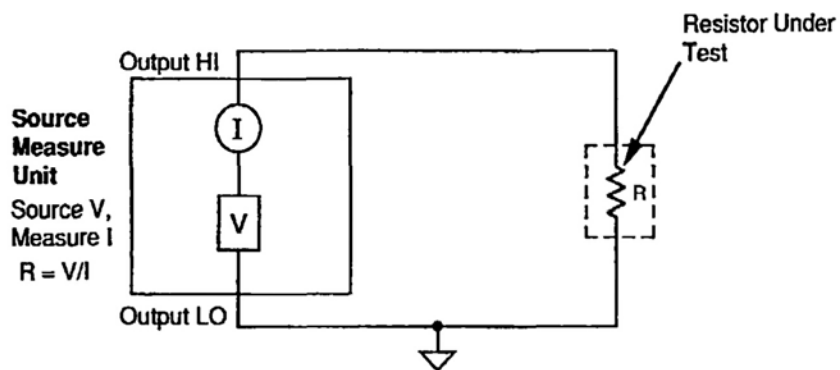
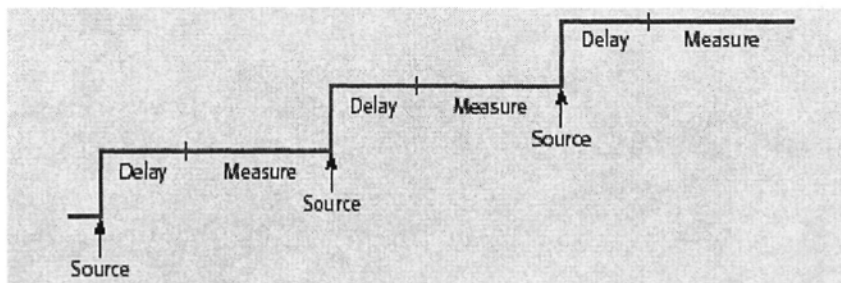


Fig. 72: Equivalent scheme of measurements (where V is a stabilized high voltage source and I is a current measurement unit).

Two different approaches for measuring current were performed. The first scheme was as presented in **Figure 73**:



**Figure 73.** Voltage - current (V-I) sweep.

According to this, at each voltage step, the instrument sources a voltage. The voltage change in the circuit will induce a transient current, so using an appropriate delay time between sourcing and measurement is critical to overall measurement integrity. This setup allows for volt-ampere characteristics measurement. The voltage ranged from 0 to 1100 Volts with 100V steps. Ten randomly selected parchments including the modern, pigmented modern and historical parchment types were measured using this setup. Each final data point included an average of 32 measurements.

**Figure 74** represents the schematic form of the source-delay-measure cycle. The baseline current (using the same experimental setup without a sample) was collected at a first step of the measurements according to the following source-delay-measure cycle procedure: averaging 32 measurements when applying 10 cycles of delay-measure procedure. The second type of measurements was performed according to the following scheme (**Figure 74**):

All the parchment samples were measured according to the second mentioned procedure in one day to ensure the same humidity and temperature initial conditions for each checked sample. Before starting the measurements, parchment samples were equilibrated in air at room temperature for 12 hours. The corrected current was finally calculated, taking into account the water content as well as the thickness of the sample.

The correction done for the thickness is obvious. The correction for water content was performed in view of some publications reporting a significant loss of water under electrical treatments (applying 100-500V) [Vanbever et al.].

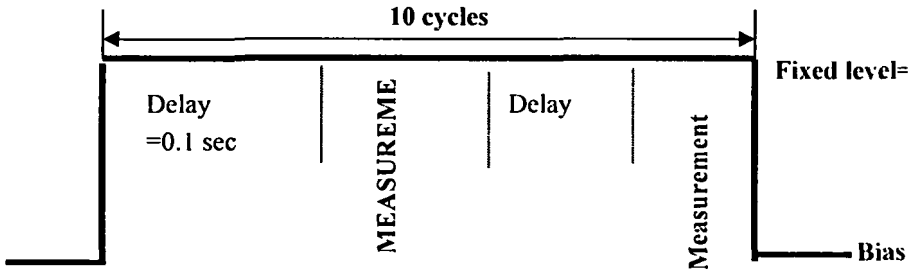


Fig. 74.: Experimental setup for current measurements.

All the parchment samples were measured according to the second mentioned procedure in one day to ensure the same humidity and temperature initial conditions for each checked sample. Before starting the measurements, parchment samples were equilibrated in air at room temperature for 12 hours. The corrected current was finally calculated, taking into account the water content as well as the thickness of the sample.

The correction done for the thickness is obvious. The correction for water content was performed in view of some publications reporting a significant loss of water under electrical treatments (applying 100-500V) [Vanbever et al.].

### 2.8.2. Current response results

As previously reported skin forms a barrier for diffusion of water and ions through it [Kalia et al.]. The potential is generated by a constant ionic gradient. Electrically, the skin can be modeled as a resistor and capacitor in parallel with most of the resistance residing in the stratum corneum (upper surface layer). Thus, if the skin were exposed to an electric pulse, most of the pulse voltage would fall across this upper layer [Gallo et al.]. The relatively thin barrier has a very high resistance. All ionic activity is seen as a change in current response.

Typical volt-ampere curves for different parchment groups are presented in Figure 75. One can observe that with the increasing of the applied voltage the measured current response increases for all examined parchment groups, but the slope of the curves representing the groups is different. An assumption is that the resistance of the historical samples is much lower than of the modern ones due to the high concentration of mobile ions in the outer layers. This could mean that in these fast measurements, the outer layers only

give the main fraction of the signal, and the real thickness of the sample is somewhere minor. Verification of this hypothesis, however, requires detailed future study.

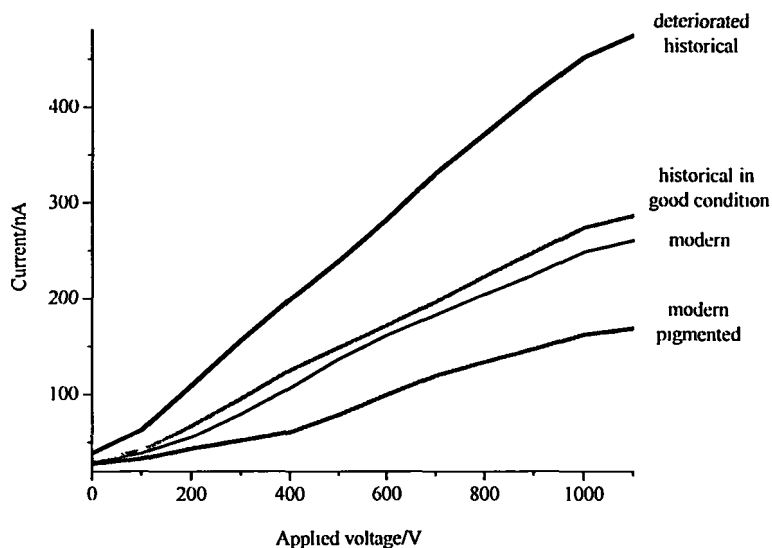


**Fig. 75:** Volt-ampere characteristics of different parchment groups.

To check the resistance of parchment samples at 1100V applied, a calibration curve based on the standard resistors measurements was provided. The correlated resistance (a product of resistance and thickness) shows statistically significant differences between modern and historical parchments (**Figure 76**). This fact supports the previously mentioned hypothesis, but the supplementary confirmation is needed since the resistance in this given case was checked at one given voltage.

### 2.8.3. Ancient samples discrimination

The discrimination of ancient samples (**Figure 77**) was based on empirical parameter which is a combination of experimentally measured data (current, background current, sample thickness and sample water content):

$$\text{Corrected current} = \frac{\text{measured current(nA)} * \text{thickness(mm)} * \text{H}_2\text{O} (\%w/w)}{\text{background current(nA)}} \quad (10)$$

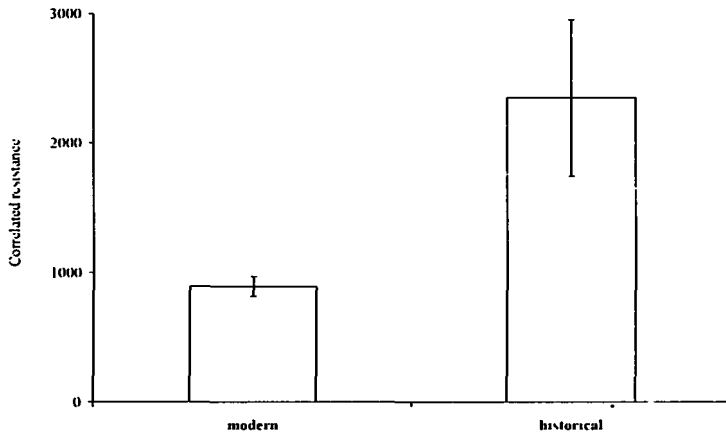


**Fig. 76:** Differences in correlated resistance (a product of resistance and thickness) between modern and historical parchments.

This formula provides a best statistical differentiation; however, the physical meaning of the calculated corrected current is unclear. In such a case, a problem of correlation between the measured signal and water content/sample thickness is of great moment, but the testing of the theory is time consuming and is out of the scope of this study. This method is very fast, semi-destructive (only a small piece is needed) and simple.

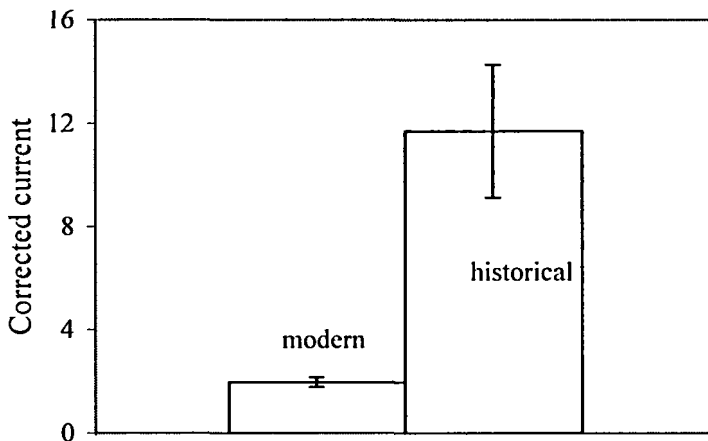


**Fig. 77:** Ancient samples discrimination based on corrected current response.

## 2.9. Electron Spin Resonance study

### 2.9.1. Experimental setup

ESR measurements were performed on Bruker EMX-10/12 X-band ( $\nu = 9.4$  GHz) digital ESR spectrometer. All spectra were recorded at microwave power 2.02mW, 100 kHz magnetic field modulation of 1G amplitude. Digital field resolution was 2048 points per spectrum, allowing all hyperfine splitting to be measured directly with an accuracy better than 0.2 G. Spectra processing was performed with Bruker WIN-EPR and SimFonia Software.

### 2.9.2. Principle of the method

Electron Spin Resonance (ESR) is a magnetic resonance technique that detects the transitions of unpaired electrons in an applied magnetic field. A large number of materials have unpaired electrons. These include free radicals, many transition metal ions, and defects in materials. When we supply an external magnetic field, the paramagnetic electrons can either orient in a direction parallel or antiparallel to the direction of the magnetic field. This splitting creates two distinct energy levels for the unpaired electrons and allows for the measuring of them as they are driven between the two levels.

Only ESR detects unpaired electrons unambiguously. Other techniques such as fluorescence may provide indirect evidence of free radicals, but ESR alone yields incontrovertible evidence of their presence. In addition, ESR has the unique power to identify the paramagnetic species that is detected. ESR is very sensitive to paramagnetic species local environments. Therefore, the technique determines the molecular structure near the unpaired electron. The shape and number of peaks in an ESR spectrum depend on the nuclear spin of the neighboring atoms.

The most basic equation of ESR describes the separation between two adjacent energy levels:

$$\Delta E = \Delta h\nu = g\mu_B B_0 \quad (11)$$

where  $h$  is Plank's constant,  $\nu$  is the actual frequency corresponding to the middle of the peak,  $g$  is the Landé factor (or  $g$ -factor), which is a proportionality constant depending on the electronic configuration of the radical or ion,  $\mu_B$  is the Bohr magneton, which is the natural unit of electronic magnetic moment,  $B_0$  is the applied magnetic field strength.

### 2.9.3. Application of ESR to parchment characterization

The ESR studies of collagen and parchment were performed recently [Larsen]. In biological tissues, protein denaturation can take place at 35-70°C, which can initiate the cleavage of the lateral bonds and the formation of free radicals. The initial collagen samples do not contain the paramagnetic species. The typical EPR spectrum of collagen irradiated with 248 nm can result from the coupling of an unpaired electron to four equidistant protons, for example with protons in the CH-CH<sub>3</sub> or CH<sub>2</sub>-CH<sub>2</sub> radical moiety. It is likely that those fragments are the most stable products in the sequence of radical transformations after UV irradiation [Bagratashvili et al.]. The relative radical amount (indicated as ESR peak height) increase was reported for photoirradiated ( $\lambda \geq 250$  nm, 4 hours) collagen [Torikai et al.]. The production of free radicals *ex vivo* under UV irradiation of mouse and human skin measured by ESR was reported [Jurkiewicz et al.].

The Maillard browning reaction between carbohydrates and amines is the basis for the brown skin color caused by UV radiation. The initial stages of the reaction are quite complex, but the ultimate products are brown polymers known collectively as melanoidins. ESR shows that radicals are produced in mouse skin *in vivo* by the Maillard reaction. The ESR signal consists of a broad single line with  $g=2.0035$  [Lloyd et al.].

The degradation of parchment during artificially aging is believed to occur via free radical formation. In accordance with the theory and with previously published results, in our study intact parchment samples have no ESR signal besides the highly pigmented ones (Figure 78). The highly pigmented samples in our opinion contain a micro amount of pigment (probably, melanin). In contrast to other samples, this pigment remained on the parchment surface after the manufacturing process was finished. Additional work should be done to prove this fact. After artificial aging, a considerable increase in the ESR signal intensity was observed, indicating free radical formation.

The mean ESR signals of modern and historical parchment samples are nearly the same with a wider distribution of modern samples (Figure 79). This fact can be described by the presence of "outliers" in the modern samples population. These "outliers" probably contain various concentrations of pigments having a relatively high ESR signal in their surface layer, as previously described. However, the mean value of intact modern parchments is lower than that of the same samples after artificial

aging (Figure 80). The distribution of signals in both cases is wide and no statistically significant differences were found. However, if the modern samples population included non-pigmented samples only (after “outliers” rejection) the difference becomes clearer.

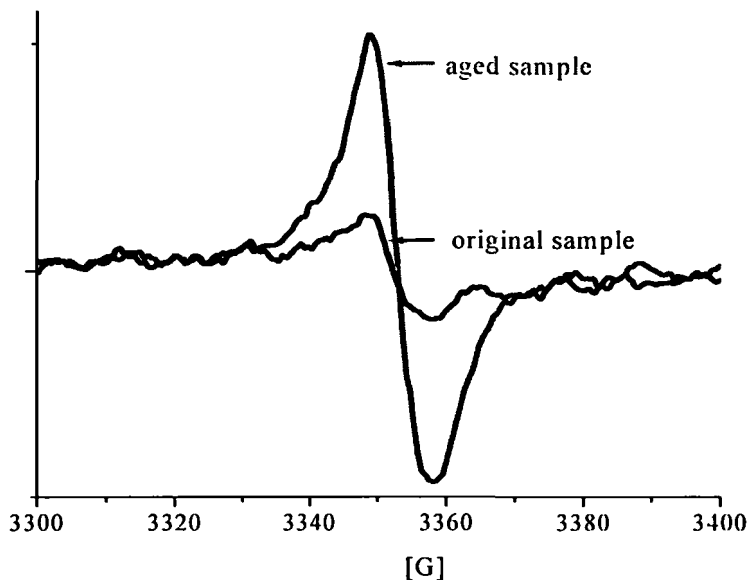


Fig. 78: ESR signal of modern and artificially aged parchment samples.

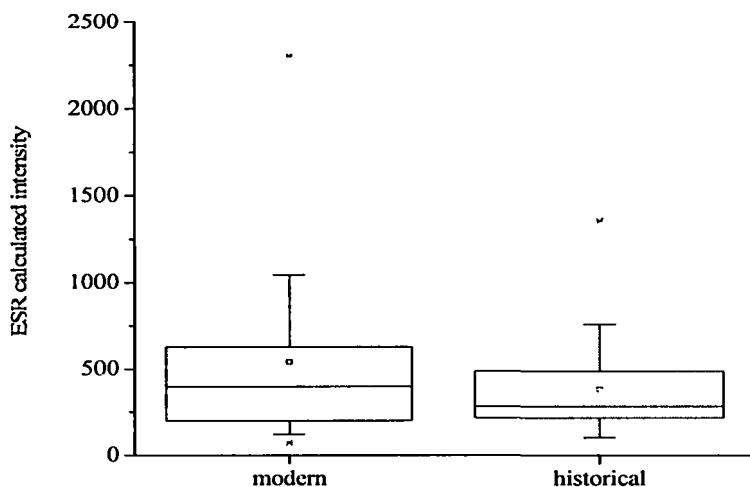
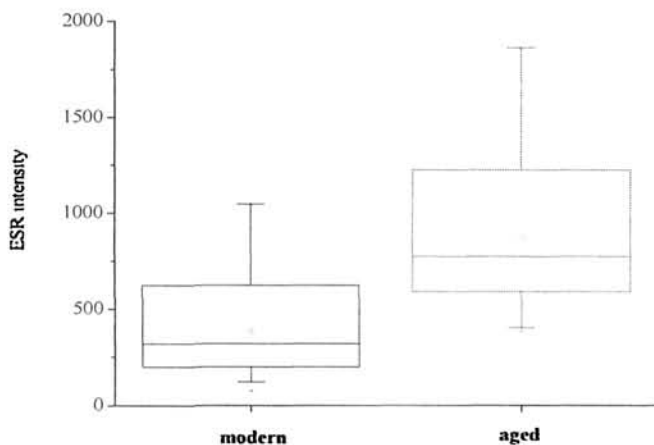
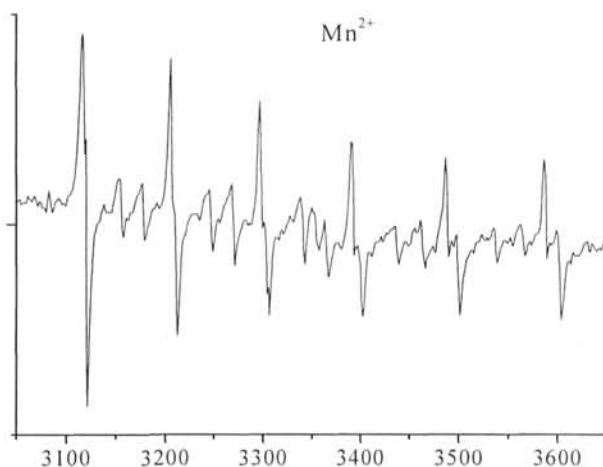


Fig. 79: Mean ESR signal of modern and historical parchment samples.



**Fig. 80:** Mean ESR signal of modern and artificially aged parchment samples.

An additional difference found in ESR spectra is in the fact that the ESR spectra of historical parchments clearly show the presence of manganese species indicating a natural calcite source (**Figure 81**). Natural calcite from limestone contains a small amount of manganese instead of calcium. Manganese has a characteristic ESR spectrum of 6 lines. Presence of the manganese lines in the modern parchment spectra was not detected. The ancient parchment manufacture included washing in sea water (containing a considerable amount of manganese) whereas at the present time urban water (containing only a trace amount of manganese) is regularly used in this process.



**Fig. 81:** ESR signal indicating presence of manganese in historical samples.

## 2.10. Organic and inorganic matter content

Some additional parameters not included in the previous chapters were examined for the parchment samples set. Statistically significant differences in organic and inorganic matter percentage in modern and historical parchment samples were found (Table 16). As is known, modern parchment contains around 95% collagen. The collagen is lost during the lifetime of the artifact due to protein hydrolysis. Additionally, the micro-organisms contribute to organic matter decomposition and this process depends on temperature, pH, and moisture content. Hence, the quality and quantity of organic material may change during aging. We found that the organic matter percentage per dry matter weight is 97% in modern and 93% in historical parchment samples. The analysis was performed gravimetrically.

Modern parchment samples should contain about 0.8% minerals [Budrugaec et al., 2003]. The inorganic matter percentage per dry matter weight is 2.5% in modern and 4.4% in historical parchment samples (the analysis was performed gravimetrically). Such a difference in ash content between young and adult pigs was previously reported [Sun et al.] where the adult animals have a higher ash percent. The differences in organic and inorganic matter percentage in modern and historical parchment samples are significant at 95% confidence; therefore, they can be used to discriminate between the two groups.

**Table 16**  
Organic and inorganic matter content in parchment samples.

%, per dry weight	Modern	Historical
Organic matter	97 ± 0.8	93 ± 0.8
Inorganic matter	2.5 ± 0.5	4.4 ± 0.6

## 2.11. Near Infrared Spectroscopy

Near Infrared Spectroscopy (NIR) has been growing very fast in recent years. However, NIR has not yet been exploited for direct measurements of parchment. This technique offers many advantages over commonly used methods, providing the information by means of a non-destructive and non-invasive technique. High quality information can be obtained rapidly with no sample preparation. The technique is relevant for both quantitative and qualitative applications and may be used throughout an on-line “decision making” process of parchment preservation and restoration. Fiber optic

technology is readily implemented in this range, allowing for remote monitoring of processes in challenging environments. The information available gives the user an understanding of the suitability of appropriate materials for particular process and the potential to predict how well a preservation method will perform.

The additional advantage is a high degree of confidence that the material will conform to a specific preservation stage when a parchment's spectral signature falls within predefined statistical limits. The technique may be applied to individual parchment components as well as to a parchment matrix in its entirety. Information from NIR data provides an objective method of analysis. Therefore, it is a possible alternate method for estimating parchment conditions and also for the determination of the appropriate restoration method.

#### 2.11.1. Principles of the method

The near infrared region of the electromagnetic spectrum covers a range from 750 nm to 3000 nm. Molecular spectra in this region are dominated by vibrational overtones and additive combinations of fundamental stretching vibrational modes of -CH, -NH, -OH and -SH bonds, which are much weaker than the fundamental vibrations encountered in the mid-IR region. Every molecule exhibits a unique signature in this region of the spectrum.

Radiation interacting with a sample can be transmitted, absorbed or reflected. Beer's law is only valid in the absence of light scattering in the sample. The scattering process changes the radiation path length. For a smooth surface, most of the radiation is reflected and no absorption takes place (so-called "specular reflection"). As a result of low light absorption in the NIR range, radiation typically penetrates several millimeters into materials. Unabsorbed radiation is diffusively reflected from the sample back to the detector. The diffusely reflected radiation ( $R$ ) can be empirically related to concentration ( $c$ ) in an analogous way to Beer's law, i.e.

$$\log(1/R) = kc \quad (12)$$

where  $k$  is a factor which incorporates both absorptivity and path length. In analogy to conventional transmission spectrophotometry, this logarithmic form is commonly called "absorbance." In transreflectance mode, the radiation is transmitted through the sample, reflected from the reflection surface behind

the sample to double the path length and then transmitted back through the sample before reaching the detector. Transflectance is thus a hybrid of transmittance and reflectance.

The chemical information is obscured by changes in the spectra caused by physical properties, such as sample inhomogeneity or variations in particle size, shape or packing and can cause shifts in spectral baselines and hence interfere with quantity. Additionally, the phenomenon of multi co-linearity when broad bands lead to overlapping of the adjacent wavelengths is observed. Hence, NIR becomes a secondary method requiring the calibration against a reference method for the constituent of interest. Due to complexity of the physics of reflectance and of the spectra, calibration is normally carried out using chemometric methods. Chemometrics is defined as “the chemical discipline that uses mathematical, statistical and other methods employing formal logic to design or select optimal measurement procedures and experiments and to provide maximum relevant chemical information by analyzing chemical data” [Massart]. A commonly used method is a multivariate analysis, which effectively reduces spectral data to relevant factors, while maintaining all the information necessary for separating the components. “In multivariate **data analysis**, models are used directly for data interpretation. In multivariate **calibration**, models relate the data to a given property in order to predict this property” [Estienne].

To summarize, NIR analysis demands the development of a calibration model based on a variety of samples analyzed by reference method. The constituent of interest or the sample characteristics may be then predicted using the calibration model and the spectral data.

In NIR analysis, the final calibration model can be used in three basic fields of analytical chemistry: identification, qualification and quantification. As determined in [Chalmers et al.]:

NIR *identification tests* are intended to ensure the identity of the analyte and/or the whole matrix and to discriminate a given material from the other materials.

NIR *qualification tests* are intended to discriminate between closely related materials that are indistinguishable by simpler identification testing. Qualification is a necessary prerequisite for admitting samples to a quantitative method; since it provides assurance that the material belongs to the correct population.

NIR *quantification procedures* are intended to measure the concentration

of an analyte in a given sample. Therefore, the derivation of the calibration model for each specific application is the most critical step towards reliable analysis. There is, however, no unique algorithm for deriving satisfactory calibration models, and various approaches should be examined.

### 2.11.2. Experimental part

Two different instruments were used in the study:

- The FOSS grating spectrometer Model 6500 (FOSS NIRSystems, Silver Springs, MD, USA) performs in the NIR and in the visible range (400-2500 nm). The spectral acquisition, the data treatment and the quantitative model development were performed using WinISI version 1.50 (developed by Infrasoft International<sup>®</sup>) software. A NIR diffuse reflectance spectrum was recorded in transmittance mode as the average of 32 scans, over the wavelength range 400 - 2498 nm, at 2 nm increments (total of 1050 data points). A standard ceramic was used as a reference before each measurement.
- The Nicolet Antaris FT-NIR analyzer (Thermo Electron Scientific Instruments Corporation, Madison, WI, USA) performs in the NIR range only (3800-12000  $\text{cm}^{-1}$ ). The spectral data was collected using Result version 2.1 software. The data treatment and quantification was performed using TQ Analyst chemometric software version 7.0 (developed by Nicolet<sup>®</sup>). A NIR diffuse reflectance spectrum was recorded in transmittance mode as the average of 32 scans obtained using a spinner to ensure homogeneity of the probing surface, over the range 4000 - 10000  $\text{cm}^{-1}$ , at 2  $\text{cm}^{-1}$  constant resolution (total of 3000 data points).

### 2.11.3. Overview of calibration procedure

A typical NIR based calibration procedure involves several steps (**Figure 82**). We will describe each step in detail according to hierarchical order.

**1) Sample selection and collection** is critical to the success of the entire application. The samples in a selected set must collectively describe the typical variation of the substance being analyzed. The number of samples should be sufficient to generate a model of good predictive ability and depend on the complexity of the matrix, analyte concentration and availability.

### *Overview of calibration procedure*

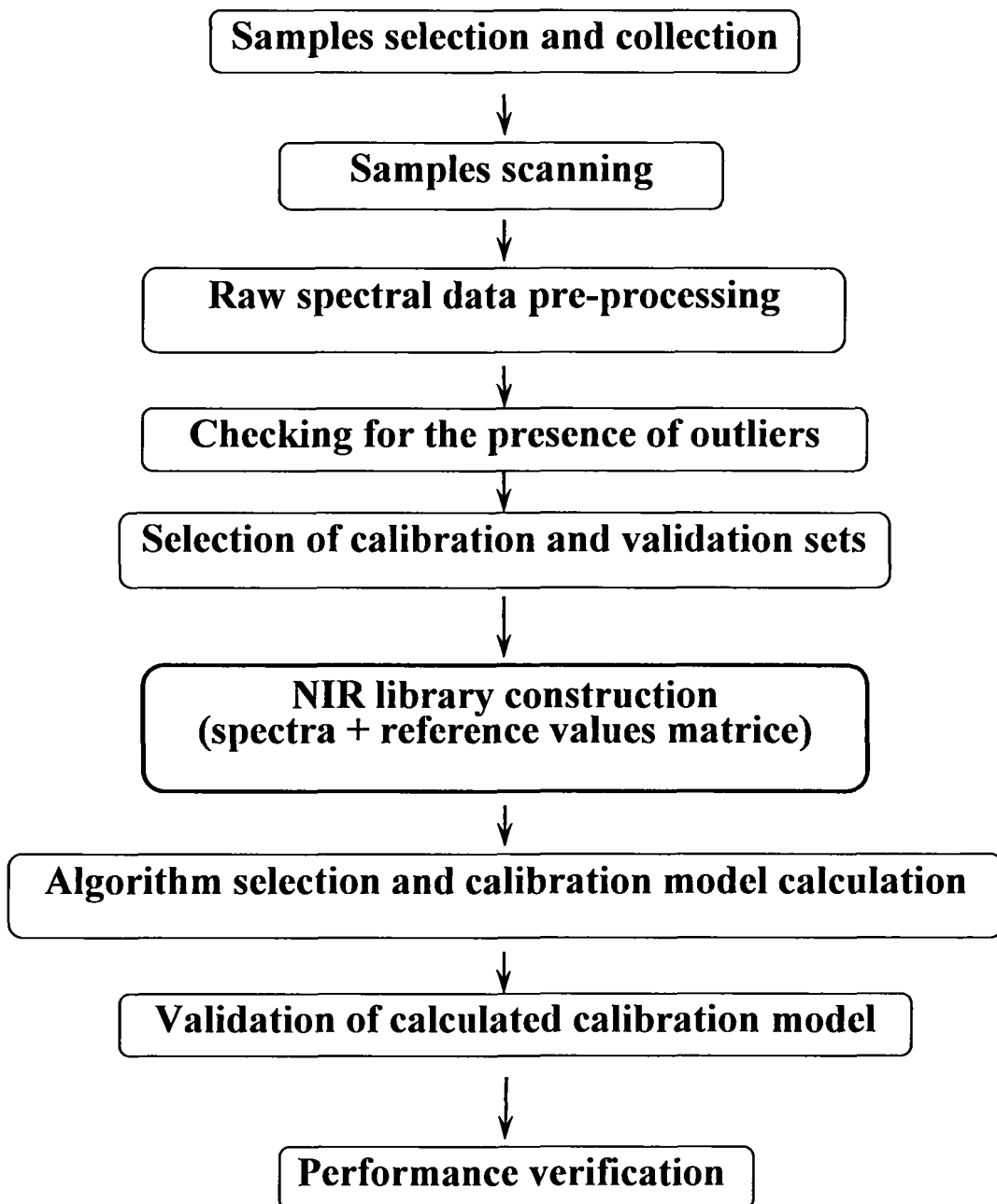


Fig. 82: Overview of calibration procedure.

**2) Sample scanning** using appropriate NIR instrument. Data acquisition mode should be planned in accordance with the sample requirements. A sufficient number of scans should be averaged to obtain suitable signal-to-noise levels for quantitative identification.

**3) Raw spectral data pre-processing** is used to enhance spectral features and/or to remove or reduce unwanted sources of variations (differences in particle size, shape, packing, and scatter light) using derivative spectroscopy, smoothing, baseline correction and scatter correction (standard normal variate, detrend and multiplicative scatter correction) algorithms. The selection of the pre-processing tool is specified by the data set and the operator rationale.

**4) Checking for the presence of outliers.** Outliers are samples which upset the expected or usual image. The question arises as to whether they should be eliminated or integrated into the model. Within the framework of the calibration outliers can usually be eliminated. However, in validation they are often retained. The rejection of outliers in routine work is dictated by the experience of the operator.

**5) Determination of calibration and validation sets.** Two sets of samples are required in chemometrical model development: one for construction of the library and an independent one for validation purposes.

**Calibration set** - representative sample set incorporating all chemical and physical variation used to generate and optimize a regression model.

**Validation set** - independent random samples set taken from the same basis as the calibration samples used to give assessment of the accuracy and precision of the calibration model.

**6) NIR library construction.** NIR methods require calibration of the NIR spectral response against authentic reference data obtained from the application of a valid routinely used reference method. For this reason, the library contains both spectral data and the correspondent reference values for each sample analyzed.

**7) Algorithm selection and calibration model calculation.** Calibration is the process of constructing a mathematical model to relate the response

from an analytical instrument to the properties of the sample. The result of the calibration is a distinct function  $Y=f(X)$ , where the  $X$  variables are the quantities we wish to measure and the  $Y$  variables are the quantities we wish to predict in future. These will be the values estimated from the  $X$  values using the regression model.

There are two distinct approaches to the generation of the calibration model: univariate and multivariate. In univariate calibration a single response from an analytical instrument is related to the concentration of a single component. Multivariate calibration (regularly used in NIR) is the process of relating multiple responses from an analytical instrument to the properties of the sample (**Figure 83**).

The essentiality of the multivariate calibration in the situation where two wavelengths that are adjacent to one another do contain mostly the same information, and one of the wavelengths is therefore redundant, is evident. Spectra can therefore be compressed by means of principal components. The aim of principal components is to describe the spectra with less data without information regarding the sample being lost. The original measured variables (e.g., absorbances at different wavelengths) are converted into new axes (principal components) so that the data scores expressed on these axes are uncorrelated, i.e. the **principal components** are orthogonal vectors that describe the independent source of spectral or content variation. By combining this spectral information, in the thousands of data points in a typical spectrum there might be only a few sources of the variation in the spectra. Once this data compression is accomplished, each reference spectrum can be approximated quite precisely as a linear combination of the principal components.

Principal components analysis provides a method for finding structure in wide data sets. Principal components are graded by the amount of variance they describe. The first principal component describes most of the variation in the calibration spectra. Each additional principal component describes most of the remaining variation. Therefore, the first principal component contains most of the common information in the data. The rest of the principal components contain information that is more specific, representing small variations in the data which are often important to analysis. The extraction of the principal components can be carried out according to principal components analysis (PCA), or partial least squares (PLS) application. The optimum number of extractable principal components is determined by the use of eigenvalues. The total variance represented by the specific principal component is

called its “eigenvalue” and decreasing variance represented by decreased eigenvalue. The detailed procedure of principal components extraction and calibration method development is described in various common books and papers on multivariate analysis [Estienne et al., Chalmers et al., Martens et al., Massart et al., Draper et al.]

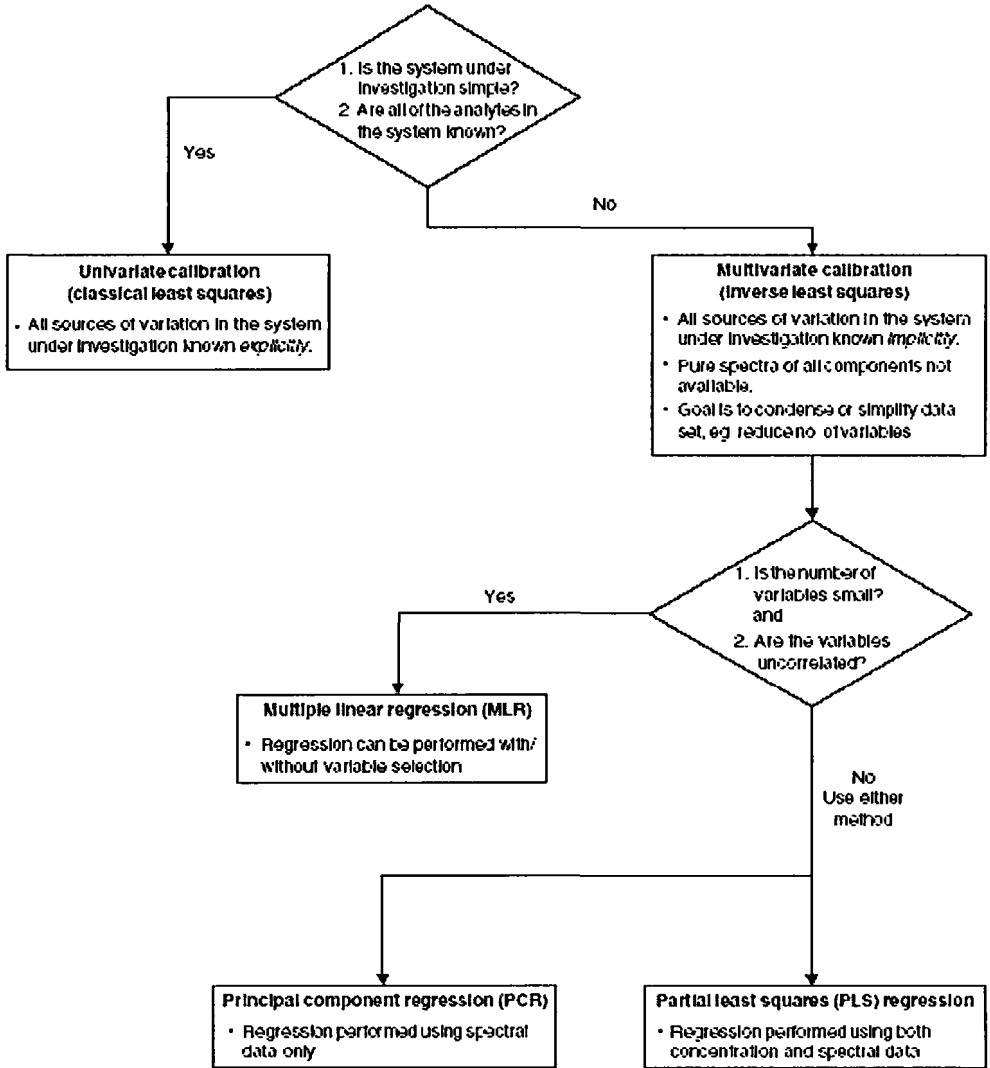


Fig. 83: Multivariate calibration decision tree. Reprinted from [Chalmers et al.].

**Quality parameters of calibration.** The main purpose of the calibration is to estimate predictor parameters from the data of available samples in such a way that the future prediction of Y has as low prediction errors as possible. To provide an estimate of the prediction error, the following parameters are used:

- **SEC (Standard Error of Calibration).** It has the same unit as the feature being examined. The standard error should be small. The SEC is calculated as the standard deviation of all NIR analysis values from the reference values of the calibration samples.

$$SEC = \sqrt{\frac{\sum_{i=1}^n (y_i - Y_i)^2}{n - p}} \quad (13)$$

where  $y_i$  is the “true” constituent content measured by reference method,  $Y_i$  is the NIR calculated value,  $n$  - is the number of samples in the calibration set,  $p$  - is the number of principal components used in the calibration model.

- $R^2$  is the portion of the variance (mean deviation squares) of the reference values, which is explained by the NIR analysis. Values close to 1 signify that the calibration can satisfactorily explain the variation in the calibration set.

$$R^2 = \frac{\sum_{i=1}^n \left( Y_i - \frac{1}{n} y_i \right)^2}{\sum_{i=1}^n \left( y_i - \frac{1}{n} y_i \right)^2} \quad (14)$$

where  $y_i$  is the “true” constituent content measured by reference method,  $Y_i$  is the NIR calculated value,  $n$  - is the number of samples in the calibration set.

- **SECV (standard error of cross-validation)** is the mean standard error from the cross-validation. During calibration with methods of multivariate regression (PCR, PLS, MPLS), a cross-validation is carried out. In this situation, in each case a part of the samples (between 10% - 50%, depending on the size of the sample set - 10% at  $n=30$ , 50% at  $n=200$ ) is estimated from a calibration on the basis of the remaining samples. The cross-validation is carried out in order to identify and prevent an overfitting (see SEC) which may be being expressed in a repeat rise of the SECV.

$$SECV = \sqrt{\frac{\sum_{i=1}^n (y_i - Y_i)^2}{n-1}} \quad (15)$$

where  $y_i$  is the “true” constituent content measured by reference method,  $Y_i$  is the NIR predicted value,  $n$  - is the number of samples in the validation set.

**8) Validation of calculated calibration model.** A calibration equation is an empirically detected statistical connection between measured reflectance values and concentrations of the content substance in the calibration samples. The quality of the examination results from these independent samples is decisive with regard to whether the calibration equation is fulfilling its task. The examination of a calibration equation on independent new samples in order to determine the error in the analysis method is the validation. At the start of a calibration development, calibration and validation samples are drawn from an existing sample set. Internal and external validation can be applied. Internal validation (cross-validation) is based on the samples selected to make up the library. External validation is verified using authenticated samples not used to generate the model.

**Quality parameters of validation.** The statistical parameters of the validation are determined, in order to establish the smallest possible errors.

- **SEP** is the standard error of the NIR analysis prediction. The SEP can be broken down into the bias (systematic error) and the SEP(C) (random error).
- **Bias** is the systematic error by which all the samples are on average incorrectly estimated. If the validation samples are representative samples from the same basic totality as the calibration samples, and if the validation and calibration samples have been examined with the same reference method in the same laboratory in a short time span, then no significant bias should arise during the validation. Bias can be corrected by calculation if a significant bias pertains.

$$\text{bias} = \frac{\sum_{i=1}^n (y_i - Y_i)}{n} \quad (16)$$

where  $y_i$  is the “true” constituent content measured by reference method,  $Y_i$  is the NIR predicted value,  $n$  - is the number of samples in the

validation set.

- **SEP(C)** - (standard error of prediction corrected for bias) - calculated as standard deviation of all NIR analysis values from the reference values for the validation samples, after the NIR analysis values have been adjusted by the bias.

$$\text{SEP(C)} = \frac{\sum_{i=1}^n (y_i - Y_i - \text{bias})^2}{n-1} \quad (17)$$

where  $y_i$  is the “true” constituent content measured by reference method,  $Y_i$  is the NIR predicted value,  $n$  - is the number of samples in the validation set.

- **Slope** relates the regression lines of the NIR analysis values to the reference values of the validation samples. The slope of the regression lines should be close to 1. With deviations greater than 1, it is particularly the samples with high and low values which are being incorrectly estimated.

**RSQ** is the determination measurement of the regression of the NIRS analysis values on the reference values of the validation samples.

**9) Performance verification** – comparison with reference method. Samples analyzed by NIR have also to be analyzed by the reference method and the results compared in order to demonstrate that the calibration model is performing correctly.

**10) Prediction** is the process of using the developed model to predict properties of an unknown sample given the output from an analytical instrument.

#### 2.11.4. NIR model

As mentioned previously, the parchment samples in the study were examined using various analytical techniques. However, some problems remained unsolved. Here the NIR technology can replace earlier mentioned methods since it has its own advantages.

Through the advantages of NIR instrument and software, we compensate for the time consuming or expensive measurements as well as solve the problem of non-destructive evaluation of parchment content. We performed

two various types of analysis in order to 1) discriminate between modern, historical and artificially aged groups and then, in each defined group 2) to quantify analytes of interest found in parchment matrices. Each of the two models proposed can be used alone, according to the specific purpose.

The discrimination model is very important for on-line recognition during the restoration process. As was mentioned earlier, the discrimination models were successfully built based on ion chromatography, LIBS and fluorescence data. However, as an ideal alternative (fast, without sample preparation, non-destructive and non-invasive, option of fiber optics readings) and/or to complete the picture NIR has to be applied.

The quantification of analytes in parchment matrices in this study was performed using common "wet chemistry" procedures. Optionally, they can be correlated with NIR spectral data simply. However, the quantification of some essential analytes in parchment matrix, like water and nitrogen, is not possible to complete non-destructively with no assistance of NIR technology due to target complexity. In this case the application of multivariate calibration is obligatory. When sufficiently accurate and precise quantification can be achieved based on these constituents, it can be expanded to other substances of interest according to the specific requirements of the restoration process.

#### 2.11.4.1. Discriminant Analysis

Discriminant analysis is a classification technique to determine which class of standards is most similar to the unknown based on the **Mahalanobis distance**. The Mahalanobis distance (H-value) is a multidimensional vector that describes the distance of a sample from the mean value of a multidimensional ellipse containing a set of standards. The purpose of discriminant analysis is to join the objects into successively large clusters using some measure of similarity between the objects.

The first step of the process is to perform a Principal Components Analysis (PCA) to reduce the original set of variables to a smaller set of factors and plot the most significant PC's in order to identify any clustering of spectra. Clusters are groups of similar objects inside a population. Once the number of clusters is defined, by use of many statistical algorithms available, a discriminant function must be developed in order to classify unknown samples.

The **performance index** is a measure of how accurately a calibrated

method can classify the validation standards. This diagnostic shows how well a calibrated discriminant analysis method performs by classifying the calibration and validation standards. The performance index for discriminant analysis ranges between 0 and 100. The higher the performance index, the closer each standard is to its actual class and the farther it is from the next closest class.

In our study, a total of 70 standards (51 calibration, 19 validation) were divided into modern, historical and artificially aged parchment groups, resulting in a model for the classification of the parchment deterioration stage. Nine principal components were extracted and 100% of variability was described. A performance index of 91% was achieved. Two standards were misclassified: the historical in very good condition as belonging to the modern group and a highly pigmented modern one as belonging to the historical group). The results are plotted in **Figure 84**.

The plot shows strong discrimination between two types of population: 1) aged samples, 2) modern and historical samples. As expected, the higher the distance of a particular sample in the specific group from other samples fitting in a different group, the greater the probability that the sample belongs to it. The discrimination between the modern and historical samples is weaker. This is understandable, because the process of parchment's artificial aging was designed to achieve maximum available damage. Additionally, some of historical parchment samples are found in very good condition; therefore, they should be closer to the modern samples than to the artificially aged ones. However, a reasonable level of separation of modern and historical samples was achieved.

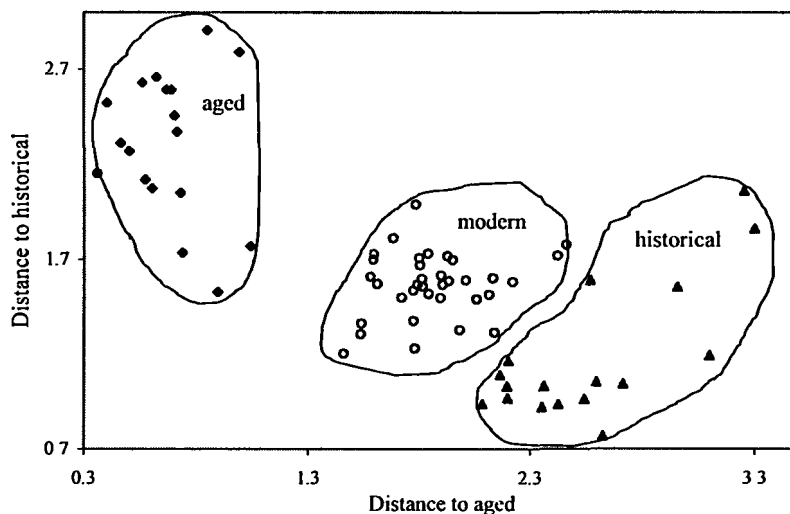


Fig. 84: Discriminant analysis results.

#### 2.11.4.2. Quantitative NIR model development: water and nitrogen evaluation

The quantification of some essential analytes in a parchment matrix, like water and nitrogen, is not possible to complete non-destructively due to target complexity. Regularly, water and nitrogen have to be analyzed using a “wet chemistry” approach and the analysis performed destructively. Moreover, in terms of water analysis, the interpretation of results is complicated. As a result, application of multivariate calibration to water and nitrogen quantification is obligatory. Based on these two constituents, we will demonstrate the ability of chemometrical model application to quantify the parameters of interest. Additionally, the general discussion on various statistical treatments and method performance will be provided.

As previously mentioned, parchment starts to deteriorate when the manufacturing process finishes. Aging of historical parchments is a complex deterioration mechanism. There are three major irreversible degradation paths: denaturation, hydrolysis and oxidation.

Denaturation is caused when collagen interacts with water to form gelatin. Gelatin is an aqueous colloidal suspension of polypeptide chains and fragments of chains. According to [Renugopalakrishnan et al.], irreversible loss of bound water in collagen was observed in the 60-140°C temperature

interval. After 140°C, no further weight loss due to collagen dehydration was mentioned. More detailed results were reported by Dong [Dong et al.]: the denaturation transitions in collagen occur at 42°C and 68°C when the triple helical structure is destroyed (biological activity lost), and at 90°C when the secondary structure of collagen is destroyed. At evaluated temperatures, water molecules can gain sufficient energy to compete for hydrogen bonds maintaining collagen triple helix configuration [Hansen et al.]. As a result, the hierarchical internal structure of protein becomes disordered. The denaturation temperature depends on water content (the lower the water content, the higher the denaturation temperature [Chanine]) and on the animal's genetic type and age [Rochdi et al.].

Collagen is lost because of hydrolytic cleavage of peptide bonds [Collins et al.]. Hydrolysis is caused by exposure of a parchment to humidity and atmospheric pollutants. Oxidation by atmospheric oxygen changes the molecular structure of protein, causing cross-linking and chemical modification of several amino acids over time.

It has been reported that the aging process affects the amino acid content of fossil collagen samples and the loss of amino acids is not uniform. The increased loss of amino groups occurs at the N-terminus [Tuross]. The rate of nitrogen loss from mineralized collagen corresponds to a pseudo-first order reaction [Collins et al.]. To conclude, changes in amino acid (nitrogen) and water content during lifetime of the artifact can be used as a precursor for parchment deterioration evaluation.

Generally, water in organic matrices (like collagen within parchment) can be divided into surface ("free" or "bulk-like") and bound water (**Figure 85**). Some models image even more than three fractions [Leikin et al.]. NIR spectroscopy has been applied recently to the determination of water in skin [Arimoto et al. 2005; Arimoto et al. 2003; Suh]. However, quantitative evaluation of water content is problematic because of the different hydration of skin layers [Arimoto et al. 2003; Martin]. Several types of water can be distinguished due to differences in skin thickness and, therefore, different depths of penetration of near-infrared radiation. The NIR calibration model was successfully utilized to differentiate between surface and bound water in drug substances [Zhou et al.].

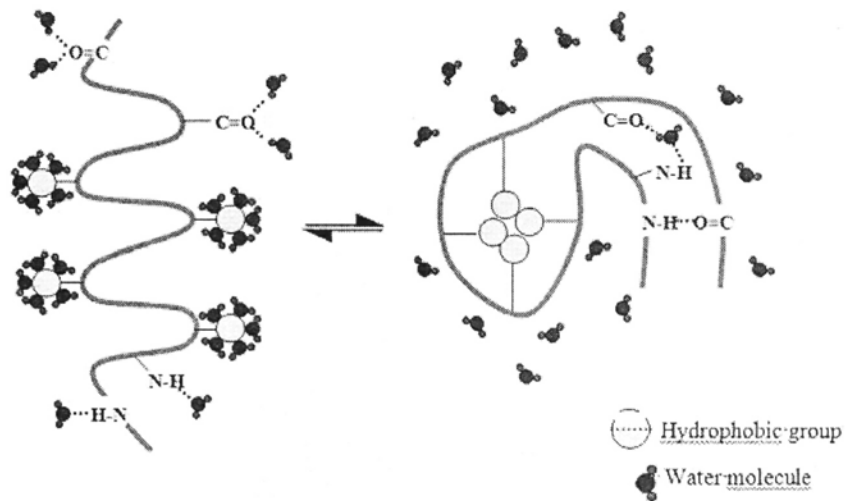


**Fig. 85:** Schematic representation of the various ways that water molecules are implicated in protein structure. (adapted from: <http://www.exobio.cnrs.fr>)

According to Kozlov et al., at 0-25% relative humidity, water in collagen is sorbed by high-energy sorption centers inside a triple helix as a monomolecular layer (0.10-0.12g/g). At 25-60% relative humidity polar groups of collagen macromolecules outside the helical fragments sorb water. Water directly bounded to macromolecules of proteins through H-bonds (both inside and outside helical fragments) should be considered as structural water (0.21- 0.23 g/g). At 60-90% relative humidity, water is sorbed by collagen into polymolecular layers (0.24-0.26 g/g).

It has been found that three stages of water desorption exist with the elapse of time within the skin after the application of humidifying agents. The rapid stage occurs during the first minute. At the second stage (1-10 min) water loss increases linearly at a rate slower than at the first stage. At the third stage (10-30 min) water content decreases exponentially at the slowest rate and tends to equilibrate [Scheuplein].

Two different constituents were determined using NIR for each parchment sample: nitrogen and water content. The Kjeldahl method for determination of total nitrogen content was chosen as a reference method. A number of investigators have reported the nitrogen content of animal food [Sosulski et.al] and different animal type skins [Eichelberger et al., Spencer

et al.]. However, the nitrogen percentage in parchment samples has not yet been measured. The water content of parchment samples has been previously measured and reported [Hansen et al.], but correlation of free and bound water in parchment matrices to deterioration stage based on NIR technology does not exist.

Based on NIR spectra, on line parchment characterization will serve the restoration rationale best. The main difficulty in parchment characterization is the correct identification of measurable properties. In order to characterize the historical parchment (for example, the Dead Sea Scrolls) we have to characterize the differences between the modern and the historical parchments.

Based on the differences, the parchment conditions may be inspected using a model based on multivariate analysis. The aim was to develop robust calibration equations capable of predicting parchment constituents on line during the restoration process. Modified partial least squares regression (MPLS) was applied to develop a calibration model. This study shows a possibility of a rapid, non-destructive and non-invasive parchment characterization and highlights the dilemma of the parchment water estimation.

#### **2.11.4.2.1. Experimental part**

##### *Nitrogen and water analysis*

Total nitrogen determination was performed by the Kjeldahl method. The calculations were done based on both wet and dry matter weight. As a reference, the value of nitrogen content in acid-soluble collagen type I from calf skin (Sigma) was determined to be 13.1% (based on wet matter).

Water content of the parchment samples at different temperatures was determined at 50°C, 70°C, 100°C and 150°C by loss of weight when drying in the oven until the constant weight was achieved at each temperature. It will be used to correlate in the study these measurements to specific structure water type within parchment samples at each temperature. The total water content of the parchment samples was determined as a loss of weight when heating in the oven at 105°C for 24 hours.

##### *Instrumentation*

NIR reflectance measurements of parchment samples were carried out

using a FOSS instrument grating spectrometer Model 6500 (FOSS NIR Systems, Silver Springs, MD, USA). For detailed procedure, see pages 124-125.

#### *NIR model*

In this study, the technique for measuring nitrogen and water content from spectral data using NIR 6500 instrument was evaluated. The calibrations were derived from the spectra and the chemical data together. The chemical data determined by the reference analytical method for parchment samples were added to the corresponding NIR spectral files. The maximum number of orthogonal components to be used in the regression models was preliminarily selected by the software to explain most of the total variance. Preliminary analysis, using the first or second derivative spectra showed that in most cases the use of a second derivative pre-treatment with a gap of four data points produced the best calibration. To achieve a single spectrum for each parchment sample (totally 88 spectra) two sides of each sample were averaged.

Two different methods of analysis were carried out. In the first, used for the nitrogen prediction, all the 88 spectra were included in calibration set and the data for each constituent was analyzed using Modified Partial Least Squares (MPLS) regression model. In this model, the maximum number of terms for each equation was determined by cross-validation, which consists of dividing the samples into two sets, a calibration set with  $\frac{3}{4}$  of the spectra and a validation set with  $\frac{1}{4}$  of the spectra. Using MPLS, separate calibration equations were developed, down weighting outliers with general Mahalanobis distance  $H > 3$  (two repeated selection passage were performed by the software).

When the calibration for water was developed the cross-validation was performed without a validation set, due to the lack of available data (in some cases only 44 samples were available).

Spectra pre-treatment in all regression models was applied to limit the influence of particle size on the prediction: a mathematical scatter correction SNV and detrend (SNVD) or standard multiplicative scatter correction (MSC).

Squared coefficients of determination in calibration ( $R^2$ ) were calculated as well as standard errors of calibration (SEC) for the equations developed for each constituent. Performance of cross validation was expressed as

squared coefficients of determination in validation ( $r^2$ ) and standard error of cross validation (SECV).

#### 2.11.4.2.2. Results and Discussion

**Figure 86** presents differences in reflectance among the spectra of the samples with different water content. **Figure 87** shows the corresponding second derivative spectra. In the NIR region water reflectance bands with peak maxima around 1420 nm (overtones) and 1920 nm (combination bands) are commonly used for determining the content of skin moisture [Zhou et al.; Arimoto et al., 2003]. Water bands associated largely with primary and secondary water of hydration on protein (1928 and 1910 nm, respectively), and free water (1890 nm) was assigned [Scheuplein]. Differences in the distribution of water types were seen due to differences in skin thickness with consequently different depths of penetration of near-infrared radiation [Scheuplein]. In our experiment, the local minima caused by water at 1422 nm, 1460 nm, 1907nm and 1937 nm can be observed, identifying the wavelengths for possible calibration. In **Figure 92**, the absorbance at 1907 nm and 1937 nm increases when total water level increases. According to [Zhou et al.], water peak at 1907 nm can be attributed to the surface water, and peak at 1937 nm corresponds to bound water. Therefore, according to the second derivative spectra, clear contribution of water to the spectra can be observed. **Figure 88** presents differences in reflectance among the spectra of the samples with different nitrogen content. The reflectance bands of protein are seen in **Figure 89** presented as a second derivative at 1184 nm, 1382 nm, 1422 nm, 1690 nm, 1973 nm, 2165 nm, 2182 nm.

Range, mean values and standard deviations of parchment constituents for the modern, artificially aged and historical samples are presented in **Table 17**. Significant differences are observed in the nitrogen content for the modern, aged and historical parchment samples. When examining the distribution of parchment samples according to nitrogen percent around pure calf collagen nitrogen content (13.1%), the clear distinction of the new samples that are found are both higher and lower than the pure collagen value and only historical samples that are lower can be seen.

Differences in the results for the calibration based on wet and dry weight basis calculations are found for nitrogen content, where the standard error of cross-validation (SECV) ranged from 0.75 to 1.16 and the squared coefficient of determination in validation (RSQ) from 0.73 to 0.35. The calibration equation for nitrogen estimation derived from the parchment samples based on the wet basis performed better in terms of the model performance (**Table 18**). The  $r^2$  varied from 0.60 to 0.86 and SEP values for nitrogen varied from 1.50 to 0.54 for the dry and wet basis calculation, respectively. The reason for this difference is the fact that the total water content used in the dry basis calculations does not correlate well. Therefore, the best predictive ability was obtained using a calibration model based on the wet basis calculations (native parchment state).

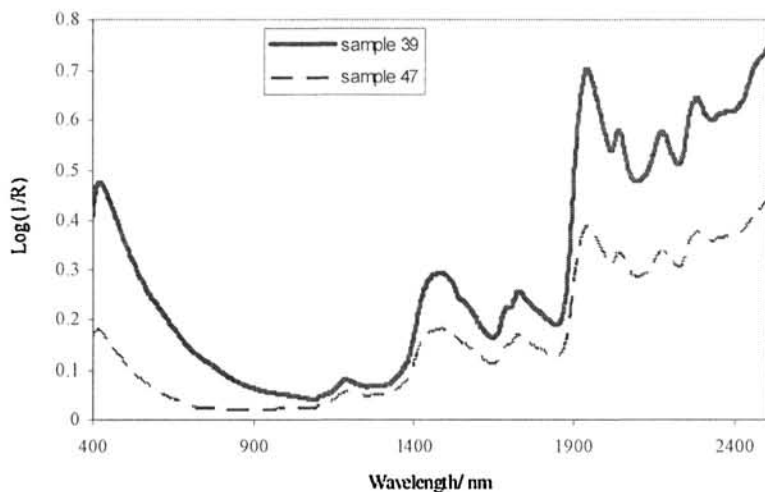


**Fig. 86:** Near infrared spectra of parchment samples with different water content (upper-high content, lower-low content), sample 39-flesh side, sample 47-grain side.

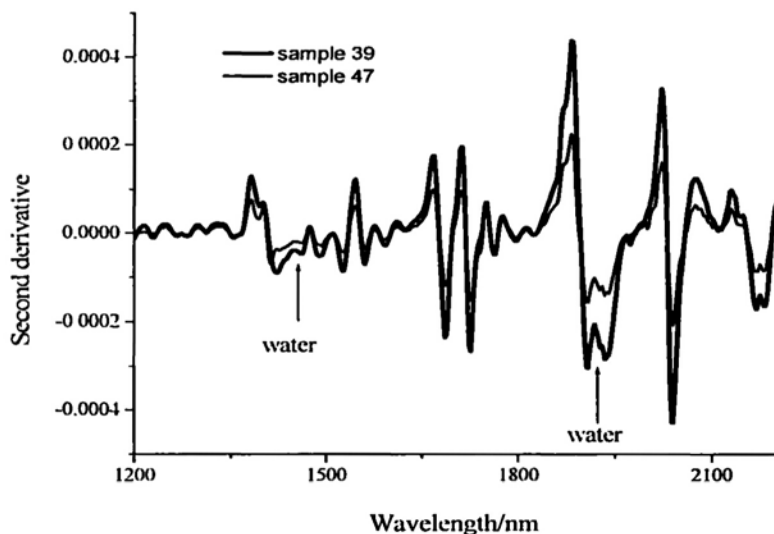


**Fig. 87:** Second derivative of near infrared spectra of parchment samples with different water content.

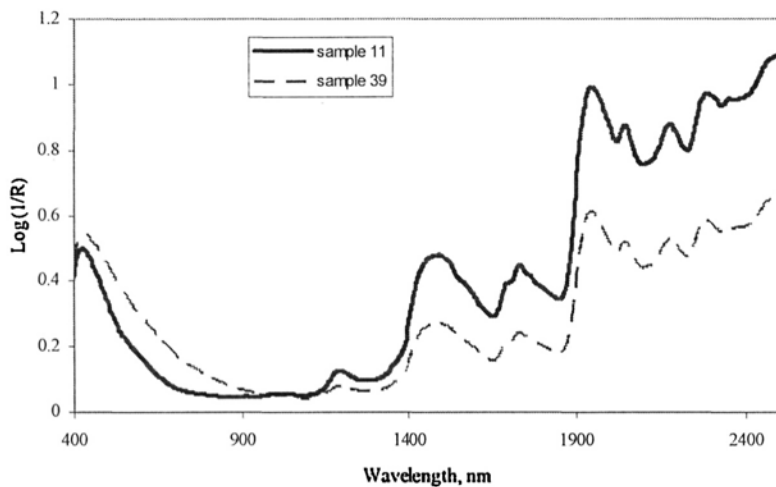


**Fig. 88:** Near infrared spectra of parchment samples with different nitrogen content.

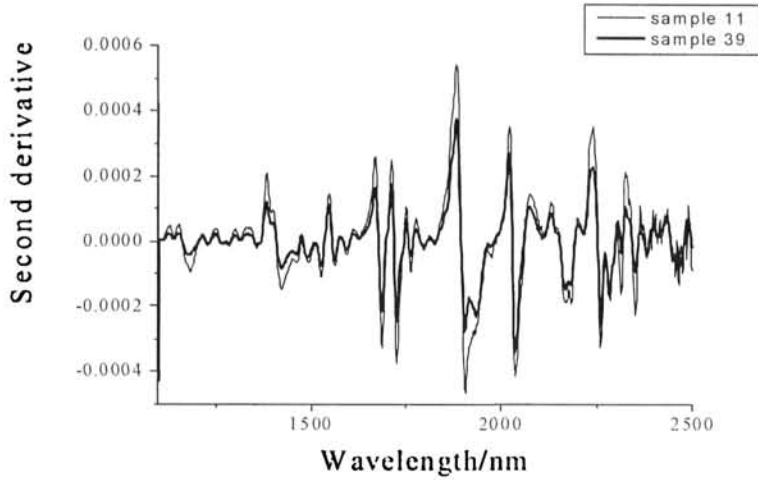


**Fig. 89:** Second derivative of near infrared spectra of parchment samples with different nitrogen content.

**Table 17**

Nitrogen and water content (on wet and dry matter basis) and descriptive statistics for parchment samples.

Constituent	Mean	SD	Range
<b>All samples</b>			
Nitrogen (%), wet basis	13.0	1.1	10.4-15.5
Nitrogen (%), DM basis	15.6	1.8	12.8-20.6
Water (%), DM basis	18.6	5.5	5.0-34.0
<b>New samples only</b>			
Nitrogen (%), wet basis	12.9	0.9	
Nitrogen (%), DM basis	16.0	1.9	
Water (%), DM basis	18.8	6.1	
<b>Aged samples only</b>			
Nitrogen (%), wet basis	13.5	1.0	
Nitrogen (%), DM basis	17.1	2.1	
<b>Historical samples only</b>			
Nitrogen (%), wet basis	12.0	0.8	
Nitrogen (%), DM basis	14.9	1.8	
Water (%), DM basis	19.2	2.2	

The experimentally measured water loss (Table 18) has a good correlation with previously reported values. It was found that the water loss during thermal degradation of parchment occurs through two processes. The first one is endothermic and consists of the 6-11% water loss only. The second one is exothermic and contains pyrolytic decomposition and thermooxidation of dry material (29-47% water loss) [Budrugaec et al., 2004]. Another study indicates that the relative mass lost up to 125<sup>0</sup>C is 18-38% [Budrugaec et al., 2003].

The calibration results for water were worse than those achieved for nitrogen content: RSQ varied from 0.24 to 0.68 depending on the water content in a specific parchment layer. The performance of the calibrations for prediction of parchment water layer content is shown in Table 18. The  $r^2$  varied from 0.48 to 0.82 and SEP values for nitrogen varied from 2.0 to 4.1 depending on the corresponding layer.

The results obtained for calibration of total water content show that the problem of the light penetration depth is critical because the specific layer water content determination depends on it. The light penetration depth depends on absorption and on the scattering properties of the sample. The scattering coefficient of biological tissue depends on many factors: water concentration, density of structural fibers, shapes and sizes of cellular structures [Kumar et al.]. The results obtained for water prediction shows that the reliable prediction model could be performed only using the specific type of structure water within a parchment sample. Depending on the specific parchment particle size, light penetration depth should be taken into account to correlate better between bulk and surface water. Water loss on drying profile was checked for all the samples to recognize the problem. The drying profile for the different samples can be seen in Figure 90 as a function of the ongoing heating. Three different stages can be recognized in the drying profile of each sample. Each stage corresponds to the specific temperature. The rate of the sample drying at the specific temperature depends on the parchment thickness and the water content. As reported by [Rochdi et al.], collagen denaturation exhibits a two-exponential behavior for the longitudinal relaxation time. Both the slow and the fast components decrease with increasing water content, and increases with the heating temperature in the range 40-70<sup>0</sup>C. At 70<sup>0</sup>C the proportion of thermal denatured collagen increased markedly with the water content. The fast component exists in a highly hydrated sample only from 60<sup>0</sup>C. The water population associated

with the fast component remains unchanged at high water content and represents ~15% of the total water signal. When the water content of collagen increases, the fraction of bound water is reduced.

It was reported that the rate of dehydration process increases with the hydration degree [Budrugaec et al., 2003]. For intact fibrillar collagen, multiple thermal transitions at temperatures between 50-110°C occurs [Brown et al.]. Budrugaec reported about the following processes in the heating of collagen: the transition of collagen from triple helix to random coil, the dehydration, the thermal degradation, the thermo-oxidative degradation [Budrugaec et al., 2003].

Actually, we have observed three different groups performing the measurements: bulk water, surface water and bonded water (**Figure 91**). The difference between the first two is distinguishable while the bond water can be found almost in every parchment layer.

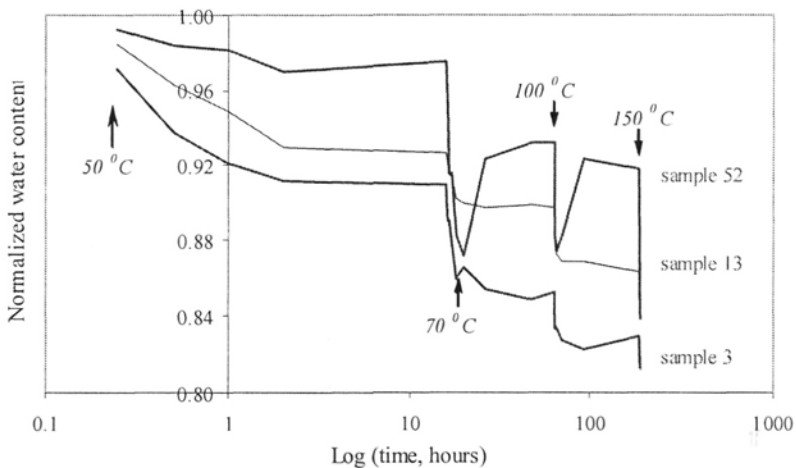


**Fig. 90:** Drying profile of the parchment samples through ongoing heating from 50°C to 150°C.

In **Figure 91**, the first group (left rectangle) includes the first water layer presented as a loss on drying at 50°C (surface water) and the second (right rectangle) includes the last layer presented as a loss on drying at 150°C. The data corresponding to loss on drying at 70°C is in between those two groups. All the parchment samples have a different thickness therefore when the light is probing the sample; the measured diffuse reflectance is actually a non-

linear function of two or more different water types together. We cannot clearly distinguish in our experiment between different water types. As a result, the calibration model for total water evaluation was not successful.

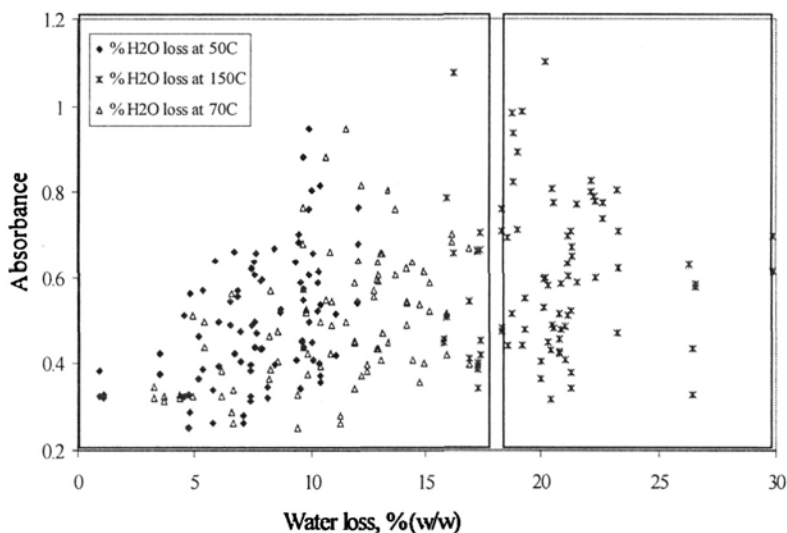


**Fig. 91:** Distribution of parchment samples according to the water loss. Absorbance was measured at 1907 nm for the surface water and at 1937 nm for the bulk water.

The performance of the calibration is presented in **Table 19**. The performance of the nitrogen calibration is shown in **Figure 92** when the predicted values are plotted as a function of the reference values. A sufficient correlation is seen ( $r^2 = 0.73$ ). The predictive ability of the model for the estimation of the surface water content (at 70°C) shows a better correlation ( $r^2 = 0.68$ ) than the total water estimation ( $r^2 = 0.24$ ) (**Figure 93**).

**Table 18**  
Statistic data of calibration developed for the prediction of nitrogen and water in parchment samples.

Constituent	Nitrogen (%), wet basis	Nitrogen (%), DM basis	Water (%), DM basis	Water loss at 50°C (%), DM basis	Water loss at 70°C (%), DM basis	Water loss at 100°C (%), DM basis	Water loss at 150°C (%), DM basis
Calibration set (range)	10.38-15.48	12.81-20.64	7.0-29.0	0.9-12.1	3.2-16.9	6.2-22.5	15.8-29.9
Calibration set (SD)	1.04	1.81	4.7	2.6	3.5	3.8	3.0
Validation set (range)	11.31-14.30	14.87-20.23					
Validation set (SD)	0.91	1.63					
Calibration set (mean)	12.99	15.86	18.5	7.8	10.9	16.4	20.5
	12.96	16.50					
Calibration model	MPLS	MPLS	MPLS	MPLS	MPLS	MPLS	MPLS
Data pre-treatment#	MSC	SNVD	MSC	MSC	MSC	MSC	MSC
Derivative	2	1	2	2	2	2	2
Calibration set (No.)	66	42	56	44	44	44	44
Validation set (No.)	22	14	0	0	0	0	0
R <sup>2</sup>	0.86	0.61	0.49	0.59	0.82	0.50	0.57
SEC	0.52	0.95	3.51	2.1	2.1	2.4	2.2
SEC(V)	0.75	1.08	3.97	2.4	3.1	2.8	2.4

#Data pre-treatment: standard normal variate coupled with quadratic baseline correction-detrend (SNVD); standard multiplicative scatter correction (MSC).

**Table 19**  
Performance of calibration for prediction of nitrogen and water in parchment samples.

Constituent	Nitrogen (%) wet basis	Nitrogen (%) DM basis	Water (%), DM basis	Water loss at 50°C (%) DM basis	Water loss at 70°C (%) DM basis	Water loss at 100°C (%) DM basis	Water loss at 150°C (%) DM basis
Calibration model	MPLS	MPLS	MPLS	MPLS	MPLS	MPLS	MPLS
t*	5	2	2	1	3	2	2
RSQ	0.73	0.37	0.24	0.34	0.68	0.25	0.33
Slope	0.95	0.87	0.84	1.00	0.99	0.87	1.17
SEP	0.54	1.37	4.14	2.05	1.96	3.28	2.42
SEP(C)	0.54	1.22	4.16	2.07	1.98	3.27	2.44
Bias	0.63	2.20	2.59	-0.01	0.11	1.73	-3.34

t\*-number of terms used in the regression model.

Generally, the major problem in this study is associated with the difficulty in providing an optimal estimate of the model's parameters, using a limited set of available data. Acquiring representative samples in the case of a historical parchment is usually a complicated trial. Consequently, the available number of samples with good statistical distribution is absolutely limited. Further analysis will be conducted with a larger number of samples representing a wider distribution and variety of parchments for assessing the general feasibility of NIR spectroscopy. However, this technique could be currently employed as a routine testing method in estimating nitrogen and water constituents in parchment samples rapidly and non-destructively.

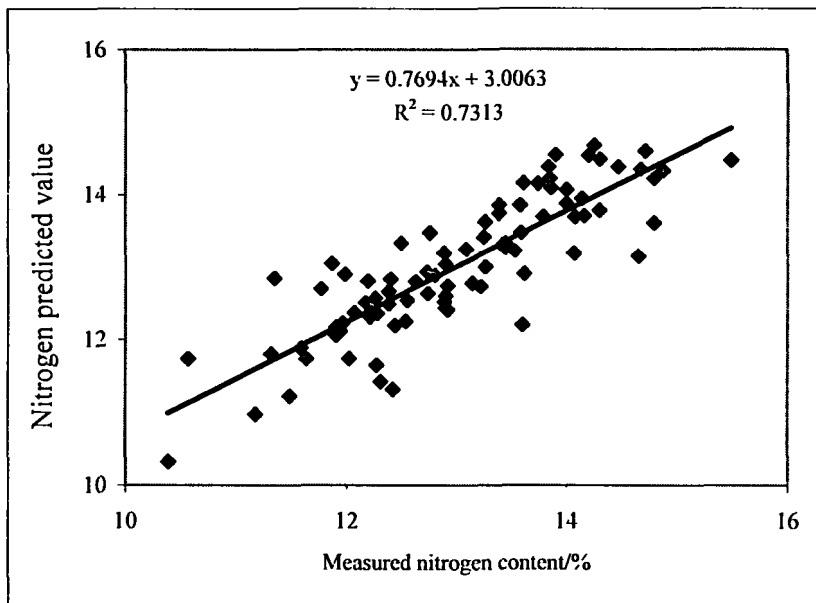


Fig. 92: Predicted nitrogen content in parchment samples calculated on wet basis (w/w%).

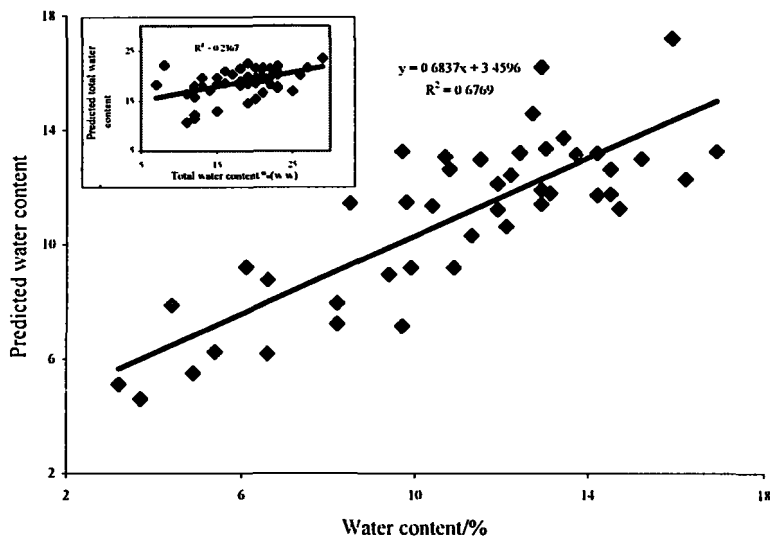


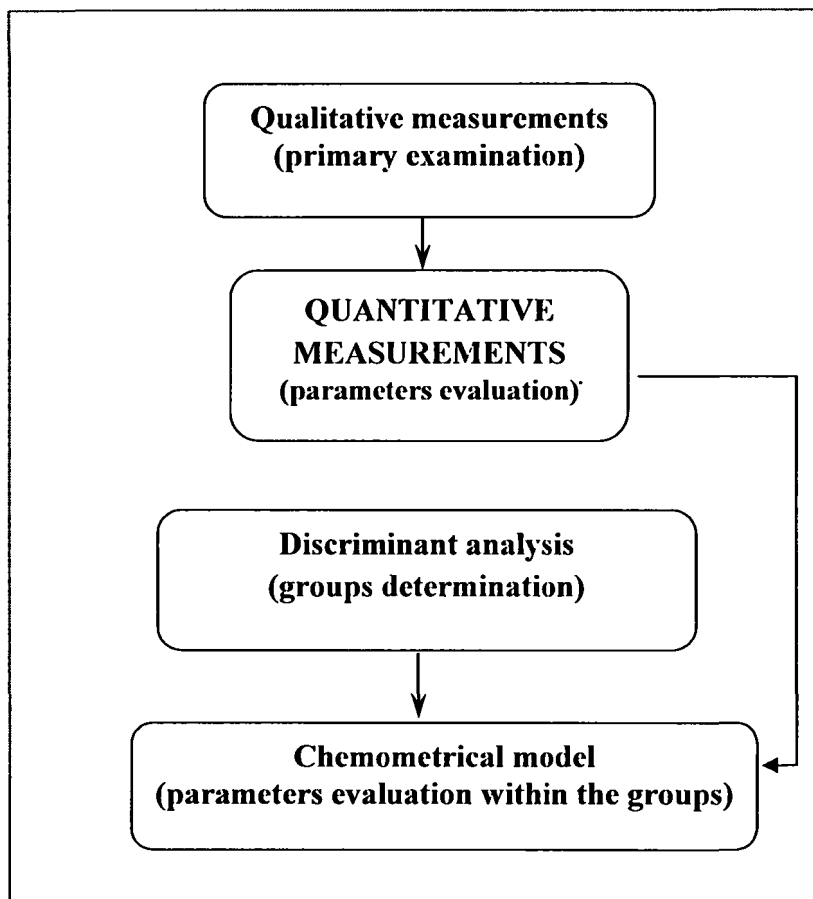
Fig. 93: Predicted water content in parchment samples (w/w %): top-total water content, bottom-water content at 70°C.

### 3. CONCLUSIONS

#### 3.1. Methods application guide

The main goal of the study was to develop a detailed complex analytical method for complete characterization of a given parchment sample. For this purpose, a wide variety of non-destructive analytical methods was applied. To simplify the “making decision” task for the final user (museum experts or laboratory investigators), the methods application diagnostic guide was created, tested and implemented to characterize parchment samples.

All the proposed methods presented in the scheme (Figure 99) were divided into four principal groups. The methods belonging to the same group reached the same target. Moreover, methods in each group enable the searching out of the answer to a predefined task. The tests to be performed are described from the simplest to the most complex group:

**METHODS APPLICATION DIAGNOSTIC GUIDE**

**Fig. 94:** Methods application diagnostic guide.

*Qualitative tests* are the very beginning, simplest possible non-destructive analysis that can be carried out on-line (for example, visualization of the fluorescence color) or in situ. The goal of these tests is to perform the preliminary examination of an artifact. These tests results in the basic classification of objects under the study. Consequently, qualification is a prerequisite for admitting samples to a quantitative method. These tests are also extremely helpful when the quantitative results are not required.

*Quantitative tests* possess an ability to quantify parameters of interest in each selected method. Then if the statistically significant difference exists

between predefined groups, the discrimination of parchment samples among these groups can be performed. The correspondent level of significance recognizes “quality control” decisions. Therefore, each of the quantitative methods can be used separately. To ensure the results completely, a combination of qualitative and quantitative tests as well as of two or more quantitative tests can be applied.

*Discrimination models* are intended to discriminate among modern, historical and artificially aged samples that are indistinguishable by simpler identification testing and/or to ensure accurate and precise classification. Regularly, a combination of statistically significant parameters under a quantitative test, or a few quantitative tests, provides assurance that the material belongs to the correct population and the discrimination method can fit the purpose in its original form. Alternatively, a discrimination model can be built. This model can be used optionally in an initial step in chemometric model development. In routine work, these two groups (discriminant model and chemometrical model) are often widely overlapping.

*Chemometrical* data analysis and models are both the most complicated and extremely helpful proposed tests. In multivariate **data analysis**, models are used directly for data interpretation. In multivariate **calibration**, models relate the data to a given property in order to predict this property.

In each sample group defined by discrimination methods, it allows quantification of specified parameters. Obviously, based on statistically significant differences found in each quantitative test, every restoration laboratory if needed can easily apply chemometric to the data to build their own prediction model. Once the model was built, fast, user-friendly and cheap non-destructive analysis can be performed on line. Additionally, the prediction of parameters regularly measured by destructive techniques (for example, water and nitrogen) becomes possible by means of non-destructive NIR analysis.

### 3.2. Summary

The results obtained in the study allow concluding two main achievements:

1. Five methods were successfully applied for the first time to parchment sample analysis, namely, synchronous fluorescence, LIBS, measurements of current sourcing high voltage, visible reflectance spectroscopy and NIR. Robust methodology of parchment characterization as an analytical object

using specified procedures was developed.

Chemometrical models (including discriminant analysis) were developed to demonstrate the feasibility and to show the perspective of using a given parchments set (with a given structure, variability and number of samples) as an origin of data.

Detailed achievements are provided in **Table 20** according to the previously described application guide. All the methods were applied to a representative set of 54 parchment samples (37 modern and 17 historical), produced from different animal skins and at different stages of deterioration. In the scale of archeological science, this set appears sufficiently big because it is understandable that the real historical samples are rare. Artificial aging of modern parchments was carried out in order to induce deterioration under well-defined controlled conditions.

### **3.3. Original contribution**

The work conducted for this study has made a number of achievements and some novel interesting features in examined parchment samples were found.

- 1) NIR analysis was successfully applied for the first time to the parchment sample analysis. The feasibility of chemometrical models development was demonstrated. We have used these models to identify and quantify parchment constituents.
- 2) LIBS was successfully applied for the first time to parchment samples. Surface elemental concentration of 7 minor and trace elements was measured by LIBS, when their bulk concentrations were measured by ICP and these two measurements found to be in good statistical correlation.
- 3) Synchronous fluorescence was successfully applied for the first time to parchment sample quantitative characterization. Layer-resolved profiling enabled the quantifying of the specific contribution of each chromophore in each given layer to the whole spectrum.
- 4) Three dimensional digital color imaging enables fast fake sample recognition.

**Table 20**  
Main results of the study according to the developed application guide.

Proposed method	Qualitative measurements	Quantitative measurements (statistically significant)	Chemometrical model (including discriminant analysis)
Fluorescence regular	fluorescence color and intensity → deterioration stage evaluation		
Fluorescence synchronous	fluorescence intensity integral and peak position → characterization of specific parchment sample → discrimination among groups	collagen-to-gelatin ratio → characterization of specific parchment sample → discrimination among groups	prediction model feasible
	layer resolved profile of parchment (based on LIBS) → individual chromophores in every parchment layer → potential to map the sample surface according to its local deterioration stage		prediction model in perspective
Digital color imaging (RGB)	blue color imaging → parchment surface examination		discrimination among parchment groups
Visible reflectance (470 nm)	3D color imaging → artificially aged samples recognition	distinction of parchment deterioration stage	prediction model in perspective
<b>LIBS&amp;ICP</b>		animal type identification; markers for ancient specimens identification	discriminant analysis based on Ca, Fe, Mg → distinction between modern and historical parchments

Table 20 (continued)

LIBS& ICP (continued)	depth profiling of parchment samples by LIBS → elemental concentration on surface → on-line ancient species identification depth profiling of parchment samples by LIBS (Mg) → principal possibility of animal type recognition	
	trace elements measured by ICP → differentiation of parchment samples to modern and historical markers → fast ancient parchments identification; environmental pollutants → evaluation of specific damage; calcium and/or nitrate content → animal type recognition	discrimination model; chemometrical analysis feasible
Ion chromatography	excellent correlation between corrected conductivity and normalized total ions amount → on-line discrimination among modern and historical parchment	
Current response at 1100V	modern, historical and artificially aged samples group distinction	
NIR		discrimination model, chemometrical model

- 5) Fluorescence decay kinetics of chromophore type I was examined.
- 6) The chromophores found in parchment samples were attributed to chemical substances based on previously published works.
- 7) Particle size evaluation based on visible reflectance spectroscopy was proposed as a perspective future study.
- 8) Measurement of current response sourcing high voltage was found as a fast method for parchment classification.
- 9) Presence of at least two types of chromophores in fluorescence spectrum of parchment samples was detected.
- 10) The procedure for “clean parchment matrix” preparation was developed.

This concept of preparation additionally permits self-made reference material preparation. Having a reference material for such a complicated matrix as the parchment can really improve the accuracy of analysis.

### **3.4. Open Questions**

The performed experiments have provided information on existing questions and opened up many new interesting ones. The first question would be to explore the artificial aging process with a lower irradiation dose and/or more gentle heating. These measurements would provide a more precise scale of the deterioration stage.

The second question deals with the chromophores found in parchment samples. It would be very useful to study in more detail the relationship between change in fluorescence spectrum of a parchment sample and specific fluorophores found in its matrix. Even in more simple matrices this problem remains unsolved. We found the original solution applying the depth resolved synchronous fluorescence using laser ablation. The obtained results are productive but a lot of routine experiments are needed to complete a picture. Consequently, working in this direction, one could potentially receive a precise mapping of parchment fluorophores distribution.

The next question to be addressed is to study more detail the effect of the animal type on the measurable properties. Some studies need to be done to better understand the behavior of each type of animal skin under high voltage application. We believe that a larger sample set with known properties would extend the proposed classification.

Another interesting question is one of polarization of the radiation on the parchment surface. This data would greatly complement the existing classification model.

#### 4. REFERENCES

- Akshaya K, Fang-Yu Y, Singh J, Shane B, (2004), *Applied Optics*, **43**: 5399-5403
- Ali B. A., Bulajic D., Corsi M., Cristoforetti G., Legnaioli S., Masotti L. F., Palleschi V., Salvetti A., Tognoni E., (2001), *Proceedings of SPIE*, **4402**: 25-31,
- Anglos D., (2001), *Applied Spectroscopy*, **55A**: 186-205
- Arimoto H., Egawa M., (2003), *Proceedings of the 25<sup>th</sup> Annual International Conference of the IEEE EMBS*, 3438-3441
- Arimoto H., Egawa M., Yamada Y., (2005), *Skin Research and Technology*, **11**: 27-35
- Bagrashvili V., Omel'chenko A., Sviridov A., Sobol' E., Lunina E., Zhitnev Y., Markaryan G., Lunin V., (2001), *High Energy Chemistry*, **35(6)**:423-429
- Beck K., Brodsky B. (1998), *Journal of Structural Biology*, **122**: 17-29
- Boyain-Goitia A., Beddows D., Griffiths B., Telle H., (2003), *Applied Optics*, **42**: 6119-6132
- Brown E., Farrell H., Wildermuth R., (2000), *Journal of Protein Chemistry*, **19(2)**:85-92
- Budrugaec P., Trandafir V., Albu M.G., (2003), *Journal of Thermal Analysis and Calorimetry*, **72**: 581-585
- Budrugaec P., Miu L., Popescu C., Wortmann F.-J., (2004), *Journal of Thermal Analysis and Calorimetry*, **77**: 975-985
- Cefalas A.C., Sarantopoulou E., Kollia Z., (2001), *Applied Physics A*, **73**: 571-578
- Chanine C., (2000), *Thermochimica Acta*, **365**: 101-110
- Chalmers J.M., Griffiths P.R., (2002), *Handbook of Vibrational Spectroscopy*, Wiley, Chichester
- Collins M., Riley M., Child A., Turnet-Walker C., (1995), *Journal of Archeological Science*, **22**: 175- 183
- Conserve O' Grams- Museum Management Program
- Cooper, M., Sportun S., Stewart A., Vest M., Larsen R., Poulsen D., (2000), *The Conservator*, **24**: 69-79.
- Corsi M, Cristoforetti G, Hidalgo M, Legnaioli S, Palleschi V, Salvetti A, Tognoni E, Vallebona C, (2003), *Applied Optics*, **42**: 6133-6137
- Danielsen L., Gniadecka M., Thomsen H.K., Pedersen F., Strange S., Nielsen

- K.G., Petersen H.D., (2003), *Forensic Science International*, **134**: 134-141
- Della Gatta G., Badea E., Ceccarelli R., Usacheva T., Mašić A., Coluccia S., (2005), *Journal of Thermal Analysis and Calorimetry*, **82(3)**: 637-649
- Derrick M., (1991), *The American Institute for Conservation Annual*, **10**
- Deyl Z., Praus R., Sulcova H., Goldman J.N., (1969), *FEBS Letters*, **5(3)**: 187-191
- Dong R., Yan X., Pang X., Liu S., (2004), *Spectrochimica Acta A*, **60**: 557-561
- Doukas A.G., Soukos N.S., Babusis S., Appa Y., Kollias N., (2001), *Photochemistry and Photobiology*, **74(1)**: 96-102
- Dramićanin T., Dramićanin M.D., Jokanović V., Vukosavljević D.N., Dimitrijević B., (2005), *Photochemistry and Photobiology*, **81**: 1554-1558
- Draper N.R., Smith H., (1981), *Applied Regression Analysis*, Wiley, New-York
- Edwards H.G.M., Farwell D.W., Newton E.M., Perez F.R., Villar S.J., (2001), *Spectrochimica Acta A*, **57**: 1223-1234
- Edwards H.G.M., Perez F.R., (2004), *Journal of Raman Spectroscopy*, **35**: 754-760
- Eichelberger L., Eisele C.W., Wertzler D., (1943), *The Journal of Biological Chemistry*, **151**: 177-189
- Estienne F., (2002), Ph.D.Thesis, University of Brussels
- Estienne F., Pasti L., Centner V., Walczak B., Despagne F., Rimbaud J. D., de Noord O. E., Massart D.L., (2001), *Chemometrics and Intelligent Laboratory Systems*, **58 (2)**: 195-211
- Fessas D., Schiraldi A., Tenni R., Zuccarello L.V., Bairati A., Facchini A., (2000), *Thermochimica Acta*, **348**: 129-137
- Fujimori E., (1966), *Biochemistry*, **5(3)**: 1034-1040
- Fujimoto D., Akiba K., Nakamura N., (1977), *Biochemical and Biophysical Research Communications*, **76 (4)**: 1124-1129
- Gallo S., Sen A., Hensen M., Wen Hui S., (1999), *Biophysical Journal*, **76**: 2824-2832
- Gavriusinas V., Vaitkus J., Vaitkuvienė A., (2000), *Lithuanian Journal of Physics*, **4094**: 232-236
- Guidelines for the conservation of leather and parchment bookbinding
- Jansen E.F., Lee S.N., Sobel H., 1992, *Journal of the American Institute of Conservation*, **31(3)**: 325-342

- Hybl J., Lithgow G., Buckley S., (2003), *Applied Spectroscopy*, **57**: 1207-1215
- Jurkiewicz B., Buettner G., (1996), *Photochemistry and Photobiology*, **64(6)**: 918-922
- Kalia Y.N., Alberti I., Sekkat N., Curdy C., Naik A., Guy R., (2000), *Pharmaceutical Research*, **17(9)**:1605-1613
- Kaminska A., Sionkowska A., (1996), *Polymer Degradation and Stability*, **51**: 15-18
- Kaminska A., Sionkowska A., (1996). *Polymer Degradation and Stability*, **51**: 19-26
- Kautek W., Pentzien S., Rudolph P., Krüger J., König E., (1998), *Applied Surface Science*, **127-129**: 746-754
- Kautek W., Pentzien S., Röllig M., Rudolph P., Krüger J., Maywald-Pitellos C., Bansa H., Grösswang H., König E., (2000), *Journal of Cultural Heritage*, **1**: S233-S240
- Kautek, W. Pentzien, A.Conradi, D.Leichtfried, L.Puchinger, (2003), *Journal of Cultural Heritage*, **4**: 179s-184s
- Kennedy C.J., Wess T.J., (2003), *Restaurator*, **24**: 61-80
- Knox K., Johnston R., Easton R.L., (1997), *Optics and Photonics News*, 30-34
- Kollia Z., Sarantopoulou E., Cefalas A.C., Kobe S., Samardzija Z., (2004), *Applied Physics A*, **79**: 379-382
- Kozlov P.V., Burdygina G.I., (1983), *Polymer*, **24**: 651-666
- Kumar G., Schmitt J.M., (1997), *Applied Optics*, **36(10)**: 2286-2293
- Larsen R., (2002) (ed.), *Microanalysis of parchment*, Archetype, London
- Leikin S., Parsegian V.A., Yang W.-H., Walrafen G.E., (1997), *Proceedings of the National Academy of Science of the United States of America-Biophysics*, **94**: 11312-11317
- Lloyd R., Fong A., Sayre R., (2001), *Journal of Investigative Dermatology*, **117**:740-742
- Massart D.L., (1988), *Chemometrics: a textbook*, Elsevier, NY
- Massart D., Vandeginste B., Buydens L., Jong S., Lewi P.J., Smeyers-Verbeke J., (1997), *Handbook of Chemometrics*, Elsevier, Amsterdam
- Martens H., Naes T., (1989), *Multivariate Calibration*, Wiley, Chichester
- Majewski A., (2001), *Ph.D. Dissertation*, New Jersey
- Majewski A., Sanzari M., Cui H. L., Torzilli P., (2002), *Physical Review E*, **65 (031920)**: 1-10

- Melessanaki K., Mateo M., Ferrence S., Betancourt P., Angos D., (2002), *Applied Surface Science*, **197-198**: 156-163
- Mannucci E., Pastorelli R., Zerbi G., Botanni C.E., Facchini A., (2000), *Journal of Raman Spectroscopy*, **31**: 1089-1097
- Martin K., (1998), *Applied Spectroscopy*, **52**: 1001-1007
- Menter J.A., Williamson G.D., Carlyle K., Moore C.L., Willis I., (1995), *Photochemistry and Photobiology*, **62(3)**: 402-408
- Meyers R.(ed), (2000), *Encyclopedia of analytical chemistry*, Wiley, Chichester
- Miles C.A., Sionkowska A., Hulin S.L., Sims T.J., Avery N.C., Bailey A.J., (2000), *Journal of Biological Chemistry*, **275 (42)**: 33014-33020
- Morel S., Leone N., Adam P., Amouroux J., (2003), *Applied Optics*, **42**: 6184-6191
- Na R., Stender I.M., Ma L., Wulf H.C., (2000), *Skin Research and Technology*, **6**: 112-117
- Odlyha M., Cohen N. S., Foster G. M., Aliev A., Verdonck E., Grandy D., (2003), *Journal of Thermal Analysis and Calorimetry*, **71(3)**: 939-951
- Ohan M.P., Weadock K.S., Dunn M.G, (2002), *Journal of Biomedical Materials Research*, **60**: 384-391
- Onwuka S., Avwioro O., Akpan M., Ahmed Y., (2001), *African Journal of Biomedical Research*, **4**: 151-154
- Orgel J. P., Miller A., Irving T. C., Fischetti R. F., Hammersley A. P., Wess T. J., (2001) *Structure (London)*, **9**: 1061-1069
- Patra D., Mishra A.K., (2002), *Trends in analytical chemistry*, **21(12)**: 787-798
- Potts P. J., Ellis A. T., Kregsamer P., Marshall J., Strelci C., West M., Wobrauschek P., (2003), *Journal of Analytical Atomic Spectrometry*, **18**: 1297-1316
- Renugopalakrishnan V., Chandrakasan G., Moore S., Hutson T.B., Berney C.V., Bhatnagar R.S., (1989), *Macromolecules*, **22**: 4121-4124
- ROCHDI A., FOUCAT L., RENO J.P., (1999), *BIOPOLYMERS*, **50**: 690-696
- Samek O., Beddows D., Telle H., Kaiser J., Liska M., Caceres J., Gonzales U., (2001), *Spectrochimica Acta*, **56 B**: 865-875
- Sattmann R., Monch I., Krause H., Noll R., Couris S., Hatziapostolou A., Mavromanolakis A., Fotakis C., Larrauri E., Miguel R., (1998), *Applied Spectroscopy*, **52**: 456-461

- Scheuplein R. J., (1964), *Journal of the Society of Cosmetic Chemists*, **15**: 111-122
- Sionkowska A., (2000), *Polymer Degradation and Stability*, **68**: 147-151
- Sionkowska A., (2000), *Polymer Degradation and Stability*, **67**: 79-83
- Sionkowska A., (2001), *Polymer Degradation and Stability*, **73**: 107-112
- Sionkowska A., Kaminska A., (1999), *Journal of Photochemistry and Photobiology A*, **120**: 207-210
- Sionkowska A., Skopinska J., Wisniewski M., (2004), *Polymer Degradation and Stability*, **83**: 117-125
- Sobel H., Ajie H., (1992), *Free Radical Biology and Medicine*, **13**: 701-702
- Sosulski F.W., Imafidon G.I., (1990), *Journal of Agricultural and Food Chemistry*, **38**: 1351-1356
- Spencer H.C., Morgulis S., Wilder V.M., (1937), *The Journal of Biological Chemistry*, **120**: 257-266
- Sportun S., Cooper M., Stewart A., Vest M., Larsen R., Poulsen D. V., (2000), *Journal of Cultural Heritage*, **1**: S225-S232
- Strli M., Kolar J., 效lih V.S., Marin 鑽k M., (2003), *Applied Surface Science*, **207**:236-245
- Sun J.S, Lu F., (2002), *Pakistan Journal of Nutrition*, **1(4)**:169-173
- Suh E.-J., Woo Y.-A., Kim H.-J., (2005), *Archives of Pharmacological Research*, **28(4)**: 458-462
- Szalay A., Antal I., Zsigmond Z., Marton S., Erős I., Regdon G., Pintyc-Hidói K., (2005), *Particle and Particle Systems Characterization*, **22**: 219-222
- Theodossiou T., Rapti G., Hovhannisyan V., Georgiou E., Politopolos K., Yova D., (2002), *Lasers in Medical Science*, **17**: 34-41
- Theodossiou T., Georgiou E., Hovhannisyan V., Politopolos K., Yova D., (2001), *Journal of Optics A*, **3**: L1-L3
- Torikai A., Shibata H., (1999), *Journal of Applied Polymer Science*, **73**:1259-1265
- Tuross N., (2002), *Archaeometry*, **44(3)**: 427-434
- Vanbever R., Fouchard D., Jadoul A., Morre N.D., Pr at V., Marty J.P., (1998), *Skin Pharmacology and Applied Skin Physiology*, **11**: 23-34
- Vandenabeele P., Wehling B., Moens L., Edwards H., Reu M.D., Hooydonk G.V., (2000), *Analitica Chimica Acta*, **407**: 261-274
- Xia T., Wang L., Bian G., Dong L., Hong S., (2006), *Microchimica Acta*, **154**: 309-314
- Xiao Y., Guo M., Parker K., Hutson M. S., (2006), *Biophysical Journal*, **91**:

1424-1432

Yova D., Theodossiou T., Hovhannisyan H., (1998), *Proceedings of SPIE*, **3565**: 174-180

Zhou G.X., Ge Z., Dorwart J., Izzo B., Kukura J., Bicker G., Wyratt J., (2003), *Journal of Pharmaceutical Sciences*, **92(5)**: 1058-1065

Wang L.Y., Wang L., Dong L., Bian G.R., Xia T.T., Chen H.Q., (2005), *Spectrochimica Acta A*, **61**: 129-133

Weiner S., Kustanovich Z., Gil-Av E., Traub W., (1980), *Nature*, **287(5785)**: 820-823

Wess T.J., Drakopoulos M., Snigirev A., Wouters J., Paris O., Fratzi P., Collins M., Hiller J. and Nielsen K., (2001), *Archaeometry*, **43**:117-129

Wess T.J., Orgel J.P., (2000), *Thermochimica Acta*, **365**: 119-128

Wouters J., (2002), 5<sup>th</sup> European Commission Conference on Research for Protection, Conservation and Enhancement of Cultural Heritage, Cracow, Poland